JPRS L/10556

1 June 1982

USSR Report

EARTH SCIENCES

(FOUO 3/82)

FBIS FOREIGN BROADCAST INFORMATION SERVICE

FOR OFFICIAL USE ONLY

APPROVED FOR RELEASE: 2007/02/09: CIA-RDP82-00850R000500070002-7

NOTE

JPRS publications contain information primarily from foreign newspapers, periodicals and books, but also from news agency transmissions and broadcasts. Materials from foreign-language sources are translated; those from English-language sources are transcribed or reprinted, with the original phrasing and other characteristics retained.

Headlines, editorial reports, and material enclosed in brackets [] are supplied by JPRS. Processing indicators such as [Text] or [Excerpt] in the first line of each item, or following the last line of a brief, indicate how the original information was processed. Where no processing indicator is given, the information was summarized or extracted.

Unfamiliar names rendered phonetically or transliterated are enclosed in parentheses. Words or names preceded by a question mark and enclosed in parentheses were not clear in the original but have been supplied as appropriate in context. Other unattributed parenthetical notes within the body of an item originate with the source. Times within items are as given by source.

The contents of this publication in no way represent the policies, views or attitudes of the U.S. Government.

APPROVED FOR RELEASE: 2007/02/09: CIA-RDP82-00850R000500070002-7

JPRS L/10556

1 June 1982

USSR REPORT
EARTH SCIENCES
(FOUO 3/82)

CONTENTS

APPROVED FOR RELEASE: 2007/02/09: CIA-RDP82-00850R000500070002-7

METEOROLOGY

UDC 551.509.32

ARTICLES ON SHORT-RANGE FORECASTING OF METEOROLOGICAL ELEMENTS AND DANGEROUS WEATHER PHENOMENA

Leningrad TRUDY ORDENA LENINA GIDROMETEOROLOGICHESKOGO NAUCHNO-ISSLEDOVATEL'SKOGO TSENTRA SSSR: KRATKOSROCHNYY PROGNOZ METEOROLOGICHESKIKH ELEMENTOV I OPASNYKH YAVLENIY POGODY in Russian No 233, 1981 (signed to press 5 Jun 81) pp 129-135

[Abstracts from collection "Short-Range Forecasting of Meteorological Elements and Dangerous Weather Phenomena," edited by E. N. Novikova, candidate of geographical sciences, and B. Ye. Peskov, Gidrometeoizdat, 880 copies, 135 pages]

UDC 551.577.1+551.578.7

CONDITIONS FOR FALLING OF HEAVY SHOWERS AND HAIL

[Article by Glushkova, N. I.]

[Text] The author sets forth the conditions governing the falling of heavy showers and hail. The dependences between the quantity of falling precipitation, macroscale vertical movements and mesoscale convective currents in a cloud are determined. Expressions are also derived for computing a precipitation sum greater than 50 mm and hail, which can inflict losses on agricultural crops over a great area. Expressions are given which represent the relationship between the product of the radar parameters of the cloud $H_m|gz_m$ and the maximum velocity of the ascending flow in the cloud, which make it possible to compute the quantity of precipitation over a great area on the basis of observational data from the network of meteorological radars. The results of the investigation can be used in the diagnosis and prediction of precipitation and heavy hail inflicting great losses on the national economy and also for evaluating the effect exerted on hail processes. Tables 5, references 8.

UDC 551.515.4

SOME RESULTS OF INVESTIGATION OF SYNOPTIC-DYNAMIC CONDITIONS FOR DEVELOPMENT OF CONVECTIVE CLOUDS AND PHENOMENA ASSOCIATED WITH THEM OBTAINED DURING MONEX

[Article by Peskov, B. Ye., Zhelnin, A. A., Shupyatskiy, A. B., Khamarina, T. V. and Casova, K. I.]

[Text] The authors have found the dependence of convective activity on the convergence of flows in the lower layers of the troposphere under favorable conditions

of stratification and humidity on the basis of data for the equatorial zone of the South China Sea. It was possible to ascertain the physical reasons for the influence of convergence. The article gives the diurnal variation of convergence, the pressure field, precipitation, altitude of the cloud tops (on the basis of radar data) at sea at a distance of 100-300 km from major land masses. An analysis is given of the role of the mesoscale pressure field in determining the divergence of surface currents in the equatorial zone and its macroscale characteristics in a forecast of convective activity. The vertical profiles of temperature, humidity, instability energy, divergence and vertical movements, averaged for different classes of cases, are given, as well at the mean values of the altitudes of the "tops" of radioechoes and the quantity of precipitation. Figures 1, tables 4, references 17.

UDC 551.588.7

RESULTS OF ROUTINE TESTING OF METHOD FOR SHORT-RANGE FORECASTING OF METEOROLOGICAL CONDITIONS FOR CONTAMINATION OF SURFACE AIR LAYER

[Article by Neronova, L. M. and Ponomarenko, S. I.]

[Text] The article gives the results of the probable success of experimental forecasts of the meteorological conditions for the accumulation and scattering of effluents on the basis of data for 1978 in the Moscow region. It was possible to determine the critical values of the parameters of the thermodynamic state of the atmospheric boundary layer and the characteristic meteorological conditions recommended for preparation of forecasts of the meteorological conditions for the contamination of urban air. Tables 5, references 3.

UDC 551.509.323

RECOMMENDATIONS ON REFINING FORECAST OF VERTICAL DISTRIBUTION OF TEMPERATURE IN ATMOSPHERIC BOUNDARY LAYER

[Article by Novikova, E. N.]

[Text] Pressure pattern maps for the standard isobaric surfaces, situated at a distance of 150-200 mbar from one another, cannot be used in a reliable analysis and prediction of the temperature fields in thinner layers of the atmosphere. The author gives practical recommendations on refining the forecast of the vertical distribution of temperature in the lower 500-m layer of the atmosphere on the basis of empirical data obtained from high structures, in the example of use of observational data from the television tower at Ostankino (Moscow). Tables 3, references 6.

UDC 551.509.5

METHOD FOR EVALUATING FORECASTS OF CONVECTIVE WEATHER PHENOMENA AND PROPOSALS FOR ITS IMPROVEMENT

[Article by Lapcheva, V. F.]

[Text] The article is an analysis of the existing method for evaluating operational methods for predicting convective weather phenomena, especially forecasts of

precipitation, in specific examples and proposals are given on improvement of the evaluation method. It is shown that the evaluation principle used in the Instructions (involving use of a small number of meteorological stations) applicable to forecasts of convective weather phenomena does not agree with the nature of formation of these phenomena and the probability of their detection using the meteorological network of observations. As a rule, the forecasts are not compared with the real, but with some artificial weather pattern in the forecast region. The need for using data obtained using artificial earth satellites and meteorological radars in the evaluation of forecasts is pointed out. Tables 2, references 12.

UDC 551.501(776+777)

COMPLEX MAPS OF CLOUD COVER AND ATMOSPHERIC PHENOMENA AND THEIR USE IN SYNOPTIC PRACTICE

[Article by Minakova, N. Ye.]

[Text] The information content of a complex map of cloud cover and atmospheric phenomena, compiled using data from radar and visual observations, is discussed. An evaluation of the effectiveness of radar data, making use of the complex maps, again confirmed the high reliability of information on thunderstorms (82%) and rains (65%). The complex maps contain a great volume of information (especially on convective phenomena), more than "microring" charts (by 35%) or "ring" charts (by 57%). The problem of the use of data from complex maps for determining the nature of an air mass and also the degree of atmospheric instability is examined in detail. Figures 1, tables 4, references 8.

UDC 551.509.52

QUANTITATIVE ESTIMATE OF WIND VELOCITY WITH ALLOWANCE FOR BREEZE AIR CIRCULATION

[Article by Masterskikh, M. A.]

[Text] A method for computing the pressure gradient governing the wind on the shores of seas, lakes and large reservoirs in summer during weather with few clouds is examined. The influence of breeze circulation on intensification (weakening) of the wind in the shore zone is demonstrated. Figures 1, references 4.

UDC 551.524.31

DIURNAL VARIATION OF AIR TEMPERATURE AT MOSCOW AND ITS SUBURBS UNDER DIFFERENT WEATHER CONDITIONS

[Article by Gerburt-Geybovich, A. A., Bakhareva, G. M. and Remizov, G. A.]

[Text] The authors computed the diurnal variation of air temperature with different wind directions and during a calm with different cloud cover or precipitation on the basis of data from the suburban meteorological station Nebol'sina and meteorological station Balchug, situated at the center of the city (observations made eight times a day during the period 1966-1975). The results can be used in

short-range weather forecasting for Moscow, and in particular, for separate allowance for the diurnal variation of air temperature in the city and in its suburbs. Figures 3, tables 3, references 7.

UDC 551.510.522

CHANGE IN METEOROLOGICAL ELEMENTS IN LOWER LAYER OF TROPOSPHERE DURING THUNDERSTORMS AND SHOWERS

[Article by Klinov, F. Ya.]

[Text] The principal characteristics of mesoscale changes in temperature, wind velocity and direction in the lower layer of the atmosphere during thunderstorms and showers are considered. Using samples of measurement data from the meteorological mast at Obninsk and the television tower at Moscow, for each of the considered elements the author gives quantitative estimates of their mesoscale changes. These characteristics are indicative for possible deviations of the values of meteorological elements from the diurnal variation. Tables 3, references 1.

UDC 551.524.31

COMPUTATION OF THERMAL TRANSFORMATION FOR MOSCOW DURING CONSIDERABLE ANOMALIES OF MEAN DAILY TEMPERATURE

[Article by Sokolova, N. G.]

[Text] Computations of the thermal transformation were made for cases of considerable anomalies and sharp day-to-day changes in mean daily temperature at Moscow. The movement of pressure formations was taken into account in constructing an air particle trajectory. The computed temperatures in the cold half-year, in comparison with the actual temperatures, were exaggerated on the average by 2°C. This value can be used as an additional correction in the computations. Figures 1, tables 1, references 2.

UDC 551.584.2

MESOSCALE REGIONALIZATION OF MOSCOW AND ITS SUBURBS WITH RESPECT TO TEMPERATURE AND WIND

[Article by Gerburt-Geybovich, A. A.]

[Text] On the basis of processing and generalization of mesometeorological observations for 1975-1978 at 50 points in Moscow and in its suburbs it was possible to develop a mesoclimatic regionalization of the Moscow metropolitan area and also validate the desirability of differentiation of the background temperature forecast for Moscow for 6-8 hours for sectors of the city and suburbs. Figures 1, tables 1, references 4.

UDC 551.515.5

INTERTROPICAL CONVERGENCE ZONE ACCORDING TO DATA FROM THE 30th VOYAGE OF THE SCIENTIFIC RESEARCH SHIP 'YU. M. SHOKAL'SKIY'

[Article by Belinskiy, O. N. and Veselov, Ye. P.]

[Text] The authors define two intertropical convergence zones (ICZ) in the western part of the Pacific Ocean -- in the northern and southern hemispheres -- and a zone of divergence of wind flows. A study is made of the correlation of their migration with pulsations of the subtropical anticyclones. It was established that ICZ movement occurs in the direction of the resultant pressure gradient (subtropical anticyclone - equator). A scheme of the development of processes in the ICZ is proposed. In the ICZ regions and beyond their limit the authors computed the velocities of ordered vertical movements, vorticity components and Ω_z, Richardson number, thermodynamic temperature gradients and other parameters. It is shown that for delineating the ICZ boundaries it is sufficient to use the vertical spatial-temporal sections of the meridional wind component, ordered vertical movements and dew point spreads. Figures 2, tables 7, references 10.

UDC 551.509.32

CORRELATION BETWEEN LOWER-LEVEL CLOUD COVER AND DEW POINT SPREAD AND AIR TEMPERATURE

[Article by Alekseyeva-Obukhov, I. A.]

[Text] On the basis of statistical processing of data from aircraft ascents during the spring and autumn seasons of 1948-1951 it was possible to obtain expressions for computing the quantity of low clouds on the basis of the dew point spread at the 850-mbar level. A checking of the results of computations on the basis of independent material indicated that the proposed method has a good probable success (the mean error in computing the quantity of clouds is from 0.8 to 2.0 scale units (tenths)) for all months of the transitional seasons, except for March and November -- months of the cold half-year, for which the mean error in computations is 3.8-4.9 scale units (tenths) respectively. Tables 2, references 9.

5303
CSO: 1865/76

OCEANOGRAPHY

UDC 551.46

COLLECTION OF PAPERS ON MARINE HYDROLOGICAL COMPUTATIONS AND FORECASTS

Leningrad TRUDY ORDENA LENINA GIDROMETEOROLOGICHESKOGO NAUCHNO-ISSLEDOVATEL'SKOGO TSENTRA SSSR: MORSKIYE GIDROLOGICHESKIYE RASCHETY I PROGNOZY in Russian No 241, 1981 (signed to press 25 May 81) pp 107-112

[Abstracts from collection of articles "Marine Hydrological Computations and Forecasts", edited by V. S. Krasyuk, candidate of geographical sciences, and K. M. Sirotov, candidate of geographical sciences, Gidrometeoizdat, 510 copies, 112 pages]

UDC 551.463.6(261)

MACROSCALE WATER SURFACE TEMPERATURE ANOMALIES IN THE PACIFIC OCEAN

[Article by Karasev, Ye. V. and Ugryumov, A. I.]

[Text] The article gives a statistical analysis of the field of water surface temperature anomalies in the northern part of the Pacific Ocean (20-50°N) on the basis of data for 5° grid squares during the period from 1949 through 1976. Using the information content index I_n, the spatial correlation and autocorrelation functions it was possible to discriminate four informative regions of the ocean, arbitrarily called: northern, central, southwestern and southeastern. It is proposed that the use of information from the ocean areas of these regions will be most useful for investigating the macroscale interaction between the ocean and atmosphere for the purposes of long-range weather forecasting. Figures 3, references 17.

UDC 551.526.6:551.465.635

CYCLICITY OF VARIATIONS IN WATER SURFACE TEMPERATURE ANOMALIES IN PACIFIC OCEAN

[Article by Karasev, Ye. V. and Ugryumov, A. I.]

[Text] The authors analyze the results of computations of the spectral density functions for water surface temperature anomalies in four informative regions of the Pacific Ocean: northern, central and two southern (southwestern and southeastern) regions. The basis for the computations was time series Δt_w for the period from 1949 through 1962. As a result of the analysis it was demonstrated that along

the North Pacific Ocean subtropical circulation there is a predominance of long-period variations with a period of 4.2 years, coinciding with the full period of circulation of water masses. Variations of water temperature anomalies with lesser periods (about 10 months) are noted in the southwestern part of the Pacific Ocean in a zone of well-expressed currents. Also examined is an approximate scheme of the interrelationship of ocean currents and the field of water temperature anomalies in accordance with the scheme proposed by V. G. Kort (1970). Figures 3, references 16.

UDC 551.465.41

PREDICTION OF WATER TEMPERATURE IN OCEAN

[Article by Kalatskiy, V. I. and Nesterov, Ye. S.]

[Text] A statistical method is proposed for taking into account the advection of heat by currents in hydrothermodynamic models of thermal structure of the ocean. The influence of advection is characterized by the error in computing water temperature in a two-layer model without advection. It is shown that the maximum errors are concentrated in zones of strong currents and are stable in time. This served as a basis for developing the proposed method. The use of this method in forecasts of the mean monthly distribution of water temperature in the North Atlantic made it possible to increase the guaranteed probability of forecasts by 5-10%. Figures 1, tables 1, references 3.

UDC 551.465.62

POSSIBILITY OF DETECTING FRONTAL ZONES USING DATA ON SURFACE WATER TEMPERATURE FROM COMMERCIAL AND FISHING VESSELS

[Article by Getman, I. F.]

[Text] On the basis of an analysis of five-day maps of surface water temperature in the northern part of the Atlantic Ocean it is shown that it is possible to detect frontal zones. An evaluation of the observation errors is made. The number of errors is 4% of the number of observations. References 5.

UDC 551.526.6

EVALUATION OF 'THERMAL INERTIA' AND USE OF SHIPBOARD OBSERVATIONS OF OCEAN WATER TEMPERATURE

[Article by Gavrilyuk, R. V.]

[Text] The fields of water temperature anomalies, given at nine points in the North Atlantic, are represented in the form of series of expansion in natural components. For an evaluation of the thermal inertia of the fields of water temperature anomalies the author finds the correlation of each preceding monthly value of the expansion coefficient with its value after two, three and four months. It

is shown that there is a possibility for predicting water temperature for 3-4 months in advance. For a more complete representation of the fields of water temperature in the North Atlantic the author also gives an analysis of maps of the mean monthly water temperature values, averaged by 5° grid squares. Rather high values of the correlation coefficients between the series of observations made on the weather ship and the series of observations in the square corresponding to the site of the ship (excepts for weather ships A and B) indicated the possibility of supplementing the weather ship data with series of observations in 5° squares. Tables 5, references 3.

UDC 551.521

COMPUTING THE INFLUX OF SOLAR HEAT AT THE SEA SURFACE

[Article by Krasyuk, V. S.]

[Text] Formulas are proposed making it possible to compute the diurnal values of the influx of total solar radiation on the water surface of the oceans on the basis of cloud cover data, taking into account the coefficient of atmospheric transparency, dependent on geographical latitude. A computation nomogram, constructed using the derived formulas, is presented. Figures 1, references 4.

UDC 551.461.25

EXPERIENCE IN USING A HYDRODYNAMIC MODEL FOR COMPUTING SURGES IN THE NORTHERN CASPIAN

[Article by Getman, I. F.]

[Text] The computations are based on a numerical solution of hydrodynamic equations for shallow water by the fractional intervals method. A peculiarity of this approach is the stipulation of the condition of an invariable level at the water boundary between the Northern and Middle Caspian. Computations of the catastrophic surge in the northwestern part of the Northern Caspian in 1952 are presented. Nomograms are constructed for computing surge level changes as a function of the velocity, direction and duration of the wind for several points in the Northern Caspian. The nomograms were checked using a 34-year series of observations. The ratio of the mean square error to the standard deviation from the mean was equal to 0.614 and 0.648 for the different surges, which is satisfactory for the used series of observations. Figures 2, tables 1, references 6.

UDC 551.465

TYPHOON EFFECT ON VERTICAL STRUCTURE OF OCEAN WATERS (MATERIALS FROM THE 'TAYFUN-75' EXPEDITION)

[Article by Makarov, Sergey]

[Text] On the basis of materials from the "Tayfun-75" experiment, carried out in July-October 1975 in the northwestern part of the Pacific Ocean, the author analyzes the fields of hydrometeorological and hydrophysical characteristics before

and after the passage of a typhoon. On the basis of a classification of vertical water temperatures it was possible to detect two oceanic formations with horizontal dimensions of some hundreds of miles. It is noted that the trajectory of movement of the typhoon coincided with the zone of separation of the mentioned formations. An explanation is given for the two-level nature of the distribution of hydrometeorological and hydrophysical characteristics in the polygon after the passage of a typhoon. Figures 2, tables 1, references 5.

UDC 551.464.3

ORIGIN OF THE SUBSURFACE SALINITY MAXIMUM IN THE NORTH ATLANTIC

[Article by Chernyavskiy, Ye. B. and Kutalo, A A.]

[Text] A study was made of the degree of correspondence of the localization of waters of maximum salinity in the North Atlantic to the extrema in the fields of wind and evaporation-precipitation difference. An evaluation is made of the relative roles of sources of advective and local origin of the subsurface salinity maximum in the Sargasso Sea. It was possible to define regions of advective origin of the subsurface salinity maximum and the regions of its local formation due to convection during evaporation without disruption of the above-lying waters ("convective puncture" mechanism). Use was made of survey materials from the 23d voyage of the scientific research weather ship "Passat" (300 hydrological stations). Figures 3, references 11.

UDC 551.465.41(520)

SOME RESULTS OF COMPUTATION OF CIRCULATION OF WATERS IN WORLD OCEAN IN 1° GRID

[Article by Sarkisyan, A. S., Demin, Yu. L., Dzhioyev, T. Z. and Brekhovskikh, A. L.]

[Text] The article gives some results of diagnostic computations of currents in the world ocean (that is, computations made from the observed density and wind fields) for the summer season. The computations were made in a 1° grid at 31 depth horizons. The basis for the computations was the fields of mean long-term temperature and salinity values obtained by Princeton University (United States). The computations were made on the basis of the A. S. Sarkisyan quasigeostrophic model. The equatorial boundary layer was smoothed in the following way. First, use was made of the procedure of continuous calculations across the equator, and second, the assumption was made that φ = const = 2.5° in the zone from 2.5°N-2.5°S. The results quite precisely reflect the principal peculiarities inherent in circulation of the waters of the world ocean during summer. This pertains especially to regions of strong jet currents, for which rather high velocity values were obtained. References 3.

UDC 551.465.41(520)

NUMERICAL INVESTIGATION OF CIRCULATION OF WATERS IN ANTILLES-GUIANA COUNTERCURRENT REGION

[Article by Dzhioyev, T. Z.]

[Text] The author gives the results of computations of currents in the region of the Antilles-Guiana Countercurrent on the basis of data on density and atmospheric pressure at sea level by means of use of a level surface and the total flows function. The equations for the level surface and the total flows function are solved by the directed differences method with use of a Gauss-Seidel iteration process. Specific computations were made for the ocean area 15-30°N, 60-80°W using a BESM-6 electronic computer. The horizontal interval of the grid region used was 0.5°; the vertical interval was nonuniform. The number of computation horizons was 10. The article gives a comparative characterization of the results obtained by the two methods. The results of the computations are represented in the form of maps of topography of the level surface and charts of the velocity vectors at the 50-m horizon. Figures 2, references 2.

UDC 551.466.2

COMPUTATION OF SPECTRAL CHARACTERISTICS OF WAVE FIELDS OVER GREAT AREAS OF NORTH ATLANTIC

[Article by Pokhil, A. E.]

[Text] A study was made of the possibility of use of the spectral theory of waves for developing a practical method for predicting wave fields. The wave parameters are computed by a method based on solution of the balance equation for wave energy written in spectral form. The optimum computation conditions are found for precomputation of large fields. The possibility of using a BESM-6 computer for computing waves over an ocean area up to $20 \cdot 10^6$ km^2 with an error not exceeding 20% was demonstrated. A nomogram is given which can be used in computing the time expenditure on a BESM-6 computer when computing wave fields of any extent in computation periods of any duration. The author estimates the computation errors for different spatial and temporal computation intervals. Figures 2, tables 2, references 6.

UDC 551.466.2

SWELL WAVES IN NORTH SEA

[Article by Sett, L. S. and Sirotov, K. M.]

[Text] For the first time for the North Sea it was possible to classify the wind fields, compute the fields of wind waves and swell for typical conditions of their generation and give the values of the parameters of wind waves and swell for each type of field. The errors in the computation method employed decrease with an

increase in wave height and increase with an increase in the advance time of the computations. For wave heights of 2.5-5 m and for an advance time of 24 hours the computation errors do not exceed 15-18%. Figures 1, tables 1, references 4.

UDC 551.467.3

LONG-RANGE FORECAST OF RATE OF WATER COOLING TO FREEZING TEMPERATURE IN THE BARENTS, WHITE AND BALTIC SEAS

[Article by Sheremetevskaya, O. I.]

[Text] A long-range forecast of the times of first appearance of ice in the Barents, White and Baltic Seas is prepared on the basis of a forecast of the rate of water cooling, taking into account the initial temperature and the freezing point. The mean rates of water cooling during the autumn for the years 1944-1976 were computed. The cooling rate field is represented analytically by expansion into a series in natural components. The forecast of the cooling rate field is prepared taking into account atmospheric circulation, water temperature in the Atlantic and position of the high-altitude frontal zone. Figures 1, tables 2, references 11.

UDC 551.467.3

USE OF ENTROPIC EXPRESSION FOR EVALUATING RELIABILITY OF PREDICTORS OF PROGNOSTIC EQUATIONS

[Article by Kutsuruba, A. I.]

[Text] A study is made of the possibility of using one of the concepts of information theory, an entropic expression, as a criterion for choosing predictors in writing new prognostic expressions. The entropic expression is a measure of the information which is acquired when allowance is made for the argumentative factor. Entropic expressions are found for the predictors entering into equations employed in predicting the clearing of ice from the Sea of Azov, Black and White Seas (for a number of years -- from 1945 through 1979). Preliminary conclusions are drawn concerning the reliability of these predictors on the basis of a comparison of the determined values of the entropic expression. Tables 1, references 8.

UDC 551.467.03

EXPERIMENT IN ALLOWING FOR ASTRONOMICAL AND GEOPHYSICAL DATA IN LONG-RANGE PREDICTION OF ICE CONDITIONS IN BALTIC SEA

[Article by Nikolayev, S. G.]

[Text] Long-range (3 and 7 months in advance) prediction of position of the edge of floating ice at the times of maximum development of the ice cover in the Baltic Sea was carried out with allowance for the cosmic and geophysical background. The prediction errors along the "Leningrad-ice edge" track did not exceed 67 miles with an admissible error of ±90 miles. Figures 1, tables 1, references 7.

5303
CSO: 1865/77

UDC 551.465.41

MODEL OF NONSTATIONARY TURBULENT HEAT AND MASS EXCHANGE IN FLUID WITH HIGHLY STABLE STRATIFICATION

Moscow IZVESTIYA AKADEMII NAUK SSSR: FIZIKA ATMOSFERY I OKEANA in Russian Vol 18, No 3, Mar 82 (manuscript received 28 Apr 81) pp 262-268

[Article by G. I. Barenblatt, Institute of Oceanology, USSR Academy of Sciences]

[Text]

Abstract: A two-phase model of nonstationary turbulent heat and mass exchange in a highly stable stratified fluid is proposed. The fluid is represented in the form of a set of two mutually penetrating phases: turbulent spots and laminar layers. Two temperature fields are accordingly introduced. The heat and mass balances are determined separately by phases. The exchange of heat and matter between phases is taken into account. The proposed model is applied to the temperature field and concentration in the upper thermocline of the ocean. It is shown that the model explains, in particular, the development of a temperature jump between the upper quasihomogeneous layer and the thermocline.

1. Introduction. The main characteristic of turbulence under conditions of a highly stable stratification is that it does not affect fluid universally. Under such conditions turbulence is concentrated in sharply defined disklike spots separated by relatively thin layers in which movement is laminar and transpires in conformity to the molecular mechanism. Such an "insular" structure of turbulence, to use the graphic expression of A. V. Gaponov-Grekhov, governs the indicative characteristics of the process of nonstationary turbulent heat and mass exchange in a highly stable stratified fluid.

The two-phase model of this process proposed in this article in general is as follows. The fluid is represented in the form of a set of two mutually penetrating phases: turbulent spots and laminar layers. At each point we therefore introduce into consideration two temperatures (and (or) concentrations) -- temperature of spots T_s and temperature of layers (interlayers) T_i. The temperature fields of the spots T_s and layers T_i constitute the result of interpolation of the temperature

field separately for spots and layers. The exchange of heat (or matter) between phases, that is, between spots and layers, is taken into account. The balance of heat (matter) is determined separately by phases, that is, for spots and layers. Here it is taken into account that the spots are isolated from one another and that the relative volume of the layers is small. With the assumptions made the very same equation is derived. It differs from the usual thermal conductivity equation, but at the limit, for slow processes, undergoes transition into the ordinary thermal conductivity equation.

The proposed two-phase scheme is tested in a model of the seasonal thermocline of the ocean in the form of a traveling thermal (diffusional) wave in front of the submerging lower boundary of the upper quasihomogeneous layer. It appears that this scheme cannot explain, in particular, the development of a temperature jump between the quasihomogeneous layer and the thermocline with rapid subsidence of the lower boundary of the upper quasihomogeneous layer.

2. Physical representations of the model and fundamental equations. A characteristic property of turbulence under conditions of a highly stable stratification is its high degree of intermittence, spottiness [1-3]. Within the spots the transport of heat and (or) matter is accomplished by turbulence and therefore the conductivity in spots is much greater than the conductivity in the layers and the temperature (concentration) gradient within individual spots can be neglected. Then, as indicated by the in situ measurements of Woods [1] and others, as well as indirect evaluations, the relative volume of the laminar layers between spots is small; it is about 1/100. The spots have the form of greatly flattened disks (the ratio of height to diameter for the most part is of the order of 10^{-2} or less), which has a theoretical validation [4]. We will discuss further the matters of temperature and heat exchange, bearing in mind that everything stated is automatically applicable to the concentration and mass exchange of diffusing matter.

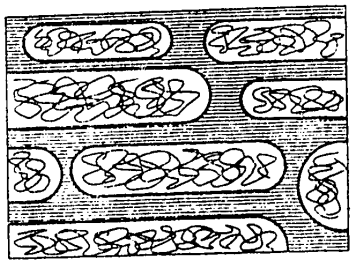

Fig. 1. Two-phase model of turbulence in case of highly stable stratification.

In accordance with what has been stated above, we will represent the model of a turbulent fluid under conditions of its highly stable stratification in the form of "brickwork" (Fig. 1): turbulent spots having the form of highly flattened disks or "bricks," separated by "cement," relatively thin laminar layers. We will introduce two temperature fields into consideration: temperature T_s of spots and temperature of layers T_i, by these notations meaning the temperature fields interpolated and smoothed in space separately for spots and layers. Thus, the turbulent fluid under conditions of a highly stable stratification is represented in the form of a set of two mutually penetrating continuous media: turbulent spots and laminar layers.

We will write the heat balance equations separately for turbulent spots and laminar layers. The turbulent spots are isolated from one another and within the spots the temperature gradient is small. Accordingly, in the heat balance equation for the spots there is no heat transfer by thermal conductivity and the rate of change in the heat content in the spots in a unit volume of fluid $\partial_t scT_s$ is equal to the rate of heat loss from the spots to the layers in this volume -q:

$$\partial_t scT_* = -q. \tag{2.1}$$

Here s is the relative volume of the spots, c is the heat capacity of the fluid, t is time, q is the quantity of heat flowing from the spots to the layers in a unit volume in a unit time.

On the assumption that the fields of both temperatures are horizontally uniform and change only with time t and in depth z, we obtain an equation for the heat balance in laminar layers

$$\partial_t (1-s) cT_l = k_{eff} \partial_{zz}^2 T_l + q, \tag{2.2}$$

where k_{eff} is the effective thermal conductivity coefficient in the medium of the laminar layers; its determination will be discussed below.

We note that the parameter (1 - s) -- the relative volume of the laminar layers -- is small. The $\partial_t cT_l$ parameter has the same order of magnitude as the parameter $\partial_t cT_s$, which, in accordance with (2.1) is close to q since s is close to unity. Accordingly, the rate of change of the heat content in the layers -- the left-hand side of equation (2.2) -- is small in comparison with the intensity of heat flow q entering into the right-hand side and equation (2.2) can be simplified:

$$k_{eff} \partial_{zz}^2 T_l + q = 0. \tag{2.3}$$

Finally, it is natural to assume that the intensity of heat flow q between the phases is proportional to the temperature difference of the spots and layers:

$$q = A(T_* - T_l). \tag{2.4}$$

Here A is a proportionality factor constant for a particular fluid and a particular turbulence field in it, whose determination will also be examined below. Expressions (2.1), (2.3), (2.4) make it possible to derive a closed system of equations for the temperatures T_s and T_l. With the simplest assumption concerning constancy of the relative volume of turbulent spots this system has the form

$$\partial_t T_* + (T_* - T_l)/\tau = 0, \tag{2.5}$$

$$\varkappa \partial_{zz}^2 T_l + (T_* - T_l)/\tau = 0. \tag{2.6}$$

Excluding, we obtain one and the same equation for both temperatures T_s and T_l:

$$\partial_t T_s = \varkappa \partial^2_{zz} T_s + \eta \partial^3_{tzz} T_s;$$

$$\partial_t T_l = \varkappa \partial^2_{zz} T_l + \eta \partial^3_{tzz} T_l. \tag{2.7}$$

The coefficients in equations (2.5)-(2.7) are determined in the following way:

$$\varkappa = k_{ett}/cs, \quad \tau = cs/A, \quad \eta = \varkappa\tau. \tag{2.8}$$

Thus, $\varkappa$ is some compound thermal diffusivity coefficient corresponding to the effective thermal conductivity of the layers but the heat capacity of the spots. Then τ is the characteristic time of thermal relaxation of the spots. The new coefficient η obviously has the dimensionality of area. Equations of the type (2.5)-(2.7) were examined earlier in relation to other physical problems [5-7].

It can be seen that equation (2.7), which satisfies both temperature fields, differs from the ordinary thermal conductivity equation. We introduce the characteristic time of the process τ_0 and the corresponding characteristic spatial scale $L = (\varkappa\tau_0)^{1/2}$ and we will proceed to dimensionless independent variables

$$\vartheta = t/\tau_0, \quad \zeta = z/L, \tag{2.9}$$

then equations (2.7) will assume the form

$$\partial_\vartheta T_s = \partial^2_{\zeta\zeta} T_s + (\tau/\tau_0)\partial^3_{\vartheta\zeta\zeta} T_s,$$

$$\partial_\vartheta T_l = \partial^2_{\zeta\zeta} T_l + (\tau/\tau_0)\partial^3_{\vartheta\zeta\zeta} T_l. \tag{2.10}$$

If we examine a slow heat exchange process for which the characteristic time τ_0 is much greater than the characteristic time of the thermal relaxation of spots τ, then the parameter τ/τ_0, entering into equations (2.10), is small and these equations are transformed to an ordinary thermal conductivity equation. Thus, a qualitative difference in turbulent thermal conductivity under conditions of a strong stable stratification from ordinary thermal conductivity must be expected for essentially nonstationary processes, whose characteristic time is comparable to the time of thermal relaxation of the spots.

3. Boundary and initial conditions. The formulation of boundary-value problems for system (2.5), (2.6) is characterized by a definite singularity because this system is degenerate: the derivative $\partial_t T_l$ is absent in it. Now we will return to the unsimplified equation (2.2) in which this derivative has been retained and we will write the full system in the form

$$\partial_t T_s = -(T_s - T_l)/\tau, \quad \varepsilon\partial_t T_l = \varkappa\partial^2_{zz} T_l + (T_s - T_l)/\tau. \tag{3.1}$$

Here $\varepsilon = (1 - s)/s$ is a small parameter. For system (3.1) it is already necessary to stipulate two initial conditions -- for T_s and for T_l. We introduce the "fast" time $\theta = t/\varepsilon$. System (3.1) is rewritten in the form

$$\partial_\theta T_s = -\varepsilon(T_s - T_l)/\tau, \quad \partial_\theta T_l = \eta\partial^2_{zz} T_l + (T_s - T_l). \tag{3.2}$$

We will take $t_1 > 0$ as small as desired. Then with $\varepsilon \to 0$ the value $\theta_1 = t_1/\varepsilon$ tends to infinity. According to the first equation (3.2), $\partial_\theta T_s \to 0$, so that T_s remains unchanged whereas T_1 instantaneously at ordinary time scales t tends to solution of the equation

$$\eta \partial_{zz}^2 T_l + (T_s - T_l) = 0 \tag{3.3}$$

with corresponding boundary conditions. Thus, with $\varepsilon \to 0$, that is, for a degenerate system, it is possible to stipulate arbitrarily only the function $T_s(z, 0)$ -- the initial distribution of temperature in the spots. The initial temperature distribution in the layers T (z,0) is obtained as a solution of the equation

$$\eta \partial_{zz}^2 T_l(z,0) - T_l(z,0) = -T_s(z,0). \tag{3.4}$$

The solution of equation (3.4) is obviously represented in the form

$$T_l(z,0) = C_1 e^{-z/\sqrt{\eta}} + C_2 e^{z/\sqrt{\eta}} + \frac{1}{\sqrt{\eta}} \int_0^z T_s(\xi, 0) \operatorname{sh}\left(\frac{z-\xi}{\sqrt{\eta}}\right) d\xi. \tag{3.5}$$

The function $T_l(z, 0)$ is continuous with its first two derivatives. Accordingly, the constants C_1, C_2 are determined from the boundary conditions (with t = 0, if the boundary conditions are dependent on time). On the other hand, the function $T_s(\xi, 0)$ can be discontinuous and have discontinuities of the derivative $\partial_z T_s$ $(\xi, 0)$. Taking into account the order of the singularity of equation (2.7) and using the known technique of generalized solutions of linear equations with partial derivatives (see [8]), we can obtain

$$[T_s] = [T_s]_{t=0} \exp(-t/\tau), \quad [\partial_z T_s] = [\partial_z T_s]_{t=0} \exp(-t/\tau). \tag{3.6}$$

Here $[\varphi]$ is the discontinuity of some φ value at the point z at the time t: $[\varphi] = \varphi(z + 0, t) - \varphi(z - 0, t)$, and $[\varphi]_{t=0}$ is the same discontinuity at the same point with t = 0: $[\varphi]_{t=0} = \varphi(z + 0,0) - \varphi(z - 0,0)$. Thus, in contrast to solution of the classical thermal conductivity equation, the temperature jumps in the spots, satisfying equation (2.7) and its depth derivative, do not disappear instantaneously but attenuate exponentially.

4. A traveling thermal wave is a model of the upper thermocline in the ocean. The authors of [9, 10] independently proposed a model of the upper thermocline in the form of a traveling thermal wave. On the assumption that the exchange processes transpiring in the upper thermocline are stationary, uniform and microscale, for the distribution of excess temperature $\theta(z, t)$ we obtain the ordinary thermal conductivity equation

$$\partial_t \theta = \varkappa \partial_{zz}^2 \theta, \tag{4.1}$$

where the excess temperature is the difference between the temperature and the mean temperature for the year. The solution of equation (4.1), of the traveling wave type, has the form $\theta = \theta(\xi)$, $\xi = z - ut - h_0$. Here u is the rate of subsidence of the lower boundary of the upper quasihomogeneous layer of the upper boundary of the thermocline -- a slowly changing function of time, h_0 is the depth of

the upper quasihomogeneous layer at some arbitrary moment in time t = 0. Satisfying the conditions $\theta(0) = \theta_0$, $\theta(\infty) = 0$, where θ_0 is the excess temperature at the upper boundary of the thermocline (a slowly changing function of time), we obtain a solution of the traveling wave type

$$\Theta=\Theta_0 \exp(-u\xi/\varkappa). \tag{4.2}$$

This model agrees well with data from laboratory measurements and also in situ observations, averaged over an adequately great time interval, about 10 days. The heat exchange processes in the upper thermocline under highly nonstationary conditions, in accordance with the above, must be described by system (2.5), (2.6). In particular, the temperature of the spots is described by equation (2.7); this same equation is correct for the excess temperature in the spots:

$$\partial_t\Theta_*=\varkappa\partial^2_{zz}\Theta_*+\eta\partial^3_{zzz}\Theta_*. \tag{4.3}$$

We will examine the solution of equation (4.3), of the traveling wave type $\theta_s = \theta_s(\xi)$, $\xi = z - ut - h_0$. Substituting this expression into (4.3), integrating once and using the boundary condition with $\xi = \infty$, we obtain

$$u\eta\frac{d^2\Theta_*}{d\xi^2}-\varkappa\frac{d\Theta_*}{d\xi}-u\Theta_*=0. \tag{4.4}$$

With $\xi > 0$ the solution of equation (4.4) evidently has the form

$$\Theta_*=\Theta_1 \exp(-\alpha\xi), \quad \alpha=[(\varkappa^2+4u^2\eta)^{1/2}-\varkappa]/2u\eta. \tag{4.5}$$

However, the constant θ_1 no longer can be determined from the continuity condition with $\xi = 0$ since the temperature in the spots must not be a continuous function of the z-coordinate. On the other hand, the temperature in the layers is a continuous function of the coordinate, so that $\theta_l(0) = \theta_0$, where θ_0 is the excess temperature of the upper quasihomogeneous layer. We will take the first equation of system (2.5), retaining validity for excess temperatures:

$$\partial_t\Theta_*=-(\Theta_*-\Theta_l)/\tau. \tag{4.6}$$

Substituting into this equation $\theta_s = \theta_s(\xi)$, $\theta_l = \theta_l(\xi)$, we have

$$-ud\Theta_*/d\xi=-(\Theta_*-\Theta_l)/\tau. \tag{4.7}$$

Using (4.5) and assuming $\xi = +0$, we obtain

$$u\alpha\Theta_1=-(\Theta_1-\Theta_0)/\tau, \tag{4.8}$$

hence we find the excess temperature in the spots at the upper boundary of the thermocline:

$$\Theta_1=\frac{\Theta_0}{1+u\tau\alpha}=\frac{2\varkappa\Theta_0}{[(\varkappa^2+4u^2\eta)^{1/2}+\varkappa]}=\frac{2\Theta_0}{1+(1+\beta)^{1/2}}, \tag{4.9}$$

$$\beta=4u^2\eta/\varkappa^2=4u^2\tau/\varkappa. \tag{4.10}$$

Thus, with not very small β the θ_1 value is not equal to θ_0, so that the excess temperature of the spots at the upper boundary of the thermocline is not equal to the excess temperature of the quasihomogeneous layer: there is a finite temperature jump (Fig. 2). This circumstance also explains why the in situ measurements with low-inertia instruments sometimes reveal an appreciable temperature jump. In actuality, it is the temperature of the spots which is for the most part measured. In the case of relatively large instantaneous u the β parameter can have an appreciable value. On the other hand, the rates of subsidence, averaged over a long time interval, are small; the parameter β is small and in a comparison with data from averaged measurements the jump should not appear. We note that a different explanation of the nature of the jump was given in a study by G. I. Shapiro [12].

5. Some evaluations. Summary. We will begin with evaluations of the coefficient k_{eff}. Layers having the molecular thermal conductivity k_{mol} and the relative volume 1 - s are separated by turbulent spots having the relative volume s and the thermal conductivity k_{turb}. Since the temperature gradient in the spots is neglected, the temperature drop in a layer of a unit thickness is created by the thermal resistance of layers with the relative thickness 1 - s and we obtain

$$k_{eff}=k_{mol}/(1-s), \tag{5.1}$$

so that in order of magnitude $k_{eff}\sim 10^2 k_{mol}$. Then for the characteristic time of thermal relaxation of spots τ we have, obviously

$$\tau\sim l^2/\varkappa_s. \tag{5.2}$$

Here l is the mean thickness of a turbulent spot for a particular flow, $\varkappa_s$ is the effective coefficient of turbulent thermal diffusivity in the spot. Bearing in mind that turbulence is not strongly developed in the spots, for $\varkappa$ it is possible to use an estimate in rather wide limits $\varkappa_s\sim 10^{-1}$-10 cm^2/sec. The thicknesses of the turbulent spots also vary in a wide range: from ten to several hundreds of centimeters Therefore, if for the $\varkappa$ coefficient we obtain a relatively stable estimate of $\varkappa\sim 10^{-1}$ cm^2/sec, the characteristic time for thermal relaxation of the spots varies in a wide range: from 10 to 10^5 sec. Depending on the τ value, prevailing under the conditions of this flow and the characteristic time of the heat exchange process, the effects considered in this study may be both significant or insignificant. In particular, depending on τ the rate of subsidence u of the quasihomogeneous layer at which the effects considered here will be significant is

$$u\sim(\varkappa/\tau)^{1/2}\sim 10^{-1}\div 10^{-3}\ \ cm/sec,$$

which falls in the region of real rates of subsidence.

There do not seem to be fundamental difficulties in taking horizontal inhomogeneity, the variability of the relative volume of spots, etc. into account in the described scheme. However, despite all the importance of these circumstances for practical computations, allowance for them does not change the qualitative picture of the phenomenon.

Since the coefficients of molecular thermal diffusivity and diffusion for sea water differ by two orders of magnitude, the rate of subsidence u of the quasihomogeneous layer at which the effects considered above become significant is an order of

magnitude less for the halocline than for the thermocline. Accordingly, it is entirely possible to observe salinity jumps in the absence of temperature jumps.

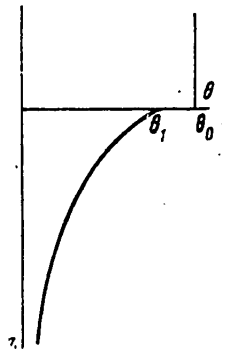

Fig. 2. With high rates of subsidence of the upper boundary of the thermocline the temperature experiences a discontinuity.

Under definite conditions the relative volume of the layers may not be small and therefore it is quite impossible to neglect the rate of change in heat content in the layers in system (3.1) and the equation for temperature in the spots assumes the form

$$\frac{1-s}{s}\tau\partial_{tt}^2 T_* + \frac{1}{s}\partial_t T_* = \varkappa\partial_{zz}^2 T_* + \eta\partial_{zzz} T_*. \qquad (5.3)$$

A similar equation is derived in this case for the temperature of the layers.

BIBLIOGRAPHY

1. Woods, J., "Wave-Induced Shear Instability in the Summer Thermocline," J. FLUID MECH., Vol 32, Pt 4, pp 791-800, 1968.

2. Monin, A. S., Kamenkovich, V. M. and Kort, V. G., IZMENCHIVOST' MIROVOGO OKEANA (Variability of the World Ocean), Leningrad, Gidrometeoizdat, 1974, 262 pages.

3. Monin, A. S. and Ozmidov, R. V., OKEANSKAYA TURBULENTNOST' (Ocean Turbulence), Leningrad, Gidrometeoizdat, 1981, 320 pages.

4. Barenblatt, G. I., "Dynamics of Turbulent Spots and Intrusions in a Stably Stratified Fluid," IZV. AN SSSR: FAO (News of the USSR Academy of Sciences: Physics of the Atmosphere and Ocean), Vol 14, No 2, pp 195-206, 1978.

5. Barenblatt, G. I., Zheltov, Yu. P. and Kochina, I. N., "Main Representations of the Theory of Filtering of Homogeneous Fluids in Fissured Rocks," PMM (Applied Mathematics and Mechanics), Vol 24, No 5, pp 852-864, 1960.

6. Barenblatt, G. I., "Some Boundary-Value Problems for the Equations for Filtration of a Fluid in Fissured Rocks," PMM, Vol 27, No 2, pp 348-350, 1963.

7. Nemchinov, I. V., "Some Nonstationary Problems in Heat Transfer by Radiation," PMTF (Applied Mechanics and Theoretical Physics), No 1, pp 36-57, 1960.

8. Gel'fand, I. M. and Shilov, G. Ye., OBOBSHCHENNYYE FUNKTSII I DEYSTVIYA NAD NIMI (Generalized Functions and Operations With Them), Moscow-Leningrad, Fizmatgiz, 1958, 440 pages.

9. Barenblatt, G. I., "Self-Similarity of Distributions of Temperature and Salinity in the Upper Thermocline," IZV. AN SSSR: FAO, Vol 14, No 11, pp 1160-1166, 1978.

10. Turner, J. S., "The Temperature Profile Below the Surface Mixed Layer," OCEAN MODELLING, No 1, pp 6-8, 1978.

11. Efimov, S. S. and Tsarenko, V. I., "On the Problem of Self-Similarity of the Temperature Distribution in the Upper Thermocline," IZV. AN SSSR: FAO, Vol 16, pp 620-627, 1980.

12. Shapiro, G. I., "Influence of Fluctuations in the Layer of Turbulent Entrainment on Heat and Mass Exchange in the Upper Thermocline," IZV. AN SSSR: FAO, Vol 16, No 4, pp 433-435, 1980.

5303
CSO: 1865/134

EXPERIMENT IN MACHINE PROCESSING OF SATELLITE OCEANOLOGICAL INFORMATION

Leningrad UCHENYYE ZAPISKI LGU, SERIYA GEOGRAFICHESKIKH NAUK: SPUTNIKOVAYA OKEANOLOGIYA, CHAST' 2 in Russian No 27(403), 1980 (signed to press 16 Apr 80) pp 118-119

[Article by V. V. Vinogradov, I. V. Likhachev and D. K. Staritsyn]

[Text] The article examines the results of processing of satellite infrared information obtained from artificial earth satellites in a direct transmission regime. In the processing use was made of data from "NOAA-2" artificial earth satellites during their flight over the polygon of the international tropical experiment GATE-74.

The results of the processing are presented in the form of profiles and temperature maps of the ocean. We compared the results of processing of artificial earth satellite data with synchronous data from radiation measurements from an IL-18 aircraft of the Main Geophysical Observatory imeni A. I. Voyeykov and subsatellite measurements from scientific research ships in the GATE-74 polygon. Aboard the aircraft and on the scientific research ship "Akademik Korolev" synchronous measurements were made using identical apparatus: IR radiometers in the spectral range 9-12 μm.

Maps of radiation temperature were obtained which have a greater information content than the mean long-term maps.

The temperature of the ocean surface is one of the principal physical characteristics determining the intensity of dynamic processes in the ocean and exerting an influence on formation of atmospheric circulation.

It is entirely obvious that there is a need for obtaining mass operational data concerning the surface of the world ocean in order to meet a whole series of needs and requirements on the part of the national economy and science. In connection with the development of new technical means for the noncontact measurement of thermal radiation in the IR spectral region it is now possible to obtain data on the temperature of the water surface from artificial earth satellites. From each quasipolar orbit, depending on the flight altitude and technical specifications of the vehicle, the artificial satellite scans a part of the ocean with a total breadth up to 3000 km [I. P. Velov, 1967; K. Ya. Kondrat'yev and Yu. M. Timofeyev, 1970; U. Bandin, 1975].

Since in a direct transmission regime an artificial earth satellite gives higher-quality information, it was received in the ocean under conditions of an insignificant cloud cover aboard the scientific research ship "Akademik Korolev." outfitted for this purpose with special receiving-recording apparatus.

The principal tasks in the reception of temperature data were the checking of the reliability of information and study of the possibility of its use in oceanological practice.

The work, for which about 40 scientific research ships, located in the GATE-74 polygon, were used in a comparison of the measured parameters, was carried out for the first time for oceanological purposes. Such a combination of subsatellite support made possible a better study of the problems related to the tie-in of the collected information, an evaluation of its reliability and planning a measurement method and operational use.

The maps of absolute temperature of the ocean surface were plotted without taking absorption into account on the basis of synchronous reference measurements in the IR range from the scientific research vessel "Akademik Korolev."

In an operational analysis the great volume of satellite information requires the use of high-capacity electronic computers. Experience in the use of digital computers indicated that using electronic computers outfitted with appropriate input-output devices it is possible to solve a wide range of problems related to the collection, registry, transmission and analysis of TV and IR information.

Now we will examine the problems involved in the preparation and input of data obtained from artificial earth satellites using special apparatus -- two-channel scanning radiometers with the information being represented in the form of an analog signal in the memory of an M-222 electronic computer for subsequent analysis -- and constructing maps of temperature distribution in digital form.

The use of two-channel scanning radiometers on "NOAA" artificial earth satellites, operating in the visible and IR spectral regions, on the one hand made it possible to obtain a line image of the earth during both daytime and nighttime, and on the other hand, created the fundamental possibility of representing the information in digital form, its coding and input into an electronic computer.

An individual scanning line for the "NOAA-2" artificial earth satellite begins with a group of synchronizing pulses which can serve as time reference points, this being followed by useful information from the IR radiometer; then comes the calibration step (the step interval corresponds to a change in the observed brightness temperature by 20°K with a temperature interval from 310°K -- black -- to 180°K -- white); the first half of the line is closed with a signal on the total amplitude value (indicator of system operating stability). The second half of the line also begins with a group of synchronizing pulses, followed by useful information in the visible part of the spectrum, "calibration wedge" and total signal (100%) (Fig. 1).

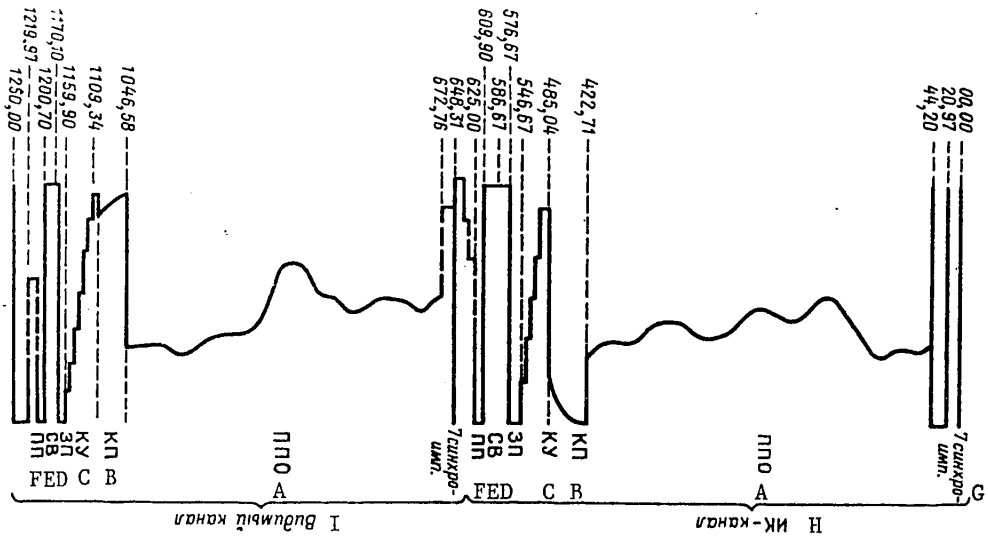

Fig. 1. Positioning of information sectors on scanning line of IR radiometer of United States artificial earth satellite "NOAA-2."

KEY:
- A) Underlying ocean surface
- B) Space
- C) Calibration levels (telemetric window)
- D) Rear area (level 100%)
- E) Reproduction synchronizing pulse (level 4%)
- F) Front area (level 100%)
- G) Synchronizing pulse
- H) IR channel
- I) Visible channel

Information from the IR channel is transmitted with the corresponding synchronization and calibration signals during the time of rotation of the radiometer dish by 180° (0.625 sec). Another kind of information is transmitted during the next 0.625 sec. Such a scanning radiometer makes it possible to scan the earth's surface with a resolution of about 7.4 km at the subsatellite point.

In the experiment, from among the best-quality records on the magnetic tape of the facsimile magnetic recorder we selected the record for 31 August 1974, which was used as the object for detailed and thorough processing.

Automated machine processing of satellite information was divided into two stages:
1) signal detection, filtering and transformation of an analog signal into a binary code;
2) extraction of information from the computer, forming a frame, geographic tie-in and construction of a map of radiation temperatures.

Figure 2 is a block diagram of the system for the input and machine processing of data, consisting of an information source (receiving station or magnetic recorder), analog signal amplifier, signal envelope detector, analog-discrete converter, group of amplifiers-shapers and the input circuits of an M-222 electronic computer. The results of processing of satellite data were fed out to the alphabetical-digital unit.

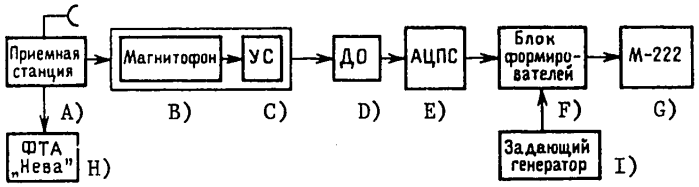

Fig. 2. Block diagram of apparatus for input of telemetric satellite information into electronic computer. Explanation in text.

KEY:

A) Receiving station
B) Magnetic recorder
C) Analog signal amplifier
D) Signal envelope detector
E) Analog-discrete converter
F) Group of amplifiers-shapers
G) M-222 computer
H) "Neva" phototelegraphic apparatus
I) Master oscillator

The analog signal, filled by the carrier frequency arriving from the information source, is amplified by a linear amplifier to the level necessary for creating a normal operating range of the converter (about 10 V), and through the envelope detector, discriminating the envelope of the high-frequency signal, is fed to the input of the analog-discrete converter of the type F-722/2, whose triggering is accomplished by a special oscillator with a frequency 1 KHz. The converter transforms the analog signal into a series of eight-digit binary-decimal numbers. The value of each number is proportional to the level of the input signal at the time of reading. The entire continuous series of discrete readings is fed through the group of shapers to the memory unit of the M-222 electronic computer. The discretization frequency is selected from the condition of a minimum loss of information and is equal to 1000 readings in the entire scanning line.

Machine processing included the selection of the type of information, its normalization, geographic and temperature tie-in of satellite data and output of the results in the form of a matrix, each of whose elements represents the radiation temperature at a particular spatial point.

On the basis of this entire mass of data we constructed a map of radiation temperatures without the averaging of data. The map was constructed by gluing on a blank the numerical values in arbitrary units at a stipulated scale and tie-in of the lines to geographic coordinates. The geographic tie-in was accomplished on the basis of a precise knowledge of the time of beginning and end of the

survey and the precise registry of the time of transit of the artificial earth satellite across the equator. The number of discrete points in the line was selected in such a way as to obtain the least distorted temperatures due to the nadir angle, which at the scale of the photograph was about 1600-2000 km. In order to exclude the influence of cloud cover on temperature we used synchronous photographs of cloud cover obtained using the "Neva" phototelegraphic apparatus.

In constructing the map of radiation temperatures atmospheric absorption was not taken into account since the tie-in to absolute temperature values was accomplished on the basis of shipboard measurements in the IR spectral region; the correction was assumed to be identical for the entire region of coverage by the satellite radiometer.

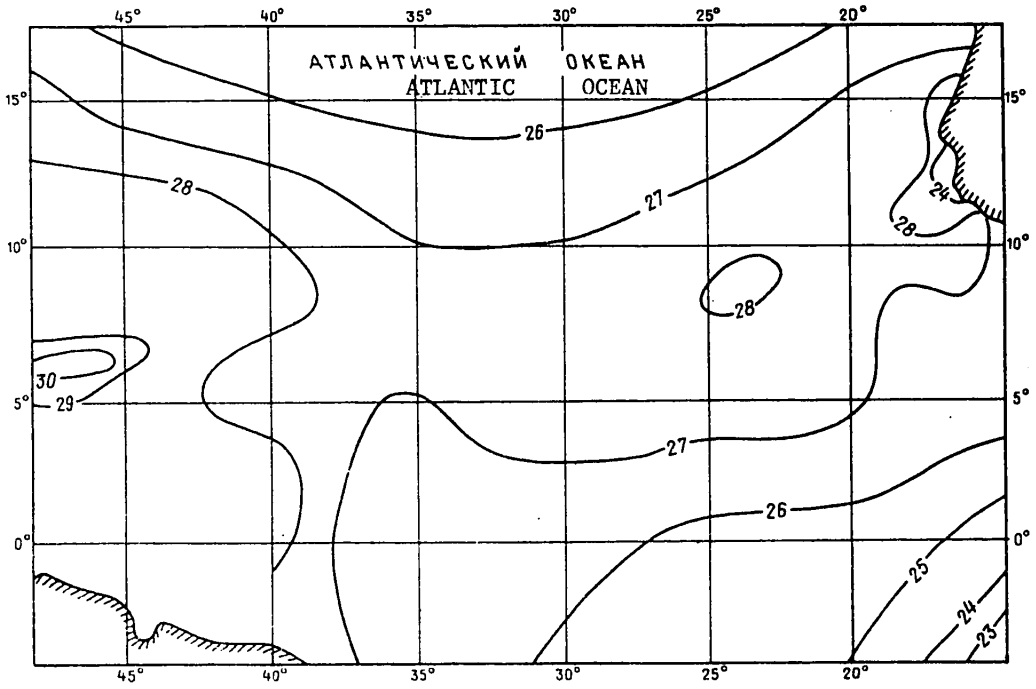

Fig. 3. Temperature of surface of Atlantic Ocean according to data from shipboard measurements on 1 September 1974 in GATE-74 polygon.

This is correct for homogeneous atmospheric conditions. With the presence of different air masses over the studied ocean area the absorption may be nonuniform and accordingly distortions will be introduced into the kinematic maps of temperature of the ocean surface. The effect of influence on the accuracy of measurement by different temperature profiles characteristic for different latitudes is given in a number of studies [W. L. Smith, et al., 1970; G. A.

Maul and M. Sidran, 1973]. Due to the presence of an IR radiometer aboard the ship and synchronous radiation measurements from an IL-18 aircraft it was possible to determine the absorption in the tropical zone of the ocean, equal to 10.5°C.

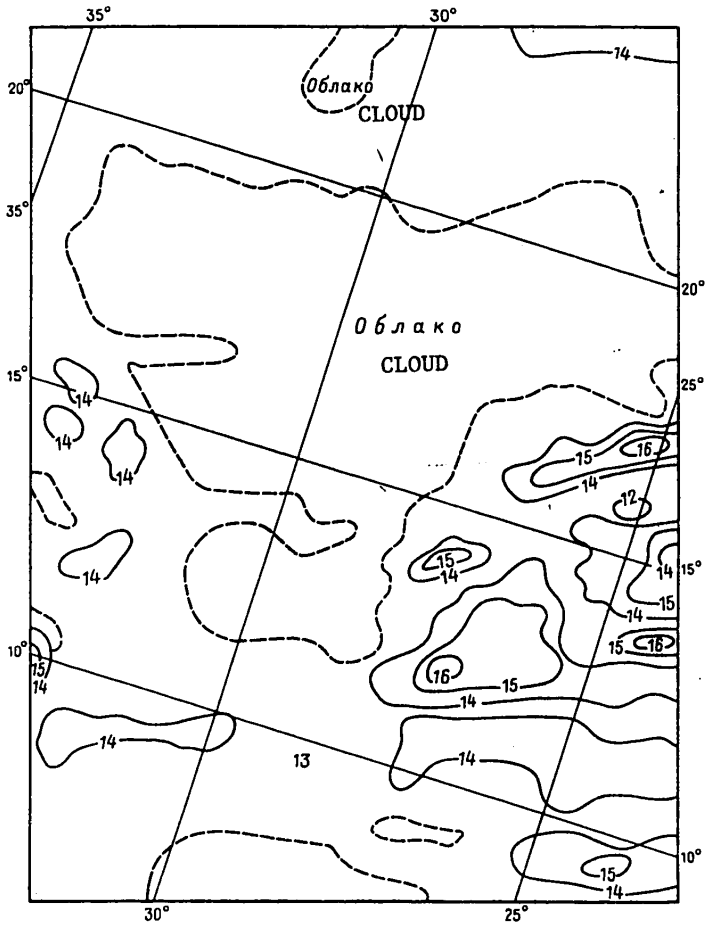

Fig. 4. Map of radiation temperature of ocean surface obtained in a direct transmission regime aboard the scientific research ship "Akademik Korolev" on 31 August 1974.

It should be noted that in regions with a well-developed Trades circulation there is an increased concentration of aerosol of continental origin. For example, the tropical zone of the Atlantic Ocean, in which the scientific research ship "Akademik Korolev" was situated, was subjected to the influence of Trade winds of a northeasterly direction with transport of aerosol of African origin. In accordance with computations and measurements of temperature at altitudes 300 and 6000 m, it was possible to determine the contribution of absorption by aerosol, which was 3.3°C. According to investigations from an IL-18

aircraft-laboratory, in the composition of aerosol particles there was a predominance of metals (Fe, Al, Zn) with a content of aerosol particles $10 \mu g/m^3$.

If it is taken into account that the horizontal temperature gradients of the surface change insignificantly with time, we can make a comparison of data from artificial earth satellites and shipboard observations collected in the polygon GATE-74 during numerous scientific and route investigations.

The experimental region was situated in the tropical zone of the Atlantic Ocean and covered its central and eastern parts where the atmospheric ICZ is situated most frequently.

The principal elements of water circulation in the tropical zone of the Atlantic Ocean at the surface are the North and South Trade Currents, Intertrades Countercurrent, Bengal, Brazilian, Guinea and Antilles Currents. The dynamic activity of these systems to a considerable degree favors the formation of the surface temperature field and horizontal inhomogeneities.

Figure 3 gives the distribution of surface temperature prepared using an objective analysis scheme on the basis of data from shipboard observations for 1 September 1974.

In the region between 6 and 10°N there is a region of high temperatures, the so-called thermal equator. Its axis runs from the southwest to the northeast. The huge region delineated by the isotherm 27°C is occupied by water whose temperature virtually does not change and falls in the range 27-27.5°C.

The horizontal gradients of this zone are exceedingly small. In the southeastern part there is some increase in the horizontal gradients, evidently associated with the existence of an upwelling in the region of the Guinea Current. This is also indicated by a decrease in temperature to 22°C in the southeastern part of the region. The temperature of the water surface in the western part is somewhat higher than the temperature of the eastern part, which is evidently associated with the transport of warm shore waters and the equatorial circulation.

The map of the radiation temperature of the Atlantic Ocean surface is represented in Fig. 4. In a comparison of this map with shipboard observations it can be noted that the temperature field constructed on the basis of data from a space survey differs from the field constructed on the basis of shipboard observations. For example, instead of a well-expressed zonality of isotherms as indicated by shipboard data, the field of radiation temperature has a rather complex configuration, evidently associated with the presence of eddy formations. The complex structure of the temperature field in a region of the ocean with strongly developed convective cloud cover, variable in time and space, creates a nonuniform heating of the upper layers of the ocean. The nonuniform heating occurs due to the screening of direct solar radiation. Prolonged anomalies in the quantity of cloud cover over any part of the ocean make a contribution to the formation of anomalies in the heat content of the upper layer in the ocean in this ocean area. Their values are cited in a study by V. V. Vinogradov and N. I. Radayev [1971].

Nevertheless, together with some differences, it is possible to note the common features in the distribution of temperature. For example, on both maps the maximum temperatures are situated to the north of the equator (tropical equator). To the north and south of the thermal equator the temperatures decrease.

Without question, the temperature maps of great expanses, constructed on the basis of data from shipboard observations, do not in their entirety reflect the complex structure of the temperature field. The lowest information content is in the atlases of mean climatic monthly maps which cannot be used for comparison with satellite measurements; the climatic data can be used only for rough evaluations of the temperature background.

Unfortunately, it is impossible to carry out a more precise checking of the reliability of satellite information since the sole means for this purpose is synchronous flights of an aircraft-laboratory in the region of the polygon. An IL-18 aircraft operated for the most part under an international program for investigating the ICZ and under our program its flights had a purely random character.

As an additional check on the correctness of the spatial distribution of temperature we used the statistical processing of observational data in the IR region obtained from a ship, aircraft and artificial satellite. Since the shipboard observations characterize the temporal variability of thermal processes at one point (the scientific research ship "Akademik Korolev" was situated at a constant point in a polygon with the coordinates 12°N, 23°3'W), as a comparison we used a number of observations for 20 days. This series was selected on the basis of the work of P. M. Saunders (1972) in which it is indicated that for the appearance of characteristic temperature features over a distance up to 100 km a period of 8-16 days is adequate. The computations of the statistical inhomogeneities of surface temperature on the basis of shipboard, aircraft and satellite measurements and employing normalized structural functions indicated a close correspondence (1.5, 2.0, 1.5°C).

At the same time, comparison with data from "Meteor-18" indicated a discrepancy in temperature variability by an order of magnitude, evidence either of gaps in transmission through the radio channel or imperfection in machine processing. The data which we used from the "Meteor-17" artificial earth satellite (with reception of IR information at Moscow), for example, for the GATE-74 polygon, gave rather good results and are entirely comparable with the shipboard observations.

It follows from the materials presented above that for a study of the character of variability of the temperature field on a global scale it is better to employ space methods which can be used for both operational and scientific oceanological purposes. The proposed and applied method for constructing maps indicated the possibility of obtaining oceanological information directly aboard a scientific research ship (weather ship or other ship outfitted with receiving apparatus and an electronic computer), the possibility of constructing maps of temperature of the ocean surface and their use for discriminating zones of well-developed currents and temperature gradients, frontal zones, upwelling of deep waters, eddy formations and other phenomena.

It must be remembered that satellite apparatus with scanning of the water surface receives the radiation of the uppermost (bounding the atmosphere) water layer whose thickness in the optical measurement range is about 0.02 mm.

In connection with the presence of vertical temperature gradients in the water in the layer 0-0.5 m from 0.2 to 3°C the tie-in of the satellite measurements must be accomplished solely on the basis of measurements with an IR radiometer or computed on the basis of the mentioned studies [P. M. Saunders, 1967; E. D. McAlister, W. L. McLeish, 1969; L. Hasse, 1971; C. A. Paulson, T. W. Parker, 1971].

BIBLIOGRAPHY

1. Vetlov, I. P., "Meteorological Observations From Artificial Earth Satellites," METEOROLOGIYA I GIDROLOGIYA (Meteorology and Hydrology), No 4, pp 3-13, 1967.

2. Vinogradov, V. V. and Radayev, N. I., "Some Results of Use of a Noncontact Thermometer for Measuring Surface Temperature Under Shipboard Conditions," KVAZIDVUKHLETNYAYA TSIKLICHNOST' I TSIRKULYATSIYA V ATMOSFERE I OKEANE (Quasi-Two-Year Cyclicity and Circulation in the Atmosphere and Ocean), Leningrad, LGMI, pp 168-178, 1971.

3. Kondrat'yev, K. Ya. and Timofeyev, Yu. M., TERMICHESKOYE ZONDIROVANIYE ATMOSFERY SO SPUTNIKOV (Thermal Sounding of the Atmosphere From Satellites), Leningrad, Gidrometeoizdat, pp 117-172, 1970.

4. Yats, G. and Bandin, U., "Use of Remote Sounding From Artificial Earth Satellites for Meteorological Purposes," TRUDY IN-TA INZHENEROV PO RADIOELEKTRONIKE (Transactions of the Institute of Radioelectronic Engineers), United States, No 12, pp 146-161, 1975.

5. Hasse, L., "The Sea Surface Temperature Deviation and the Heat Flow at the Sea-Air Interface," BOUNDARY-LAYER METEOROL., No 1, pp 368-379, 1971.

6. Maul, G. A. and Sidran, M., "Atmospheric Effects on Ocean Surface Temperature Sensing From NOAA Satellite Scanning Radiometer," J. GEOPHYS. RES., Vol 78, No 19, pp 1909-1916, 1973.

7. McAlister, E. D. and McLeish, W. L., "Heat Transfer in the Top Millimeter of the Ocean," J. GEOPHYS. RES., Vol 74(13), p 3408, 1969.

8. Paulson, C. A. and Parker, T. W., "Cooling of a Water Surface by Evaporation. Radiation and Heat Transfer," J. GEOPHYS. RES., Vol 76, pp 491-495, 1971.

9. Saunders, P. M., "The Temperature at the Ocean-Air Interface," J. ATMOS. SCI., Vol 24, pp 269-273, 1967.

10. Saunders, P. M., "Space-Time Variability of Temperature in the Upper Ocean," DEEP SEA RESEARCH, Vol 19, pp 467-480, 1972.

11. Smith, W. L., Rao, P. K. and Curtis, W. R., "The Determination of Sea Surface Temperature From Satellite High Resolution in Fraud Window Radiation Measurements," MONTHLY WEATHER REVIEW, Vol 98, No 8, 1970.

5303
CSO: 8144/1065

UDC 551.46

COLLECTION OF ARTICLES ON OPTICS OF OCEAN AND ATMOSPHERE

Moscow OPTIKA OKEANA I ATMOSFERY in Russian 1981 (signed to press 19 Aug 81) pp 2, 231

[Annotation and abstracts from collection "Optics of the Ocean and Atmosphere", edited by K. S. Shifrin, doctor of physical and mathematical sciences, Institut okeanologii imeni P. P. Shirshov, Izdatel'stvo "Nauka", 1200 copies, 232 pages]

[Text] Annotation. This collection of articles deals with the most timely problems in oceanic optics: modern concepts concerning the optical properties of sea water; optical methods for investigating the ocean and atmosphere over the ocean, including remote methods (satellite oceanology); also considered are the conditions for the formation of light fields in the ocean, hydrooptical characteristics, etc. The book is intended for physicists specializing in the field of optics and oceanologists.

Abstracts

UDC 551.46

MODERN CONCEPTS CONCERNING OPTICAL PROPERTIES OF SEA WATER

[Article by Kopelevich, O. V. and Shifrin, K. S.]

[Text] The article gives generalized concepts concerning the optical properties of sea water and their dependence on the governing factors. Also considered are the principal optically active components of sea water: pure water, inorganic salts, yellow matter, suspended particles and phytoplankton pigments. The authors analyze the characteristics of the spectral absorption of light by sea water and its light-scattering properties. Information is given on the statistical characteristics of absorption and scattering. A model with few parameters is proposed for the absorbing and scattering properties which with a satisfactory accuracy describes both these properties themselves and the characteristics of their variability. Figures 17, tables 13, references 142.

UDC 551.46

LIGHT FIELD FROM PULSED SOURCE IN SEA WATER

[Article by Gol'din, Yu. A., Pelevin, V. N. and Shifrin, K. S.]

[Text] The results of an experimental study of the processes of propagation of signals of short-pulse lasers in the sea are presented. A study was made of distortion of the shape of light pulses (time blurring) during their propagation in sea water for different distances and relative orientations of the source and receiver. The authors analyze the influence of the absorption and scattering of light by the medium on the pulsed transfer function of the process. Also examined are the characteristics of the nonstationary light field near the axis of the beam and outside the axial region. Data are given on polarization of the nonstationary light field in the sea and the computed Green functions for the nonstationary light field. Figures 18, references 47.

UDC 551.46.05

FUNDAMENTAL PRINCIPLES OF OPTICAL MEASUREMENTS IN SEA AND SOME HYDROPHOTOMETRIC COMPUTATIONS

[Article by Kozlyaninov, M. V.]

[Text] A study was made of the principal parameters of the field of optical radiation in the sea and hydrooptical characteristics, both primary and secondary, as well as the effective characteristics. The author gives the principles of the method for sea hydrophotometric measurements. Some approximate solutions are given for the radiation transfer equation, primarily in its differential form. The relationships of different hydrooptical characteristics are analyzed in detail. Some hydrophotometric computations are given. In these computations an evaluation is made of the accuracy in solving the transfer equation in a two-flow approximation and the dependence of the depth of visibility of a white standard disk on the optical properties of water and observation conditions is considered. Figures 10, tables 3, references 94.

UDC 551.46.06

HYDROOPTICAL INVESTIGATIONS IN PACIFIC, INDIAN AND ATLANTIC OCEANS

[Article by Voytov, V. I.]

[Text] Information on Soviet and foreign expeditionary investigations in the oceans carried out up to 1980 is examined and systematized. It is shown that there is a correlation between hydrooptical investigations and the general development of oceanology, and also with practical needs and the increase in the level of technology. The author defines regions of the oceans which are well covered by hydrooptical observations and regions where observations have not been made. Figures 1, tables 3, references 54.

UDC 551.46

STATISTICAL CHARACTERISTICS OF TOTAL RADIATION FLUX OVER DIFFERENT REGIONS OF WORLD OCEAN

[Article by Avaste, O. A., Karner, O. Yu., Lamden, K. S. and Shifrin, K. S.]

[Text] This article is devoted to the theoretical computation of radiation influxes at the ocean surface in the presence of cloud cover. The basis for the study is artificial earth satellite data on the seasonal-geographical distribution of cloud cover over the oceans and the results of aircraft sounding for determining the optical thickness of clouds. The computations were made for different regions of the world ocean (from 60°N to 60°S) for clouds of different morphology and a set of solar altitude values. The results with solar altitudes greater than 30° agree well with the experimental data of other authors. Possible reasons for the discrepancies in the case of a low sun are discussed at the end of the article. Figures 14, tables 9, references 56.

5303
CSO: 1865/73

UDC 551.463.5:535.31

SOME OPTICAL METHODS FOR INVESTIGATING WAVE-COVERED WATER SURFACE

Moscow IZVESTIYA AKADEMII NAUK SSSR: FIZIKA ATMOSFERY I OKEANA in Russian Vol 18, No 3, Mar 82 (manuscript received 25 Nov 80, after revision 10 Feb 81) pp 286-295

[Article by V. L. Veber, Institute of Applied Physics, USSR Academy of Sciences]

[Text]

Abstract: The authors give principles for determining the statistical characteristics of a wave-covered water surface from the images of luminescent test objects observed through this surface in reflected or refracted light.

Optical methods are being used more and more extensively at the present time, together with contact, acoustic and radar methods, in solving problems in the "diagnosis" of the wave-covered water surface. Due to high resolution and low inertia optical systems make it possible in principle to obtain extremely detailed information on waves. An interesting direction within the framework of development of optical methods for investigating waves is the development of special procedures for the extraction of information on the spatial structure and temporal variability of the wave-covered water surface from its optical images obtained with a certain illumination. Definite positive results have already been attained in this direction. For example, in [1], on the basis of images of the "sun glitter," an experimental determination was made of the distribution function for the slopes of sea waves [1]. In [2, 3] a study was made of the possibility of determining some "instantaneous" and correlation characteristics of waves on the basis of images of the sea surface in scattered skylight. A distinguishing characteristic of these methods is that they operate with images of the wave-covered surface, obtained, as a rule, under definite natural illumination conditions. This circumstance to a certain degree limits the field of their use.

The content of this article is a formulation of the theoretical principles for determining some statistical characteristics of the wave-covered water surface by optical methods with the use of luminescent test objects (artificial light sources).

1. For solving the problem we will use the model proposed in [4]. In a geometrical approximation it describes the process of transfer of an image through the interface of media with different refractive indices. Figure 1 is a diagram of the observations. The object of observation -- a diffusely luminescent surface with distributed luminosity $B_0(r_0)$ -- is situated in the plane z_1.

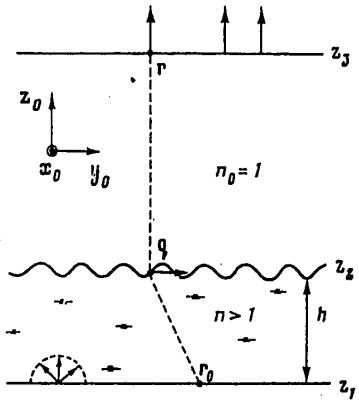

Fig. 1. Observation diagram.

The observation process essentially involves measurement (in the plane z_3) of the brightness $B_i(r) \equiv B_i(r, z_0)$ in the direction of a unit fixed vector z_0*. The object is situated in a medium with the refractive index $n>1$ and the "observer" is situated in the air ($n_0 = 1$). The image formation process is considered taking into account the variation in slopes of the interface, stipulated in the plane z_2 of the vector-function $q(r, t)$ -- the projection of the unit vector of the normal to the surface onto the plane $z = 0$.

As indicated in [4], the expression determining the relationship between the brightness distribution B_i in the image and the brightness distribution B_0 in the object has the following form:

$$B_i(\mathbf{r};\ t)=B_0[\mathbf{r}_0=\mathbf{r}+a\mathbf{q}(\mathbf{r};\ t)]; \tag{1}$$

where $a = h(n - 1)/n$, h is the distance from the object plane to the interface. This expression is also correct in a case when the "observer" and the test object are in the air. In this case the image is formed by light rays reflected from the wave-covered surface; the a coefficient has the form $a = -2h$. We note that in the derivation of formula (1) no allowance was made for the scattering properties of water and air and it was also assumed that the surface slopes are small, that is, $q^2 \ll 1$.

The author of [4], within the framework of the already described image transfer model, derived expressions for the first (m_i) and the second (M_i) statistical distribution moments for brightness in the image $B_i(r; t)$ of a test object with a determined luminosity distribution function $B_0(r)$. We will cite these expressions here:

$$m_i(\mathbf{r})=\langle B_i(\mathbf{r};\ t)\rangle=\frac{1}{(2\pi)^2}\iint_{-\infty}^{\infty}F_0(\mathbf{k})\,\theta_1(a\mathbf{k})\,e^{i\mathbf{k}\mathbf{r}}\,d\mathbf{k}; \tag{2}$$

$$M_i(\mathbf{r}_1;\ \mathbf{r}_2;\ \tau)=\langle B_i(\mathbf{r}_1;\ t_1)B_i(\mathbf{r}_2;\ t_2)\rangle= \tag{3}$$

$$=\frac{1}{(2\pi)^4}\int\limits_{-\infty}^{\infty}\ldots\int F_0(\mathbf{k}_1)F_0(\mathbf{k}_2)\,\theta_2(a\mathbf{k}_1;\ a\mathbf{k}_2;\ \rho,\ \tau)\,e^{i(\mathbf{k}_1\mathbf{r}_1+\mathbf{k}_2\mathbf{r}_2)}\,d\mathbf{k}_1 d\mathbf{k}_2,$$

* Such an idealization is correct for image detectors with a high resolution and a small angular field of view.

$$F_0(\mathbf{k}) = \iint_{-\infty}^{\infty} B_0(\mathbf{r}) e^{-i\mathbf{k}\mathbf{r}}\, d\mathbf{r}; \tag{3}$$

where

$$\theta_1(\mathbf{k}) = \iint_{-\infty}^{\infty} w_1(\mathbf{q}) e^{-i\mathbf{k}\mathbf{q}}\, d\mathbf{q}$$

is a single-point characteristic function of surface slopes; $w_1(\cdot)$ is a single-point distribution function of the probabilities of slopes;

$$\theta_2(\mathbf{k}_1; \mathbf{k}_2; \rho; \tau) = \int_{-\infty}^{\infty} \dots \int w_2(\mathbf{q}_1; \mathbf{q}_2; \rho; \tau) e^{i(\mathbf{k}_1\mathbf{q}_1 + \mathbf{k}_2\mathbf{q}_2)}\, d\mathbf{q}_1\, d\mathbf{q}_2$$

is a two-point characteristic function of slopes; $w_2(\cdot)$ is a two-point distribution function of the probabilities of slopes (the surface is assumed to be statistically homogeneous and stationary); $\rho = r_2 - r_1$; $\tau = t_2 - t_1$. For a normal (Gaussian) water-air interface (the "traditional" model of well-developed wind waves [5]) the expressions for $\theta_1(\cdot)$ and $\theta_2(\cdot)$ have the following form [4]:

$$\theta_1(\mathbf{k}) = \exp[-0{,}5(\sigma_\xi^2 k_x^2 + \sigma_\eta^2 k_y^2)]; \tag{4}$$

$$\begin{aligned}\theta_2(\mathbf{k}_1; \mathbf{k}_2; \rho; \tau) = \exp\{-0{,}5[&\sigma_\xi^2(k_{1x}^2 + k_{2x}^2) + \\ &+ \sigma_\eta^2(k_{1y}^2 + k_{2y}^2) + 2M_\xi(\rho; \tau) k_{1x}k_{2x} + 2M_\eta(\rho, \tau) k_{1y}k_{2y} + \\ &+ 2M_{\xi\eta}(\rho; \tau)(k_{1x}k_{2y} + k_{2x}k_{1y})]\},\end{aligned} \tag{5}$$

where M_ξ, M_η are the autocorrelation functions of slopes in two mutually perpendicular directions; σ_ξ^2, σ_η^2 are the corresponding dispersions; $M_{\xi\eta}$ is the cross-correlation function of slopes of the wave-covered water surface.

2. The simplest test object by means of which it is possible to have direct registry of a series of slopes of the wave-covered sea is an optical wedge, a test-object with a linear luminosity distribution function:

$$B_0(\mathbf{r}) = A(1 + \lambda x). \tag{6}$$

The brightness distribution in the image B_1 contains a component proportional to the surface slopes in the direction of the x-axis:

$$B_i(\mathbf{r}; t) = A[1 + \lambda x + \lambda a q_x(\mathbf{r}; t)]. \tag{7}$$

Information on the spatial structure of the random field of slopes $q_x(\mathbf{r})$ can be obtained, for example, by photographing the test object (6) with a small exposure and subsequent analysis (photometric measurements) of the photograph. In actual practice it is far simpler to measure the function $q_x(t)$. Information on the temporal variability of slopes at a fixed point in space can be obtained using a lucimeter oriented at the nadir (downwards). The constant component present in the signal $B_1(t)$ can be easily filtered out.

In actuality the same principle of use of a test object of the type (6) for the purpose of "diagnosis" of the wave-covered surface lies at the basis of the method for determining the slopes of the sea surface on the basis of the characteristics of

the scattered light field under natural illumination conditions [2].

3. We will examine a test object with a brightness distribution in the form:

$$B_0(\mathbf{r})=B_0+B_1\cos(k_0x+\psi). \tag{8}$$

Substituting the expression for the spatial spectrum of the test object (8) into formula (2) and taking (4) into account, we will compute the first moment of the image B_i:

$$m_i(\mathbf{r})=B_0+B_1e^{-\beta/2}\cos(k_0x+\psi), \tag{9}$$

where $\beta = a^2\sigma_\xi{}^2k_0{}^2$ is a parameter characterizing the degree of image distortions.

On the basis of the contrast of the averaged image (9)

$$Q = (m_{i\ max} - m_{i\ min})/(m_{i\ max} + m_{i\ min}) = Q_0e^{-\beta/2}(Q_0 = B_1/B_0)$$

it is possible to judge the dispersion of slopes of the wave-covered surface.

The expression for the second moment* of the image B_i can be obtained using formulas (3) and (8):

$$M_i(\mathbf{r}_1;\mathbf{r}_2\tau)=\frac{1}{2}B_1^2\{\theta_2'(\beta;\rho;\tau)\cos k_0\rho_x+\theta_2''(\beta;\rho;\tau)\cos[k_0(x_1+x_2)+ +2\psi]\}+B_0^2+B_0B_1\theta_1(\beta)[\cos(k_0x_1+\psi)+\cos(k_0x_2+\psi)], \tag{10}$$

here

$$\theta_1(\cdot)=e^{-\beta/2};\ \theta_2'(\cdot)=e^{-\beta[1-R_\xi(\rho;\tau)]};$$

$$\theta_2''(\cdot)=e^{-\beta[1+R_\xi(\rho;\tau)]};\quad R_\xi(\rho;\tau)=\frac{1}{\sigma_\xi{}^2}M_i(\rho;\tau).$$

The expression for the second time moment of the "image" $B_i(t)$ is obtained from (10) with $\rho = 0$:

$$M_i(x;\tau)=\frac{1}{2}B_1^2[\theta_2'(\beta;\tau)+\theta_2''(\beta;\tau)\cos 2(k_0x+\psi)]+C$$

(all the terms in (10) not dependent on time are denoted by C). This expression assumes a particularly simple form when $x = 0$, $\psi = \pi/2$:

$$M_i(\tau)=B_1^2e^{-\beta}\operatorname{sh}[\beta R_\xi(\tau)]+C_0,$$

where $C_0 = B_0{}^2 = M_i(\tau\to\infty)$.

Hence it is already simple to express the normalized correlation function of slopes:

$$R_\xi(\tau)=\frac{1}{\beta}\operatorname{Arsh}\left[\frac{M_i(\tau)-M_i(\infty)}{M_i(0)-M_i(\infty)}\operatorname{sh}\beta\right]. \tag{11}$$

We emphasize that all the described operations over the "image" $B_i(t)$ are technically relatively easy to carry out.

* In this article in all cases we examine the second moments, not the correlation functions, since the measurement of the latter in actual practice is more difficult.

A somewhat different approach to the problem of studying the statistical properties of the wave-covered surface involves an examination of the spectral characteristics of the test object image.

We will examine the time energy spectrum of the function $B_i(t)$:

$$\Phi_i(\omega)=B_i^2 e^{-\beta}\int_{-\infty} \mathrm{sh}[\beta R_\xi(\tau)]e^{-i\omega\tau}\,d\tau+2\pi C_0\delta(\omega).$$

We will investigate this expression in two limiting cases.

a) Case of weak distortions $\beta \ll 1$; in this case $e^{-\beta}\,\mathrm{sh}\,(\beta R_\xi)\approx\beta R_\xi$

$$\Phi_i(\omega)\approx a^2k_0^2B_i^2\Phi_\xi(\omega)+2\pi^2B_0^2\delta(\omega),$$

where

$$\Phi_\xi(\omega)=\int_{-\infty}^{\infty} M_\xi(\tau)\,e^{-i\omega\tau}\,d\tau$$

is the time energy spectrum of the slopes $q_x(t)$. As indicated by the derived expression, the spectrum of the "image" $B_i(t)$ is simply proportional to the spectrum of slopes.

b) Case of strong distortions $\beta \gg 1$; in this case:

$$\Phi_i(\omega)\approx\frac{1}{2}B_i^2\sqrt{\frac{2\pi}{2R_\xi''}}\,e^{-\frac{\omega^2}{2\beta R_\xi''}}+2\pi B_0^2\delta(\omega);$$

where $R_\xi'' = -d^2R_\xi(\tau)/d\tau^2|_{\tau=0}\geqslant 0$. It follows from this expression that the image spectrum is described by a Gaussian function, on the basis of whose characteristic width it is possible to determine the parameter R_ξ'' and accordingly the time correlation interval of slopes $\tau_\xi=\sqrt{2/R_\xi''}$.

Now we will proceed to an examination of the spatial characteristics of images of the "sinusoid." The expression for the second space moment of the $B_i(r)$ image can be obtained using formula (10) with $\tau = 0$. Averaging expression (10) for ψ (in practice this operation may not be so simple), we obtain the following dependence of M_i on R_ξ:

$$M_i(\rho)=B_0^2+0{,}5B_i^2\theta_2'(\beta;\rho)\cos k_0\rho_x.$$

We will examine the space energy spectrum of the $B_i(r)$ image averaged for ψ [4]:

$$\Phi_i(\mathbf{k})=\frac{1}{2}B_i^2\int_{-\infty}^{\infty}\int e^{-\beta[1-R_\xi(\rho)]}\cos k_0\rho_x e^{-i\mathbf{k}\rho}\,d\rho+4\pi^2B_0^2\delta(\mathbf{k}).$$

In the case of weak distortions ($\beta \gg 1$) we obtain:

$$\Phi_i(\mathbf{k})=\frac{1}{4}B_i^2a^2k_0^2[\Phi_\xi(\mathbf{k}-\mathbf{k}_0)+\Phi_\xi(\mathbf{k}+\mathbf{k}_0)+$$

$$+\pi^2B_i^2(1-\beta)[\delta(\mathbf{k}-\mathbf{k}_0)+\delta(\mathbf{k}+\mathbf{k}_0)]+4\pi^2B_0^2\delta(\mathbf{k}),$$

where

$$\Phi_\xi(\mathbf{k})=\int_{-\infty}^{\infty}\int M_\xi(\rho)e^{-i\mathbf{k}\rho}\,d\rho.$$

As indicated by the derived expression, the energy spectrum of the image $B_i(r)$ in the neighborhood of the frequencies $\pm k_0$ with an accuracy to the factor coincides with the space spectrum of slopes of an uneven interface*.

* This is correct in a case when the Φ_ξ spectra, spaced by $\pm k_0$, do not overlap one another.

In the case of strong distortions ($\beta \gg 1$) the image spectrum is written in the following way:

$$\Phi_i(\mathbf{k}) = \Phi_i^0(\mathbf{k}-\mathbf{k}_0) + \Phi_i^0(\mathbf{k}+\mathbf{k}_0) + 4\pi^2 B_0^2 \delta(\mathbf{k}),$$

where

$$\Phi_i^0(\mathbf{k}) = \frac{\pi B_i^2}{2\beta\sqrt{R_{xx}''R_{yy}''-R_{xy}''^2}} \exp\left\{-\frac{R_{xx}''k_y^2 + R_{yy}''k_x^2 - 2R_{xy}''k_x k_y}{2\beta(R_{xx}''R_{yy}''-R_{xy}''^2)}\right\}, \qquad (12)$$

$$R_{ij}'' = -\partial^2 R_\xi(\rho)/\partial\rho_i\partial\rho_j|_{\rho=0} \quad (i, j \sim x, y).$$

The coefficients R_{ij}'' are related to the dispersions of the second space derivatives of the rises $\zeta(\mathbf{r})$ of an uneven interface in the following way:

$$R_{xx}'' = \frac{1}{\sigma_\xi^2}\left\langle\left(\frac{\partial^2\zeta}{\partial x^2}\right)^2\right\rangle = \frac{\sigma_{xx}^2}{\sigma_\xi^2}; \quad R_{yy}'' = \frac{1}{\sigma_\xi^2}\left\langle\left(\frac{\partial^2\zeta}{\partial x\,\partial y}\right)^2\right\rangle = \frac{\sigma_{xy}^2}{\sigma_\xi^2};$$

$$R_{xy}'' = \frac{1}{\sigma_\xi^2}\left\langle\frac{\partial^2\zeta}{\partial x^2}\frac{\partial^2\zeta}{\partial x\,\partial y}\right\rangle = 0.$$

Accordingly, expression (12) can be transformed to the form:

$$\Phi_i^0(\mathbf{k}) = \frac{\pi B_i^2}{2a^2k_0^2\sigma_{xx}\sigma_{xy}} \exp\left[-\frac{1}{2a^2k_0^2}\left(\frac{k_x^2}{\sigma_{xx}^2}+\frac{k_y^2}{\sigma_{xy}^2}\right)\right].$$

It follows from this expression that by measuring (in the case of strong distortions) the width of the energy spectrum of the image of the "sinusoid" in the form of two sections $k_z = 0$ and $k_y = 0$, it is possible to compute the values of the dispersions of the curvature of the wave-covered surface σ_{xx}^2 and σ_{xy}^2.

4. The principal shortcoming of the methods for measuring the characteristics of waves from the practical point of view is the need for fabricating, and most importantly, the placement of light sources having large ($\geqslant a\sigma_\xi \times a\sigma_\eta$) dimensions under or over the water. This circumstance is not particularly important when carrying out a model experiment; it is a different matter when making in situ measurements. Here it is desirable to employ test objects of the smallest area possible.

This requirement is met by a test object with a brightness distribution of the following form:

$$B_0(\mathbf{r}) = B_0\delta(x). \qquad (13)$$

The task of determining the statistical characteristics of images of a test object (13) for a random interface, not changing in time, was examined in [4]. We will cite an expression for the second statistical moment of an image, also taking into account the "dynamics" of the surface [4]:

$$M_1(\mathbf{r}_1; \mathbf{r}_2; \tau) = \frac{B_0^2}{2\pi a^2\sigma_\xi^2}\cdot\frac{1}{\sqrt{1-R_\xi^2}}\exp\left[-\frac{x_1^2+x_2^2-2R_\xi x_1x_2}{2a^2\sigma_\xi^2(1-R_\xi^2)}\right], \qquad (14)$$

where $R_\xi \equiv R_\zeta(\rho; \tau)$.

The second time moment of the "image" $B_1(t)$ is obtained from (14) with $r_1 = r_2 = 0$:

$$M_i(\tau)=B_0^2/2\pi a^2\sigma_\xi^2\sqrt{1-R_\xi^2(\tau)}. \tag{15}$$

The expression for the second space moment of the image $B_i(r)$ is obtained by assuming in (14) that $\tau = 0$, $r_1 = 0$ ($r_2 \equiv \rho$):

$$M_i(\rho)=\frac{B_0^2}{2\pi a^2\sigma_\xi^2}\frac{1}{\sqrt{1-R_\xi^2(\rho)}}\exp\left\{-\frac{\rho_x^2}{2a^2\sigma_\xi^2[1-R_\xi^2(\rho)]}\right\}. \tag{16}$$

It is easy to confirm that in the region of values $\rho_x \leqslant \rho_{\xi x}$, $\rho_y < \rho_{\xi y}$ ($\rho_{\xi x}$ and $\rho_{\xi y}$ -- are the characteristic correlation intervals of the slopes q_x along the x- and y-axes respectively) with satisfaction of the inequality $\rho_{\xi x} \ll \sqrt{2}\sigma_\xi$ a the exponential factor in (16) is equal to approximately 1. In this case expression (16) is reduced to a form similar to (15):

$$M_i(\rho)\simeq B_0^2/2\pi a^2\sigma_\xi^2\sqrt{1-R_\xi^2(\rho)} \quad (\rho_x \leqslant \rho_{tx},\ \rho_y \leqslant \rho_{ty}).$$

5. The relationship between the moments of the images of the test object (13) to the correlation function of surface slopes is rather complex (in particular, with $\rho \to 0$; $M_i \to \infty$). A simpler relationship is observed when using a test object with a brightness distribution of a "stepped" type:

$$B_0(r)=B_0 1(x), \quad \text{where } 1(x) - \begin{cases} 1 \text{ with } x \geqslant 0, \\ 0 \text{ with } x < 0. \end{cases} \tag{17}$$

As follows from (3) and (5), the expression for the second statistical moment of the image of a one-dimensional test object $B_0(x)$ is written in the following way:

$$M_i(r_1; r_2; \tau)=\frac{1}{(2\pi)^2}\int_{-\infty}^{\infty}\int F_0(k_1)F_0(k_2)\exp\{-0{,}5a^2\sigma_\xi^2[k_1^2+k_2^2+2R_\xi(\rho;\tau)k_1k_2]+i(k_1x_1+k_2x_2)\}dk_1\,dk_2.$$

We will differentiate this expression for R_ξ and, using the relationship

$$kF_0(k)=\frac{1}{i}\int_{-\infty}^{\infty}\frac{dB_0(x)}{dx}e^{-ikx}dx,$$

as a result we obtain:

$$\frac{dM_i}{dR_\xi}=\frac{a^2\sigma_\xi^2}{(2\pi)^2}\int_{-\infty}^{\infty}\int\frac{dB_0}{dx}(x')\frac{dB_0}{dx}(x'')\exp\{-0{,}5a^2\sigma_\xi^2(k_1^2+k_2^2+2R_\xi k_1k_2)\}\times$$
$$\times\exp\{i[k_1(x_1-x')+k_2(x_2-x'')]\}dk_1\,dk_2\,dx'\,dx''.$$

Here we will substitute the expression (17), and carrying out integration for all the variables, we derive the differential equation

$$\frac{dM_i}{dR_\xi}=\frac{B_0^2}{2\pi\sqrt{1-R_\xi^2(\rho;\tau)}}\exp\left\{-\frac{x_1^2+x_2^2-2R_\xi(\rho;\tau)x_1x_2}{2a^2\sigma_\xi^2[1-R_\xi^2(\rho;\tau)]}\right\}. \tag{18}$$

The time correlation function of the "image" $B_i(t)$ is obtained from the differential equation (18) with $r_1 = r_2 = 0$; the expression for it has the following form:

$$M_i(\tau)=(B_0^2/2\pi)\arcsin R_\xi(\tau). \tag{19}$$

A similar solution of the differential equation (18) can be obtained for the space correlation function of the image $B_i(r)$, if the condition $\rho_{\xi x} \ll \sqrt{2}a\sigma_\xi$ is satisfied (see preceding problem). The solution for this case is written in the following way:

$$M_i(\rho)=(B_0^2/2\pi)\arcsin R_i(\rho)\quad(r_1=0;\ r_2=\rho;\ \rho_x\leqslant\rho_{ix};\ \rho_y\leqslant\rho_{iy}).\tag{20}$$

We note that in the practical realization of this method there is no need to use a test object of the type (17). An image of an object in the form (13) can be subjected to correlation analysis if we first carry out the operation of "filling" of the intervals between contour lines "alternately" with black and white colors (Fig. 2) on this image. The result of the analysis of the images "processed" in this way is described by formulas (19) and (20).

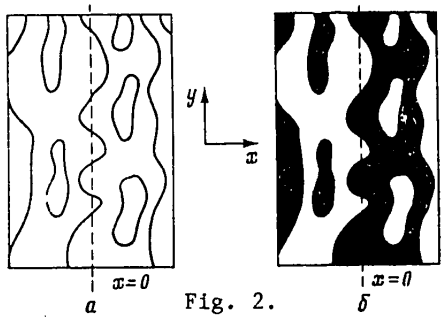

Fig. 2.

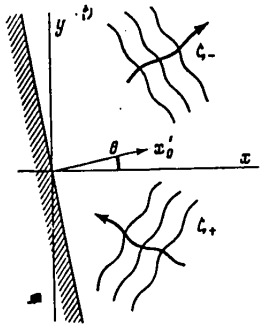

Fig. 3.

Fig. 2. Images: a) "linear" and b) "stepped" test objects obtained with observation through uneven surface.

Fig. 3. Diagram of reflection of waves from fixed rigid screen.

A further modification of this method involves the following. We will assume that a light source with a distribution of luminosity in the form

$$B_0(\mathbf{r})=B_0\exp(-|\mathbf{r}|^2/r_0^2)$$

moves over (or under) a water surface with the velocity v relative to some observation system. We will also assume that the image of this source is integrated over a long time interval. The brightness distribution in the image, "fixed" in such a way, is described by the following expression:

$$B_i(\mathbf{r})=\int_{-\infty}^{\infty}B_0[\mathbf{r}+\mathbf{v}t+a\mathbf{q}(\mathbf{r};t)]\,dt.\tag{21}$$

We will determine the second statistical moment of this image. Substituting (21) into formula (3) and assuming $\mathbf{v}=\mathbf{y}_0 v$, we obtain the expression:

$$M_i(\mathbf{r}_1;\mathbf{r}_2)=\frac{1}{(2\pi)^3}\int_{-\infty}^{\infty}\!\!\cdots\!\int F_0(k_{1x};-k_y)F_0(k_{2x};k_y)\times$$
$$\times\frac{1}{v}\theta_2(ak_{1x};ak_{2x};ak_y;-ak_y;\rho;\tau)\exp\{i[k_{1x}x_1+k_{2x}x_2+k_y(\rho_y+v\tau)]\}\times\tag{22}$$
$$\times dk_{1x}\,dk_{2x}\,dk_y\,d\tau.$$

With a great velocity of motion of the source the time variability of the waves can be neglected, that is, the interface can be considered "frozen-in." In this case expression (22) (with $r_0\to 0$) is identical to expression (16).

An analysis of the conditions under which it is possible to adopt the hypothesis of a "frozen-in" character of the surface directly on the basis of expression (22) is difficult primarily due to a lack of knowledge concerning the precise form of the functions $M_\xi(\rho;\tau)$, $M_\eta(\rho;\tau)$, $M_{\xi\eta}(\rho;\tau)$. However, such an analysis can be carried out by examining the expression for dispersion following from (22) with $r_1 = r_2 = 0$. Carrying out integration for the variables k_{1x}, k_{2x}, k_y, as a result we obtain the expression:

$$\sigma_i^2 = \langle B_i^2(0)\rangle \sim \int_{-\infty}^{\infty} f_1(\tau) f_2(\tau) f_0(\tau)\, d\tau,$$

where

$$f_1(\tau) = (\alpha^2-1)^{0,5}[\alpha^2 - R_\xi^2(\tau)]^{-0,5},$$
$$f_2(\tau) = (\alpha-1)^{0,5}[\alpha - R_\eta(\tau)]^{-0,5},$$
$$f_0(\tau) = \exp\{-p\tau^2/[\alpha - R_\eta(\tau)]\},$$

$\alpha = 1 + r_0^2/2a^2\sigma_q^2$, $p = v^2/4a^2\sigma_q^2$ (as a simplification we will assume that the waves are isotropic: $\sigma_\xi^2 = \sigma_\eta^2 = \sigma_q^2$). The functions $f_n(\tau)$, entering into this expression, have a monitonically decreasing character; the integration region is determined by the function $f_0(\tau)$. The characteristic scales of change in the functions f_n, determined using the formula

$$\tau_n = \sqrt{2/f_n''}, \qquad \text{where} \qquad f_n'' = -d^2 f_n/d\tau^2|_{\tau=0},$$

have the following values:

$$\tau_1 = \tau_2 = \tau_q r_0/a\sigma_q,\ \tau_0 = \sqrt{2}\frac{r_0}{v},\ \tau_q = \sqrt{2/R_\xi''}.$$

When there is satisfaction of the condition $\tau_0 \ll \tau_1$ (the function f_0 is "narrow" in comparison with f_1 and f_2), the integration region $\sim r_0/v \ll \tau_q$ and the dependence of the functions R_ξ and R_η under the integral on τ can be neglected, which is equivalent to the nondependence of the function Θ_2 in expression (22) on τ. Thus, the hypothesis of a "frozen-in" character of the wave-covered surface is correct with satisfaction of the condition:

$$v \gg \sqrt{2}a\sigma_q/\tau_q.$$

6. The single-point characteristics of waves are measured most simply by optical (as, however, by other) methods. In this section we will examine a method for determining the space correlation function of rises or slopes of the wave-covered surface on the basis of the results of measurements of the corresponding dispersions.

Assume that the random water-air interface is described by the function of rises $\zeta_+(r; t)$. This function can be represented in the form of a linear combination of elementary monochromatic plane waves with a random complex amplitude dA_k, propagating in different directions with the wave vectors k and the frequencies $\omega_k = \omega(k)$*:

$$\zeta_+(r; t) = \mathrm{Re}\int_k dA_k e^{i(kr-\omega_k t)}.$$

We will assume that a rigid screen (a wall reflecting waves) has been placed in the water. The orientation of the screen is stipulated by the vector x_0' -- the normal to its plane (Fig. 3). The function of rises of the "disturbed" interface is represented in the form of the sum of the functions ζ_+ and ζ_-, describing the random

wave fields of the "incident" and "reflected" systems of waves respectively:

$$\zeta(\mathbf{r};t)=\zeta_+(\mathbf{r};t)+\zeta_-(\mathbf{r};t);\quad \zeta_-(\mathbf{r};t)=\mathrm{Re}\int_{\varkappa} d\dot{B}_\varkappa e^{i(\varkappa\mathbf{r}-\omega_\varkappa t)}.$$

The condition for the reflection of an elementary plane wave from a rigid wall is written in the following way:

$$d\dot{B}_\varkappa=d\dot{A}_k \quad \text{with} \quad \varkappa=\varkappa(\mathbf{k})=\mathbf{k}-2(\mathbf{k}\mathbf{x}_0')\mathbf{x}_0'.$$

The expression for the correlation function of surface rises ζ

$$M_\zeta(\mathbf{r}_1;\mathbf{r}_2;t_1;t_2)=\langle\zeta(\mathbf{r}_1;t_1)\zeta(\mathbf{r}_2;t_2)\rangle$$

has the following form:

$$M_\zeta(\cdot)=\frac{1}{2}\mathrm{Re}\iint\{\langle A_{k_1}A_{k_2}\rangle+\langle A_{k_1}B_{\varkappa_2}\rangle+\langle B_{\varkappa_1}A_{k_2}\rangle+\langle B_{\varkappa_1}B_{\varkappa_2}\rangle+ \\ +\langle A_{k_1}A_{k_2}^*\rangle+\langle B_{\varkappa_1}B_{\varkappa_2}^*\rangle+\langle A_{k_1}B_{\varkappa_2}^*\rangle+\langle A_{k_1}^*B_{\varkappa_2}\rangle\}, \tag{23}$$

where

$$A_{k_i}=d\dot{A}_{k_i}e^{i(\mathbf{k}_i\mathbf{r}_i-\omega_{k_i}t_i)};\quad B_{\varkappa_i}=d\dot{B}_{\varkappa_i}e^{i(\varkappa_i\mathbf{r}_i-\omega_{\varkappa_i}t_i)};\quad i=1,2.$$

Using the assumption of a delta correlation of the spectral amplitudes of elementary waves, it is possible to write the following expressions:

$$\langle d\dot{A}_{k_1}d\dot{A}_{k_2}\rangle=\langle d\dot{A}_k d\dot{B}_\varkappa\rangle=\langle d\dot{B}_{\varkappa_1}d\dot{B}_{\varkappa_2}\rangle=0;$$

$$0{,}5\langle d\dot{A}_{k_1}d\dot{A}_{k_2}^*\rangle=\Phi_{\zeta_-}(\mathbf{k}_1)\delta(\mathbf{k}_2-\mathbf{k}_1)d\mathbf{k}_1d\mathbf{k}_2;$$

$$0{,}5\langle d\dot{B}_{\varkappa_1}d\dot{B}_{\varkappa_2}^*\rangle=\Phi_{\zeta_-}(\varkappa_1)\delta(\varkappa_2-\varkappa_1)d\varkappa_1d\varkappa_2$$

$$0{,}5\langle d\dot{A}_{k_1}d\dot{B}_{\varkappa_2}^*\rangle=0{,}5\langle d\dot{B}_{\varkappa_1}d\dot{A}_{k_1}^*\rangle=\Phi_{\zeta+}(\mathbf{k}_1)\delta[\varkappa_2-\varkappa(\mathbf{k}_1)]d\mathbf{k}_1d\varkappa_2;$$

here Φ_{ζ_+} is the energy spectrum of rises of the undisturbed surface $\zeta_+(\mathbf{r};t)$.

Carrying out integration in (23), we obtain:

$$M_\rho(\mathbf{r}_1;\mathbf{r}_2;\tau)=2M_{\zeta+}(\rho,\tau)+M_{\zeta+}(\rho_1)+M_{\zeta+}(\rho_2), \tag{24}$$

where $M_{\zeta+}$ is the correlation function of surface rises ζ_+;

$$\rho=\mathbf{r}_2-\mathbf{r}_1;\ \tau=t_2-t_1;$$

$$\rho_1\sim\begin{cases}\rho_{1x}=x_1+x_2\cos 2\theta+y_2\sin 2\theta;\\ \rho_{1y}=y_1-y_2\cos 2\theta+x_2\sin 2\theta;\end{cases}$$

$$\rho_2\sim\begin{cases}\rho_{2x}=-x_2-x_1\cos 2\theta-y_1\sin 2\theta;\\ \rho_{2y}=-y_2+y_1\cos 2\theta-x_1\sin 2\theta.\end{cases}$$

The dispersion of rises of a random surface ζ is:

$$\sigma_\zeta^2(\mathbf{r})=M_\zeta(\mathbf{r};\ \mathbf{r};\ 0)=2\sigma_{\zeta+}^2+2M_{\zeta+}(\rho_0), \tag{25}$$

where

$$\rho_0\sim\begin{cases}\rho_{0x}=2(x\cos\theta+y\sin\theta)\cos\theta;\\ \rho_{0y}=2(x\cos\theta+y\sin\theta)\sin\theta.\end{cases}$$

As indicated by (25), the space correlation function of the "undisturbed" surface is represented in the dispersion $\sigma_\xi^2(r)$ by its section along the straight line $\rho_{0y} = \rho_{0x} \operatorname{tg} \theta$. By measuring the position of the screen (angle θ) and measuring the dispersion σ_ζ^2 it is possible to obtain complete information on the form of the correlation function $M_{\zeta+}(\rho)$.

In most cases when reference is to optical methods for investigating waves it is simpler to make measurements of the dispersion of slopes, not water surface rises. The expression for the dispersion of slopes and the direction of the x-axis can be obtained from (24) using the formula

$$\sigma_\xi^2(r) = \frac{\partial^2}{\partial x_1 \partial x_2} M_\xi(r_1; r_2; 0)\big|_{r_1 - r_2 = r}.$$

It has the following form:

$$\sigma_\xi^2(r) = 2\sigma_{\xi+}^2 - 2M_{\xi+}(\rho_0)\cos 2\theta - 2M_{\xi\eta+}(\rho_0)\sin 2\theta, \tag{26}$$

where $M_{\xi+}$, $M_{\xi\eta+}$ are the correlation functions of slopes of the "undisturbed" interface.

The expression for the dispersion of slopes in the direction of the y-axis is determined similarly and has the form:

$$\sigma_\eta^2(r) = 2\sigma_{\eta+}^2 + 2M_{\eta+}(\rho_0)\cos 2\theta - 2M_{\xi\eta+}(\rho_0)\sin 2\theta. \tag{27}$$

It follows from expressions (26) and (27) that a "pure" measurement of the functions $M_{\xi+}$ and $M_{\eta+}$ can be carried out only for the sections $\theta = 0$ and $\theta = \pi/2$, whereas "pure" measurement of the function $M_{\xi\eta+}$ can be accomplished only for the sections $\theta = \pm\pi/4$. For measuring the dispersions of slopes σ_ξ or σ_η it is possible to use the optical methods described in sections 2, 3, 4 of this work.

We note in conclusion that for practical purposes this method for determining the space correlation functions of waves can be convenient in measurements made from aboard a ship or from stationary structures in the sea.

The author expresses appreciation to L. S. Dolin and T. G. Talipova for an extremely useful discussion of the results of this study.

BIBLIOGRAPHY

1. Cox, C. and Munk, W. H., "Statistics of the Sea Surface Derived From Sun Glitter," J. MAR. RES., Vol 13, No 2, pp 198-204, 1954.

2. Stilwell, D. J., "Directional Energy Spectra of the Sea From Photographs," J. GEOPHYS. RES., Vol 74, No 8, pp 1974-1986, 1969.

3. Titov, V. I., "Determination of the Spectrum of Sea Waves by a Spectral Analysis of Aerial Photographs," manuscript deposited at the All-Union Institute of Scientific and Technical Information, 3 September 1981, No 4324-81 DEP.

4. Veber, V. L., "Statistical Characteristics of Images Obtained in Observations Through an Uneven Interface of Media With Different Refractive Indices," IZV. VUZOV: RADIOFIZIKA (News of Higher Educational Institutions: Radiophysics), Vol 22, No 8, pp 989-1001, 1979.

5. Longuet-Higgins, M. S., "Statistical Analysis of a Random Moving Surface," VETROVYYE VOLNY (Wind Waves), Moscow, IL, pp 125-218, 1962.

6. Sinitsyn, Yu. A., Leykin, I. A. and Rozenberg, A. D., "Spatial-Temporal Characteristics of Ripples in the Presence of Long Waves," IZV. AN SSSR: FAO (News of the USSR Academy of Sciences: Physics of the Atmosphere and Ocean), Vol 9, No 5, pp 511-519, 1973.

5303
CSO: 1865/134

UDC 551.466.81

PROPAGATION OF PACKET OF SLIGHTLY NONLINEAR INTERNAL WAVES IN MEDIUM WITH CONSTANT VÄISÄLÄ FREQUENCY

Moscow IZVESTIYA AKADEMII NAUK SSSR: FIZIKA ATMOSFERY I OKEANA in Russian Vol 18, No 3, Mar 82 (manuscript received 8 Dec 80) pp 320-324

[Article by A. G. Voronovich, Institute of Oceanology, USSR Academy of Sciences]

[Text] It was demonstrated in [1] that during the propagation of a packet of slightly nonlinear internal waves (IW) belonging to a mode with some fixed number the evolution of the packet envelope is described by a nonlinear Schrödinger equation. The packet generates some mean flows and corrections to density not disappearing with averaging for the wave period. It is not impossible that these corrections are related to the fine structure of hydrophysical fields in the ocean [2, 3]. It is of interest to examine this problem applicable to a three-dimensional packet of IW not having a modal structure. A similar problem for a compressible medium was examined in [4], where, in particular, it was demonstrated that a packet of powerful acoustic waves generates internal waves during its propagation (Cherenkov radiation).

Thus, assume that there is an unbounded fluid with a constant Väisälä frequency N_0 = const and a packet of internal waves of a small but finite amplitude is propagated in it. An examination of the corresponding slightly nonlinear effects is conveniently carried out using Hamiltonian formalism proposed in [5]. We will solve the problem using the Boussinesq approximation. Applicable to a medium with a constant Väisälä frequency N_0 the results in [6] give the following. In the equations of hydrodynamics we will convert from the ρ, v values to the variable b_k such that

$$\mathbf{v}=\nabla\Phi+\lambda\nabla(\rho_0+\rho), \tag{1a}$$

$$\Phi=-\Delta^{-1}\{\lambda\nabla(\rho_0+\rho)\}, \tag{1b}$$

$$\rho=-\frac{\rho_0'}{N_0}(2\pi)^{-3/2}\int\sqrt{\frac{\omega_k}{2}}\,b_k e^{i\mathbf{kr}}\,d\mathbf{k}+\text{к.с.}, \tag{1c}$$

complex conjugate

$$\lambda=\frac{ig}{N_0}(2\pi)^{-3/2}\int\frac{1}{\sqrt{2\omega_k}}\,b_k e^{i\mathbf{kr}}\,d\mathbf{k}+\text{к.с.} \tag{1d}$$

Here $N_0^2 = -g(\rho_0)'$, $\omega_k = N_0|\varkappa|/|k|$ is the frequency of a linear internal wave with the wave vector $k = (\varkappa, \nu)$, where $\varkappa$ and ν are the projections of the vector k onto the horizontal plane and vertical respectively; the prime here and in the presentation which follows denotes $\partial/\partial z$. Then in the new variables b_k the equations of motion are Hamiltonians $\dot{b}_k + i\delta H/\delta b_k^* = 0$, where

$$H = \int \omega_k b_k b_k^* \, dk + \int |V_{kk_1k_2} b_k^* b_{k_1} b_{k_2} \delta_{k-k_1-k_2} \, dk \, dk_1 \, dk_2 + \text{к.с.} + \\ + \frac{1}{3} \int U_{kk_1k_2} b_k b_{k_1} b_{k_2} \delta_{k+k_1+k_2} \, dk \, dk_1 \, dk_2 + \text{к.с.} + \\ + \frac{1}{2} \int W_{kk_1k_2k_3} b_k^* b_{k_1}^* b_{k_2} b_{k_3} \delta_{k+k_1-k_2-k_3} \, dk \, dk_1 \, dk_2 \, dk_3 \tag{2}$$

(here only the "significant" term [5] has been left from the fourth-order terms). The b_k values are simply related to the vertical displacement $\zeta(r)$:

$$\zeta = (2\pi)^{-n} \frac{1}{N_0} \int \sqrt{\frac{\omega_k}{2}} b_k e^{ikr} \, dk + \text{к.с.} \tag{3}$$

The full expressions for the coefficients V, U and W have the form

$$\begin{pmatrix} V \\ U \end{pmatrix}_{kk_1k_2} = \mp \frac{i}{4N_0} (2\pi)^{-n} \left(\frac{1}{2} \omega_k \omega_{k_1} \omega_{k_2} \right)^{1/2} \left\{ \nu \left[\frac{\omega_k}{\varkappa^2} \left(\frac{\varkappa\varkappa_1}{\omega_{k_1}} + \frac{\varkappa\varkappa_2}{\omega_{k_2}} \right) + \right. \right. \\ + \frac{\pm\omega_{k_1} \pm \omega_{k_2} - \omega_k}{\omega_k} \Big] \mp \nu_1 \left[\frac{\omega_{k_1}}{\varkappa_1^2} \left(\frac{\varkappa_1\varkappa_2}{\omega_{k_2}} + \frac{\varkappa_1\varkappa}{\omega_k} \right) + \frac{\pm\omega_k - \omega_{k_1} - \omega_{k_2}}{\omega_{k_1}} \right] \mp \\ \left. \mp \nu_2 \left[\frac{\omega_{k_2}}{\varkappa_2^2} \left(\frac{\varkappa_2\varkappa}{\omega_k} + \frac{\varkappa_2\varkappa_1}{\omega_{k_1}} \right) + \frac{\pm\omega_k - \omega_{k_1} - \omega_{k_2}}{\omega_{k_2}} \right] \right\} \tag{4a}$$

(the upper and lower signs in this formula relate to V and U respectively) and

$$W_{kk_1k_2k_3} = \frac{1}{4} (2\pi)^{-3} (f_{k_2kk_3k_1} + f_{k_2k-k_1k_3} + f_{-k_1-k_2k_3k} + \\ + f_{k_1k_2kk_3} - f_{k_2-k_3-kk_1} - f_{-k_1kk_3-k_2}), \tag{4b}$$

where

$$f_{k_1k_2k_3k_4} = \left(\frac{\omega_{k_1}\omega_{k_2}}{\omega_{k_3}\omega_{k_4}} \right)^{1/2} \left[(k_1k_2) - \frac{(kk_1)(kk_2)}{k^2} \right],$$

$$k = k_1 + k_3 = k_2 + k_4.$$

We will examine the propagation of a spectrally narrow packet of IW with the characteristic wave vector k_0 such that b_k is substantially different from zero in a linear approximation only when $|k - k_0| \ll k_0$ (here and in the text which follows $k_0 = |k_0|$). It is convenient to make a standard canonical replacement of the variables [7, 8], excluding third-order terms in the Hamiltonian H:

$$b_k = a_k - \int \frac{V_{kk_1k_2} a_{k_1} a_{k_2} \delta_{k-k_1-k_2}}{\omega_k - \omega_{k_1} - \omega_{k_2}} \, dk_1 \, dk_2 + 2 \int \frac{V_{k_2kk_1}^{\cdot} a_{k_1}^{\cdot} a_{k_2} \delta_{k_2-k+k_1}}{\omega_{k_2} - \omega_k - \omega_{k_1}} \, dk_1 \, dk_2 - \\ - \int \frac{U_{kk_1k_2} a_{k_1}^{\cdot} a_{k_2}^{\cdot} \delta_{k+k_1+k_2}}{\omega_k + \omega_{k_1} + \omega_{k_2}} \, dk_1 \, dk_2 + O(a^3). \tag{5}$$

In this case additional fourth-order terms appear in H and the value of the W coefficient changes. The general formula for the coefficient obtained as a result, denoted T_1, is also given in [7]. In the variables a_k the equation of motion $\dot{a}_k + i\delta H/\delta a_k^* = 0$ assumes the form

$$\dot{a}_k + i\omega_k a_k + i\int T_{kk_1k_2k_3} a_{k_1} a_{k_2} a_{k_3} \delta_{k+k_1-k_2-k_3}\, dk_1\, dk_2\, dk_3 = 0. \tag{6}$$

The unwieldy expression for the T coefficient is substantially simplified if we examine the following situation. Assume that the wave is modulated only in the direction of the unit vector e (Fig. 1) $\zeta(r) = \zeta(er)$. Then a_k will contain the δ-functions for the k components perpendicular to e and in formula (6) in actuality only a single integration for the k component parallel to e remains. It is easy to confirm that in this case

$$(2\pi)^3 T_{kk_1k_2k_3} \approx T_0 - \frac{T_1}{\omega_e^2 - [C_g(k-k_2)]^2},$$
$$T_0 = k_0^2 - (k_0 e)^2 = k_0^2(1-(\sin\alpha\sin\theta\cos\varphi + \cos\alpha\cos\theta)^2), \tag{7}$$
$$T_1 = N_0^2 k_0^2 (\cos\alpha\sin\theta - \sin\alpha\cos\theta\cos\varphi)^2,$$

where $\omega_e = N_0 \sin\theta$ is the frequency of the IW traveling in the direction of the e vector; C_g is the group velocity (the sense of the angles α, θ and φ is clear from the figure). Using the approximate expression (7), it is convenient to rewrite equation (6) in a different form. We will assume that

$$\psi(r, t) = (2\pi)^{-3/2}\int e^{i(k-k_0)r} a_k\, dk.$$

With an accuracy to terms quadratic in wave amplitude ψ is simply related to the complex amplitude of the wave of vertical displacements ζ:

$$\zeta = \frac{1}{N_0}\sqrt{\frac{\omega_{k_0}}{2}}\, e^{-ik_0 r}\psi.$$

In addition, the value $\rho_0 \omega_{k_0} |\psi|^2$ is the energy density in the packet of IW. Carrying out the Fourier transform in (6), we rewrite it, taking (7) into account, in the following form:

$$\dot{\psi} + i\omega_0\psi + C_e\psi_\xi - \frac{i}{2}\omega''\psi_{\xi\xi} + iT_0|\psi|^2\psi - iT_1 Q\psi = 0, \tag{8a}$$

$$C_e^2 Q_{\xi\xi} + \omega_e^2 Q = |\psi|^2. \tag{8b}$$

Here ξ is the coordinate in the direction of the e vector: $\xi = er$, k_ξ is the projection of k onto this same direction,

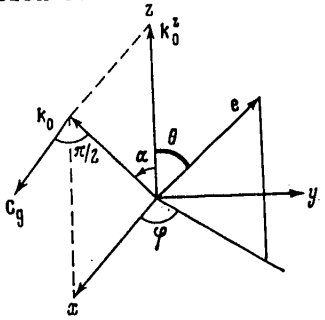

$$C_e = C_g e = \frac{N_0}{k_0}\cos\alpha(\cos\alpha\sin\theta\cos\varphi - \sin\alpha\cos\theta), \tag{9}$$
$$\omega'' = \partial^2\omega/\partial k_\xi^2 = \frac{\omega_e^2 - \omega_0^2 - C_e^2 k_0^2}{\omega_0 k_0^2} - 4\frac{(k_0 e)}{k_0^2}C_e \text{ и}$$
$$Q(\xi) = \frac{1}{2\pi}\int \frac{e^{i\Lambda(\xi-\xi')}}{\omega_e^2 - C_e^2 k^2}|\psi(\xi')|^2\, d\xi'\, dk.$$

Transforming in equations (8a), (8b) into a coordinate system related to the packet: $x = \xi - C_e t$ and substituting $\psi \to \psi e^{-i\omega_0 t}$, we obtain

$$i\psi_t + \frac{1}{2}\omega''\psi_{xx} - T_0|\psi|^2\psi + T_1 Q\psi = 0, \tag{10a}$$

$$C_e^2 Q_{xx} + \omega_e^2 Q = |\psi|^2. \tag{10b}$$

The Q parameter is related to the low-frequency IW generated by the packet. In actuality, if formulas (5) and (1c) are used in transforming from the new variable a_k to the initial parameter ρ, we obtain the following quadratic correction to ρ:

$$\zeta_{\text{low frequency}} = \rho/\rho_0' = -\frac{C_e T_1^{1/4}}{N_0}\frac{\partial Q}{\partial x}$$

($\zeta_{\text{low frequency}}$ obviously has the sense of a vertical displacement of fluid particles in the generated low-frequency IW). If it is assumed that the packet is finite in the ξ coordinate and it is assumed that Q = 0 with $\xi \to +\infty$, from equation (10b) it is easy to find the Q value and accordingly $\zeta_{\text{low frequency}}$ with $\xi \to -\infty$:

$$\zeta_{\text{low frequency}} = \exp\left\{i\left(\frac{\omega_e}{C_e}\text{er} - \omega_e t\right)\right\}\frac{T_1^{1/4}}{2C_e N_0}\int |\psi(\xi')|^2 \exp\left\{-i\frac{\omega_e}{C_e}\xi'\right\} d\xi' + \text{к.с.} \tag{11}$$

Thus, during its propagation the packet leaves behind itself a wake of low-frequency IW. It is clear that an appreciable amplitude of the generated waves will be observed only under the condition $(\omega_e/C_e)L \lesssim 2\pi$, where L is the dimension of the packet in the direction e. It therefore follows that generation occurs when $\theta \lesssim (\sigma'/k_0 L)\sin 2\alpha$, that is, the vector e must be directed almost vertically; in this case

$$\zeta_{\text{low frequency}} \approx k_0\overline{\zeta_0^2}\cos\varphi, \tag{12}$$

where

$$\overline{\zeta_0^2} = \frac{\omega_e}{C_e}\int |\zeta_0(\xi)|^2 \exp\left\{-i\frac{\omega_e}{C_e}\xi\right\} d\xi.$$

is some mean square amplitude of a wave in the packet. Assuming, for example, that $\zeta_0 \sim 5$ m, $2\pi/k_0 \sim 100$ m, $\cos\varphi \sim 1$, we find $\zeta_{\text{low frequency}} \sim 1$ m. We note that the total amplitude of displacement of the fluid particles in the low-frequency IW will be $1/\sin\theta$ times greater (and can considerably exceed the amplitude of the initial wave since this examination is suitable only if there is no violation of the requirements: $k_0\zeta \ll 1$, $k_0 L \gg 1$). It can be seen from formula (12) that if the packet envelope has a cylindical symmetry relative to the vertical the generation has a dipole character in the horizontal plane (relative to the direction defined by the wave vector k_0 of filling of the packet).

We also note that in contrast to the effect described in [2], the generated "flows" do not have a rapidly oscillating character in the vertical coordinate. This circumstance is obviously related to the fact that in the considered problem it was assumed that N_0 = const and accordingly the interaction transpires only for the

difference components of the wave vectors, and this means that a packet with a narrow spectrum can generate only waves with small projections of the wave vector along all the directions. Thus, with N_0 = const in the Boussinesq approximation the three-dimensional wave packet, like the mode [2], does not create a fine structure. However, in comparison with the case of propagation of the mode, when the generation of the "flows" was completely reversible [1], in this situation there is an irreversible radiation of packet energy into low-frequency waves. Physically this is related to the fact that in a modal case there was an almost resonance interaction [6], whereas in this case the radiated waves are in precise synchronism with the spectral components of the packet.

If small θ ($\theta \gg \sin^2\alpha/k_0L$) are not considered, then, as it can be seen, $C_e^2/L^2 \ll \omega_e^2$ and in (10b) it can be assumed that $Q = |\psi|^2/\omega_e^2$. In this case (10) is evidently reduced to a nonlinear Schrödinger equation:

$$i\psi_t + \frac{1}{2}\omega''\psi_{xx} - T|\psi|^2\psi = 0,$$

where $T = T_0 - T_1/\omega_e^2 = k_0^2 \sin^2\alpha \sin^2\varphi > 0$. In a plane case ($\varphi = 0$) there are no nonlinear effects. The stationary solution of this equation

$$\psi = \psi_0 \exp(-iT|\psi_0|^2 t)$$

is stable relative to a harmonic perturbation with the wave number $\varkappa$ if $\omega''T > 0$, and unstable if $\omega''T < 0$. The maximum instability gradient

$$\delta_{\max} = T|\psi_0|^2 = 2\omega_0 \sin^2\varphi k_0^2 |\zeta_0|^2$$

is attained with $\varkappa_{\max} = |\psi_0|(-2T/\omega'')^{1/2}$. Accordingly, this type of instability can be significant only for extremely short IW. As a simplification we will examine the case $\varphi = \pi/2$, when

$$\omega'' = \frac{N_0}{k_0^2 \sin\alpha}\left[\cos^2\alpha - \left(1 - \frac{3}{4}\sin^2 2\alpha\right)\cos^2\theta\right].$$

In this case the instability of the packet can occur only for high-frequency waves: $\omega_0 > (2/3)^{1/2}N_0 \approx 0.82N_0$, and the packet must be modulated in a direction adequately close to the vertical: $\cos^2\theta > \cos^2\alpha/1 - 3/4 \sin^2 2\alpha)$.

We will examine a packet modulated in an arbitrary way so that its spectrum no longer has a one-dimensional character. If the modulation effects in an almost vertical direction, considered above, are neglected, in formula (7) we can assume that

$$(2\pi)^3 T_{k_1k_2k_3} \approx T_0 - T_1/\omega_e^2 = k_0^2(\omega_0^2/N_0^2)\sin^2\varphi.$$

In this case, as is easy to confirm by direct computation

$$H \approx \int \psi^* \left(\omega_0 + i(C_g\nabla) - \frac{1}{2}\omega_{ij}''\frac{\partial^2}{\partial x_i\,\partial x_j}\right)\psi\,dr + \\ + \frac{1}{2}k_0^2\frac{\omega_0^2}{N_0^2}\int |\psi|^2 \frac{\partial^2}{\partial y^2}\Delta_H^{-1}|\psi|^2\,dr,$$

where $\Delta_H = \partial^2/\partial x^2 + \partial^2/\partial y^2$ and $\omega_{ij}'' = \partial^2\omega/\partial k_i \partial k_j$. The equations of motion after transformation to a coordinate system related to the packet acquires the form of Davey-Stewartson equations [9]

$$i\psi_t + \frac{1}{2}\omega_{ij}''\frac{\partial^2}{\partial x_i\,\partial x_j}\psi - k_0^2\frac{\omega_0^2}{N_0^2}\psi Q = 0,$$

$$\frac{\partial^2 Q}{\partial x^2} + \frac{\partial^2 Q}{\partial y^2} = \frac{\partial^2}{\partial y^2}|\psi|^2.$$

For the considered problem these equations were derived in [10] by the multiscale expansions method.

BIBLIOGRAPHY

1. Borisenko, Yu. D., Voronovich, A. G., Leonov, A. I. and Miropol'skiy, Yu. Z., "On the Theory of Nonstationary Slightly Nonlinear Internal Waves in a Stratified Fluid," IZV. AN SSSR: FAO (News of the USSR Academy of Sciences: Physics of the Atmosphere and Ocean), Vol 12, No 3, pp 293-302, 1976.

2. Voronovich, A. G., Leonov, A. I. and Miropol'skiy, Yu. Z., "On the Theory of Formation of Fine Structure of Hydrophysical Fields in the Ocean," OKEANOLOGIYA (Oceanology), Vol 16, No 5, pp 750-759, 1976.

3. Leonov, A. I., Miropol'skiy, Yu. Z. and Tamsalu, R. E., "Computing Fine Structure of the Density and Velocity Fields (In the Example of the Baltic Sea)," OKEANOLOGIYA, Vol 17, No 3, pp 389-394, 1977.

4. Goncharov, V. P., Krasil'nikov, V. A. and Pavlov, V. I., "Cerenkov Radiation of Internal Gravitational Waves," IZV. AN SSSR: FAO, Vol 12, No 12, pp 1310-1314, 1976.

5. Zakharov, V. Ye., "Hamiltonian Formalism for Waves in Nonlinear Media With Dispersion," IZV. VUZOV. RADIOFIZIKA (News of Schools of Higher Education. Radiophysics), Vol 17, No 4, pp 431-453, 1974.

6. Voronovich, A. G., "Hamiltonian Formalism for Internal Waves in the Ocean," IZV. AN SSSR: FAO, Vol 15, No 1, pp 82-92, 1979.

7. Zakharov, B. Ye. and Rubenchik, A. M., "Nonlinear Interaction of High-Frequency and Low-Frequency Waves," PMTF (Applied Mathematics and Technical Physics), No 5, pp 84-98, 1972.

8. Zakharov, V. Ye., L'vov, V. S. and Starobinets, S. S., "Instability of Monochromatic Spin Waves," FIZIKA TVERDOGO TELA (Solid-State Physics), Vol 11, No 10, pp 2972-2984, 1969.

9. Davey, A. and Stewartson, K., "On Three-Dimensional Packets of Surface Waves," PROC. ROY. SOC. LONDON, A338, pp 101-110, 1974.

10. Shrira, V. I., "On the Propagation of a Three-Dimensional Packet of Weakly Nonlinear Internal Gravity Waves," INT. J. OF NONLINEAR MECHANICS, Vol 16, No 2, pp 129-138, 1981.

5303
CSO: 1865/134

UDC 551.463.5:535.31

SOME PROPERTIES OF OPTICAL TRANSFER FUNCTION OF WAVE-COVERED SEA SURFACE

Moscow IZVESTIYA AKADEMII NAUK SSSR: FIZIKA ATMOSFERY I OKEANA in Russian Vol 18, No 3, Mar 82 (manuscript received 18 Nov 80) pp 330-333

[Article by A. G. Luchinin, Institute of Applied Physics, USSR Academy of Sciences]

[Text] The influence of waves on the properties of an image formed by an optical system was investigated in [1-4]. Depending on the purpose of the investigation, the authors have neglected different factors whose importance to a considerable degree is determined by the observation conditions. In this article it will be demonstrated how it is possible to modify the optical transfer function (OTF) of the wave-covered discontinuity in dependence on the difference in angles between the radiation incident on the surface and the direction of sighting. In order to simplify the problem we will neglect the effects of scattering in water, assuming that the object plane is situated at a small optical depth.

If the sea surface is illuminated by an infinitely wide beam of parallel rays and the image is formed by scanning with a narrow receiving diagram, the following expression [4] is correct for the optical transfer function in a small-angle approximation:

$F_\pi = F_{rec}$;
$n_\mu = n_{rad}$;
$n_\pi = n_{sight}$;
$z_\pi = z_{rec}$

$$K(\mathbf{h}) = \frac{\int\int\int\int_{-\infty}^{\infty} F_\pi\left(\mathbf{h}, \mathbf{h}z_\pi + \frac{\mathbf{k}L}{m}\right)\theta((\mathbf{h}-\mathbf{k})qL, \mathbf{k}qL)\, e^{-i(\mathbf{h}-\mathbf{k})(\rho+\Delta\rho)}\, d\rho\, d\mathbf{k}}{\int\int\int\int_{-\infty}^{\infty} F_\pi\left(0, \mathbf{k}\frac{L}{m}\right)\theta(-\mathbf{k}qL, \mathbf{k}qL)\, e^{i\mathbf{k}(\rho+\Delta\rho)}\, d\rho\, d\mathbf{k}}, \quad (1)$$

where $F_{rec}(h, h(z_{rec} + L/m))$ is the frequency-contrast characteristic of the receiving system; θ is a two-point characteristic function of the surface slopes; $\Delta\rho = (n_{rad} - n_{sight})L/m$, n_{rad} and n_{sight} are the projections of unit vectors describing the direction of the incident radiation and the direction of sighting onto the horizontal plane; m is the refractive index of water; $q = (m - 1)/m$, z_{rec} is the height of the receiver above the surface.

As is well known, the function K(h) characterizes the contrast transfer coefficient when making observations of an infinite sinusoidal mire with a period and direction described by the vector h and represents the normalized complex spectrum for the point scattering function. Our objective is a study of the behavior of this function (its modulus and phase) with different values of the $\Delta\rho$ parameter. The value

of this parameter gives some idea of how close to one another the rays incident and scattered on the plane at the depth L, participating in image formation, are refracted at the surface. Thus, reference is to that influence which is exerted on the OTF by the statistical dependence of the incident radiation and the radiation emanating from beneath the surface.

We will stipulate the function F_{rec} in the form $F_{rec} = \exp[-(hz_{rec} + kL/m)^2/2\beta^2]$.

With respect to the surface properties, we will assume that the waves are normal and uniform and that the correlation function of the surface rises has the form

$$B_\xi(\rho_x) = \sigma_\xi^2 \exp(-a\rho_x^2) \cos k_0\rho_x.$$

Omitting below the subscript indicating the one-dimensionality of the problem, in this case we write an expression for the OTF following from (1):

$$K(h) = \frac{\int_{-\infty}^{\infty} g^{-1/2} \exp\left\{\frac{(hp - i(\rho+\Delta\rho))^2}{4g}\right\} d\rho}{\int_{-\infty}^{\infty} g^{-1/2} \exp\left\{-\frac{(\rho+\Delta\rho)^2}{4g}\right\} d\rho}, \qquad (2)$$

where

$$g = q^2L^2(\sigma_\theta^2 - B_\theta(\rho)) + L^2\beta^2/2m^2,$$
$$p = g + L^2\beta^2/2m^2 + z_n L\beta^2/m,$$
$$B_\theta(\rho) = -d^2B_\xi/d\rho^2, \quad \sigma_\theta^2 = B_\theta(0).$$

The denominator in (2) is proportional to $\bar{P}(\Delta\rho)$ -- the mean power scattered by an infinite plane with a uniform reflection coefficient. As indicated in [5], this parameter, depending on the observation conditions, may be greater than or less than the corresponding value in the case of a smooth discontinuity. In essence this means that the wave-covered surface on the average plays the role of a collecting or scattering lens and our task is an investigation of its resolution.

Here we will introduce three cases differing qualitatively from one another.

I. The $\Delta\rho$ parameter is much greater than the correlation radius of the waves, so that $B_\theta(\Delta\rho)$ is close to zero. Then it is easy to see that in the region significant for integration in (2) the g function can be considered constant, the OTF is real and is described by the formula

$$K(h) \approx \exp(-0{,}5h^2\sigma_\theta^2 q^2 L^2),$$

derived in [1].

II. $\Delta\rho = 0$. In this case the OTF is also purely real (the imaginary part is rigorously equal to zero), but, as will be demonstrated, its form differs substantially from case I.

III. $\Delta\rho$ is finite, the imaginary part, and accordingly the phase of the OTF is different from zero.

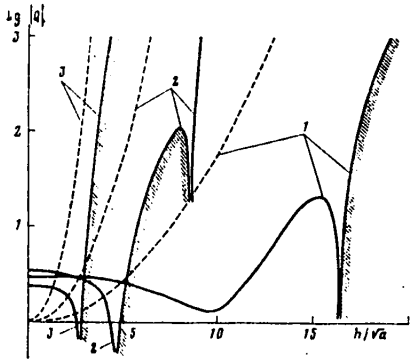

Fig. 1.

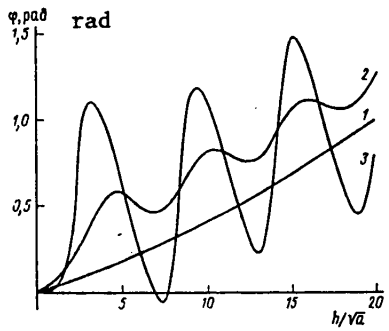

Fig. 2.

Fig. 1. Modulus of function Q(h) with $\Delta\rho = 0$; $\sigma_\xi^2 = 3.5\cdot10^{-4}$ m^2; a = 7.6 m^{-2}; k_0 = 1.8 m^{-1}; $\beta = 2.5\cdot10^{-5}$; z_{rec} = 100 m: 1) L = 5, 2) 10, 3) 20 m.

Fig. 2. Phase of optical transfer function with $\Delta\rho\sqrt{a} = 1$. For the remaining parameters see Fig. 1.

We will examine cases II and III in greater detail. In order to emphasize the effect of cross-correlation of fluctuations of incident and emerging radiation we will compute the function

$$Q(h)=K(h)[\bar{P}(\Delta\rho)/\bar{P}(\Delta\rho\to\infty)]\exp(0{,}5h^2\sigma_\theta^2q^2L^2),$$

which reveals the difference, first of all, of the mean transfer coefficient (with h = 0) and, second, the optical transfer function proper from case I. This function has the form:

$$Q(h)=\frac{1}{2\gamma\pi}\int_{-\infty}^{\infty}g^{-1/2}\exp\left\{\frac{(hp-i(\rho+\Delta\rho))^2}{4g}\right\}d\rho.$$

The results of the computations for case II are given in Fig. 1. We note the following significant properties of this function. In some regions (in Fig. 1 they are bounded by curves with a dashed line) it is negative, which corresponds to a change in the sign of contrast for the observed mire. This makes it possible to conclude that the scattering function in this case has a multimode character. The fact that a change in the contrast sign with an increase in the depth of the object plane occurs with lesser values of spatial frequency seems rather natural, as the scattering function in this case has a general tendency to broadening. The second peculiarity of the Q(h) function is an increase in the envelope of its extrema with an increase in h; that is, the presence of the correlation, which was mentioned above, leads to some contrast increase in comparison with case I. The true value

of the determined contrast can be judged by dividing the value Q(h)/Q(0) by $\exp(0.5h^2\sigma_\theta^2 q^2 L^2)$ (the dashed curves in Fig. 1 represent the value of this exponent at a logarithmic scale).

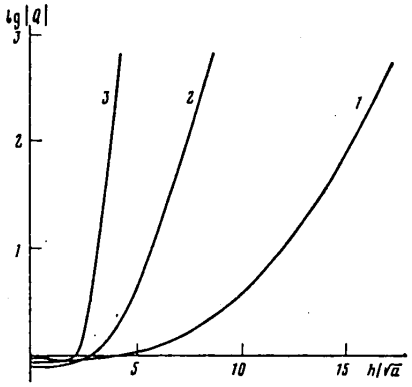

Fig. 3.

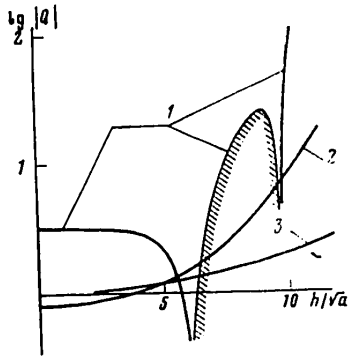

Fig. 4.

Fig. 3. Modulus of function Q(h) with $\Delta\rho\sqrt{a} = 1$.

Fig. 4. Modulus of function Q(h) with L = 20 m; $\sigma_\xi^2 = 1.1\cdot10^{-2}$ m^2; a = 0.4 m^{-2}; $k_0 = 0.46$ m^{-1}: 1) $\Delta\rho\sqrt{a} = 0$, 2) 1, 3) 2.5.

Now we will turn to case III. As already mentioned above, its most important criterion is a complexity of Q(h). Figure 2 shows the dependence of its phase value, which is identically equal to the phase of the OTF, on the spatial frequency for different depths with a fixed value of the $\Delta\rho$ parameter. In the case of a small depth (L = 5 m) the phase increases monotonically in the region of spatial frequencies shown in Fig. 2. In the case of greater depths its increase is accompanied by oscillations whose depth increases with an increase in the depth of the object plane L. With respect to the modulus of this function, it also increases with an increase in frequency; its value virtually coincides with the envelope of the extrema Q(h) in case II with the exception of the region of small spatial frequencies where it is close to unity (Fig. 3). With an increase in the $\Delta\rho$ parameter this region expands and the described effects become appreciable only for large spatial frequencies for which, however, the absolute value of the contrast is very small (see Fig. 4, whose curves were computed for larger-scale waves).

We emphasize in conclusion that the results cited here to a certain degree are of an illustrative character since the number of combinations of parameters exerting an influence on the magnitude of the effects is extremely great. For a quantitative description of their values under real conditions it is necessary, first of all, to have information on the form of the correlation functions of slopes for nonuniform waves for different wind velocities over the surface. It is also necessary to clarify the role of scattering in the water and to evaluate its influence

with different relationships of the length of the free path of protons and the correlation radii for surface waves.

The author expresses appreciation to I. M. Nefedov for assistance in carrying out the numerical computations and L. S. Dolin for useful discussions.

BIBLIOGRAPHY

1. Mullamaa, Yu.-A. R., "Influence of Wave-Covered Sea Surface on Visibility of Underwater Objects," IZV. AN SSSR: FAO (News of the USSR Academy of Sciences: Physics of the Atmosphere and Ocean), Vol 11, No 2, pp 199-206, 1975.

2. Veber, V. L., "Statistical Characteristics of Images Obtained in Observations Through an Uneven Discontinuity of Media With Different Refractive Indices," IZV. VUZOV. RADIOFIZIKA (News of Higher Educational Institutions. Radiophysics), Vol 22, No 8, p 989, 1979.

3. Veber, V. L. and Dolin, L. S., "Fluctuations of Images During Observations Through a Randomly Uneven Nonstationary Discontinuity," IZV. AN SSSR: FAO, Vol 17, No 11, pp 1168-1177, 1981.

4. Luchinin, A. G., "Some Patterns in Forming of the Image of the Shelf During its Observation Through the Wave-Covered Sea Surface," IZV. AN SSSR: FAO, Vol 17, No 7, pp 732-736, 1981.

5. Luchinin, A. G., "Influence of Wind Waves on the Characteristics of a Light Field Backscattered by the Bottom and a Water Layer," IZV. AN SSSR: FAO, Vol 15, No 7, pp 770-775, 1979.

5303
CSO: 1865/134

UDC 551.463.7

ONE MECHANISM FOR FORMING OF OCEANIC ELECTRIC FIELDS

Moscow IZVESTIYA AKADEMII NAUK SSSR: FIZIKA ATMOSFERY I OKEANA in Russian Vol 18, No 3, Mar 82 (manuscript received 30 Dec 80) pp 333-335

[Article by A. L. Virovlyanskiy and A. N. Malakhov, Gor'kiy State University]

[Text] In this communication we bring the attention of researchers to one possibility of the appearance of an electric field in a solution of electrolyte, specifically, sea water. The mechanism of field development, which is under discussion, is governed by the separation of charges due to different displacements of cations and anions during accelerated hydrodynamic motion of the solution. This effect applicable to the propagation of acoustic waves in an electrolyte solution was for the first time predicted theoretically by Debye [1] and then was confirmed repeatedly experimentally [2]. For this reason the electric field developing in the solution will henceforth be called a Debye field.

Another mechanism of the development of a field during the motion of sea water, caused by the movement of a conducting fluid in the earth's magnetic field (EMF), is well known [3-5]*. It is understandable that one and the same hydrodynamic motion is responsible for both of the mentioned effects. Below we will compare the contributions to the electric field from both effects for the simplest models of fluid motion. In these examples we will strive to understand in what cases it makes sense to take the Debye field into account and when it is masked by a field induced by motion in the EMF. In the computations we will neglect the influence of electric forces on macroscopic motion of the solution.

It was demonstrated in [7] that a Debye field develops with any accelerated motion of the solution. In [7] a formula was derived which makes it possible to find the strength of this field for arbitrary hydrodynamic motion:

$$E(r, t)=\beta \int_{-\infty}^{t} e^{-\alpha(t-t_1)} u_g(r, t_1)\, dt_1. \qquad (1)$$

* In addition, there are a number of reasons for the appearance of an electric field in the ocean associated with the presence of foreign bodies in the water, influence of the bottom, etc. [3-6]. These will not be considered here.

Here E(r, t) is the strength of the Debye field at the point r at the time t;

$$\alpha=(1/\varepsilon\varepsilon_0)\sum_{p=1}^{N}e_p^2\nu_p b_p;\qquad \beta=(1/\varepsilon\varepsilon_0)\sum_{p=1}^{N}e_p\nu_p m_p b_p;$$

e_p, m_p, b_p are the charge, mass and mobility of an ion of the p-th species; ν_p is the mean number of ions of the p-th species in a unit volume; $\varepsilon\varepsilon_0$ is the dielectric constant of the solvent; N is the number of species of ions in the solution; $\dot{u}_g(r, t_1)$ is the eddy-free component of the vector field of accelerations in the fluid, taken at the point r at a moment in time $t_1 \leqslant t$. In the examples considered below reference will be to the eddy-free motions of a fluid and therefore there $\dot{u}_g = \dot{u} \equiv \partial u/\partial t + (u\nabla)u$ is the total acceleration of the solution.

As indicated in [7], the numerical values of α and β can be computed theoretically only with a great error which it is difficult even to estimate. This is attributable to the fact that in determining m_p and b_p it is necessary to take into account the phenomenon of hydration of ions, the theory of which at the present time has not been adequately developed*. Accordingly, α and β, strictly speaking, must be determined experimentally.

In the evaluation we will use the values of these parameters, computed on the assumption that sea water is a 0.5-molar NaCl solution. In order to determine m_p we will reckon the Na^+ and Cl^- hydration numbers to be equal to 6 and 8 respectively [8]. In determining the mobilities we will employ the values of the equivalent conductivities of these ions [9]. Thus, we obtain $\alpha = 0.9\cdot10^{10}$ 1/sec, $\beta = 0.7\cdot10^4$ kg/A·sec^2.

The principal contribution to the integral (1) is from acceleration values in the time interval $(t - 1/\alpha, t)$. Since $1/\alpha \sim 10^{-10}$ sec, which is known to be much less than any time scales of hydrodynamic motion, the factor $\dot{u}_g(r, t)$ can be removed from beneath the integral. Formula (1) in this case is transformed into

$$E(r, t)=(\beta/\alpha)\dot{u}_g(r, t)\quad(\beta/\alpha=0{,}8\cdot10^{-6}\ \text{kg/A·sec}). \tag{1a}$$

As we see, computation of the Debye field for any stipulated motion of sea water presents no difficulties. The situation is different with computation of the electric field induced by motion in the EMF. However, there are also no fundamental difficulties here: it is necessary to solve the Maxwell equations in a moving conducting fluid with corresponding boundary conditions at the water-air and water-bottom interfaces. However, it is possible to obtain a solution of such a system of equations in partial (although linear) derivatives in analytical form only for the simplest motions of a fluid; the corresponding formulas usually have a rather unwieldy form [5]. Precisely for this reason as examples we selected very simple models of hydrodynamic motions, especially since we are interested primarily in an evaluation in order of magnitude.

---

* Debye [1] proposed that the mass of a hydrate shell be determined on the basis of measurements of the electric field arising during the propagation of an acoustic wave in the electrolyte solution.

As the first example we will examine a monochromatic surface gravitational wave propagating in a fluid of infinite depth. Assume that the undisturbed surface coincides with the xy-plane and the z-axis is directed vertically dowanward. The wave travels along the x-axis and its amplitude is sufficiently small so that in the computations it is possible to use the linearized equations of hydrodynamics. Using the known formulas for the field of velocities in such a wave (see, for example [10]) and formula (1a), we obtain an expression for the components of strength of the Debye field

$$E_x=-i\omega v_x\beta/\alpha, \quad E_y=0, \quad E_z=-i\omega v_z\beta/\alpha, \tag{2}$$

where $v_x(r, t)$, $v_z(r, t)$ are the projections of velocity onto the x- and z-axes, ω is the angular frequency of the wave.

The strength of the electric field of the surface wave induced by motion in the EMF has been computed in many studies (see [5] and the citations given there). For this case

$$E_x'=\mu\mu_0 H_y v_z, \quad E_z'=-\mu\mu_0 v_x H_y, \quad E_y'=\mu\mu_0(v_x H_z-v_z H_x), \tag{3}$$

where $E_{x,y,z}(r, t)$ are the projections of the electric field onto the coordinate axes, $\mu\mu_0$ is the permeability of sea water (usually μ is very close to 1), $H_{x,y,z}$ are the projections of EMF strength onto the x-, y- and z-axes.

It is easy to show that E_x and E_x' (and in exactly the same way, E_z and E_z') are shifted in phase by $\pi/2$ relative to one another.

Since v_x and v_z differ from one another only in phase, it follows from (2) and (3) that:

$$|E_z/E_x'|=|E_x/E_z'|=(\omega\beta/\alpha)/\mu_0|H_y|. \tag{4}$$

This ratio is highly dependent on the projection of the EMF onto the y-axis, that is, on the direction of wave propagation. In evaluating the minimum value of this ratio we will assume H_y = 0.5 oe. Then

$$|E_z/E_x'|=|E_x/E_z'|\approx\omega\cdot 10^{-2}, \tag{5}$$

where ω is measured in degrees/sec. The waves really existing in the ocean usually have $\omega\lesssim 1$ degree/sec. Thus, it follows from (5) that in this case the Debye field is greatly masked by a field caused by motion in the EMF. Formally the ratio (4) increases to infinity with $H_y\to 0$, that is, if the direction of wave propagation coincides with the projection of the EMF onto the xy-plane, but scarcely never does the Debye field become "predominant," since, to be sure, there are no plane surface waves in the ocean.

It can be seen from (2) and (3) that for the given example of fluid motion the fields caused by the two considered mechanisms differ in directions. This circumstance is characteristic for many fluid motions. Its cause can be seen particularly graphically from an examination of the following very simple model of a current [3, 5]. Assume that in a fluid (the positioning of the axes is the same as in the

preceding example) there is a moving layer of the thickness h. The motion occurs along the y-axis; the velocity in the layer varies in conformity to the law $v_y = v_0(x)e^{i\omega t}$. In this case the velocity and acceleration vectors are collinear and therefore the Debye field is also directed along the y-axis. The field induced by motion in the EMF is perpendicular to this axis since the Lorenz force perpendicular to velocity does not create separations of charges in the y-direction. Thus, for this hydrodynamic motion the developing electrical fields are orthogonal to one another.

In conclusion we will examine the propagation of longitudinal compressional-dilatational (acoustic and shock) waves in sea water. As in the preceding example, acceleration and velocity here are directed in the same direction. Accordingly, the Debye electric field and the electric field induced by motion in the EMF in this case are also orthogonal to one another.

Assume that a plane acoustic wave, the velocity of the fluid in which changes in conformity to the law $v(r, t) = u_0 e^{i(kr-\omega t)}$, travels in the water; the vectors u_0 and k are collinear. From (1a) we obtain the value of strength of the Debye field

$$E(r, t) = -i(\beta/\alpha)u_0\omega \exp[i(kr-\omega t)]. \quad (6)$$

In the evaluation we take $\omega = 10^5$ rad/sec, $u_0 = 10^{-2}$ m/sec. In this case $|E| \sim 10^{-3}$ V/m.

For computing the field induced by motion in the EMF, we use the general method in [5]. Omitting the elementary computations, we immediately cite the result:

$$E'(r, t) = (i\omega\mu_0^2\sigma[u_0 \times H]/(k^2 - i\omega\mu_0\sigma))\exp[i(kr-\omega t)], \quad (7)$$

σ is the conductivity of sea water. In the evaluations we assume $\sigma = 4.5$ cm/m. The ratio of the amplitudes (6) and (7) is equal to ($\omega = 10^5$ rad/sec): $|E/E'| = 1.2 \cdot 10^7$. In this case $|E \gg E'|$.

Since the Debye field is proportional to the acceleration of the fluid, it can attain especially high values at the front of an explosive wave. It is easy to visualize that the amplitude of this field at the shock wave front can be evaluated using the formula

$$E \approx (\beta/\alpha)Mc_0^2/l, \quad (8)$$

where M is the Mach number of the wave, c_0 is the speed of sound, l is front width. In the evaluation taking the real characteristics of the explosive wave: $M = 10^{-2}$, $c_0 = 1.5 \cdot 10^{-2}$, $l = 1.5$ cm, from (8) we find that $E \approx 1.2$ V/m.

On the basis of the considered examples some conclusions can be drawn concerning the role which the Debye effect plays in the general pattern of formation of the electric field in the ocean. First of all, we note that the Debye field, in accordance with (1a), is directly proportional to the eddy-free part of fluid acceleration. For the natural movements of water in the ocean the acceleration will rarely be more than 1 m/sec^2, which corresponds to an amplitude of the Debye field of 1 μV/m. The experimentally measured electric fields of natural origin in

the ocean usually have a strength from tenths to tens of μV/m [3-5]. Thus, it can be said qualitatively that the Debye field introduces a real, although a small contribution to the creation of the general pattern of the natural electromagnetic field in the ocean. This can also be seen in the considered examples. In addition, it can be concluded from these examples that the Debye field usually differs from the field induced by movement in the EMF either in phase or in direction.

Hydrodynamic movements with an acceleration substantially greater than 1 m/sec^2 are usually related to man's activity. As indicated by the third example, for such movements the Debye field in its amplitude considerably exceeds the field induced by movement in the EMF.

BIBLIOGRAPHY

1. Debye, P. A., "A Method for the Determination of the Mass of Electrolytic Ions," J. CHEM. PHYS., Vol 1, p 13, 1933.

2. Styuer, Dzh. and Yeger, E., "Propagation of Ultrasonic Waves in Electrolyte Solutions," FIZICHESKAYA AKUSTIKA (Physical Acoustics), edited by U. M. Mason, Mir, 1968.

3. Shuleykin, V. V., FIZIKA MORYA (Sea Physics), Moscow, Nauka, 1968.

4. Akindinov, V. V., Naryshkin, V. I. and Ryazantsev, A. M., "Electromagnetic Fields in Sea Water (Review)," RADIOTEKHNIKA I ELEKTRONIKA (Radio Engineering and Electronics), Vol 21, No 5, pp 913-944, 1976.

5. Sachel'nikov, V. V., OSNOVY TEORII YESTESTVENNOGO ELEKTROMAGNITNOGO POLYA V MORE (Principles of the Theory of the Natural Electromagnetic Field in the Sea), Leningrad, Gidrometeoizdat, 1979.

6. Leybo, A. B., "Electrokinetic Phenomena Associated With Sea Waves," GEOMAGNETIZM I AERONOMIYA (Geomagnetism and Aeronomy), Vol 17, No 3, pp 502-506, 1977.

7. Virovlyanskiy, A. L. and Malakhov, A. N., "Electric Field of an Arbitrarily Moving Electrolyte," IZV. VUZOV: RADIOFIZIKA (News of Higher Educational Institutions: Radiophysics), Vol 24, No 7, pp 851-854, 1981.

8. Izmaylov, N. A., ELEKTROKHIMIYA RASTVOROV (Electrochemistry of Solutions), Moscow, Khimiya, 1966.

9. KRATKIY SPRAVOCHNIK FIZIKO-KHIMICHESKIKH VELICHIN (Concise Handbook of Physicochemical Parameters), Leningrad, Goskhimizdat, 1959.

10. Uizem, Dzh., LINEYNYYE I NELINEYNYYE VOLNY (Linear and Nonlinear Waves), Moscow, Mir, 1977.

5303
CSO: 1865/134

UDC 551.466.4

GENERATION OF INTERNAL WAVES BY BOTTOM IRREGULARITY AT DISCONTINUITY OF TWO FLUIDS FLOWING AT ANGLE TO ONE ANOTHER

Novosibirsk ZHURNAL PRIKLADNOY MEKHANIKI I TEKHNICHESKOY FIZIKI in Russian
No 6, Nov-Dec 81 (manuscript received 12 Sep 80) pp 41-47

[Article by I. V. Sturova, Novosibirsk]

[Text]

Abstract: The simplest example of three-dimensional internal waves in a flow whose velocity changes with depth both in intensity and direction are waves at the discontinuity of two fluids flowing at an angle to one another. The investigation of the kinematic characteristics of wave movement in such a fluid under the condition that the depth of the lower layer is infinite was made in [1]. The asymptotic behavior of the waves at the discontinuity arising during flow around a body for the case of infinitely deep layers and an obstacle at the bottom under the condition of an infinite thickness of the upper layer was examined in [2]. The stability of waves arising at the discontinuity of two unlimited flows flowing at an angle to one another was investigated in [3].

We will examine flow around a rise described by the function f(x, z), unbounded in horizontal directions by a flow, in whose upper layer of the thickness H_1 the density of the fluid is equal to ρ_1, in the lower layer of the thickness H_2 -- $\rho_2 = \rho_1(1 + \varepsilon)(\varepsilon \geqslant 0)$. The velocity of the lower flow is equal to U_2 and is directed along the x-axis, the velocity of the upper flow is U_1 and forms the angle α with the x-axis. The x- and z-axes are situated at the undisturbed discontinuity, the y-axis is directed vertically upward, the axis of symmetry of the obstacle passes through the origin of coordinates.

Assuming the motion of the fluid within each layer to be eddy-free and the disturbances at the free surface and the discontinuity are small, the equations for the velocity potentials of disturbed motion in each layer are written in the form

$$\Delta\varphi_1 = 0 \text{ with } 0 \leqslant y \leqslant H_1,\ \Delta\varphi_2 = 0 \text{ with } H_2 \leqslant y < 0 \qquad (1)$$

with the boundary conditions at the free surface ($y = H_1$)

$$\partial\varphi_1/\partial y + L_1\zeta = 0,\ L_1\varphi_1 = g\zeta; \tag{2}$$

at the discontinuity ($y = 0$)

$$\partial\varphi_1/\partial y + L_1\eta = 0,\ \partial\varphi_2/\partial y + L_2\eta = 0,\ \rho_2 L_2\varphi_2 - \rho_1 L_1\varphi_1 = g(\rho_2 - \rho_1)\eta; \tag{3}$$

at the bottom ($y = -H_2$)

$$\partial\varphi_2/\partial y + L_2 f = 0,\ \varphi_1,\ \varphi_2 \to 0 \quad \text{with } x^2 + z^2 \to \infty,$$

where

$$L_1 \equiv U_1(\cos\alpha\cdot\partial/\partial x + \sin\alpha\cdot\partial/\partial z),\ L_2 \equiv U_2\partial/\partial x.$$

Here the functions $\zeta(x, z)$ and $\eta(x, z)$ describe the vertical displacements of the free surface and discontinuity respectively, g is the acceleration of gravity. In the investigation of internal waves in many cases at the free surface instead of condition (2) use is made of the simpler "solid lid" condition, for which $\partial\varphi_1/\partial y = 0$ with $y = H_1$.

We introduce dimensionless variables, as the scale units for length and velocity using the values $h = f(0, 0)$ (height of rise) and U_2 and employing the Fourier transform

$$\varphi_*(\mu, y, \nu) = \int_{-\infty}^{\infty} e^{-i\mu x}dx \int_{-\infty}^{\infty} e^{-i\nu z}\varphi(x, y, z)\,dz$$

for real μ and ν, from equation (1) we obtain a system of ordinary differential equations whose solution gives the following representations for the functions $\zeta_*(\mu, \nu)$ and $\eta_*(\mu, \nu)$, being the Fourier transform of the functions ζ and η:

$$\zeta_* = \frac{4k^2d_1^2d_2^2f_*(1+\varepsilon)e^{-k(H_1+H_2)}}{(1+e^{-2kH_1})(1+e^{-2kH_2})D},$$

$$\eta_* = \frac{2kd_2^2f_*(1+\varepsilon)e^{-kH_2}}{(1+e^{-2kH_2})D}(kd_1^2 - \Lambda\,\mathrm{th}\,kH_1),$$

$$D = \Lambda D_1 - kd_1^2D_2;$$

$$D_1(k, \theta) = [\varepsilon\Lambda\,\mathrm{th}\,kH_2 - (1+\varepsilon)kd_2^2]\,\mathrm{th}\,kH_1 - kd_1^2\,\mathrm{th}\,kH_2;$$

$$D_2(k, \theta) = (\varepsilon\Lambda - kd_1^2\,\mathrm{th}\,kH_1)\,\mathrm{th}\,kH_2 - (1+\varepsilon)kd_2^2;$$

$$d_1 = V\sin(\theta+\alpha);\quad d_2 = \sin\theta;\quad \Lambda = gh/U_2^2;\quad V = U_1/U_2;$$

f_* is the Fourier transform $f(x, z)$ and the following substitution is made

$$\mu = k\sin\theta,\ \nu = k\cos\theta.$$

With use of the "solid lid" condition at the free surface η_* assumes the form

$$\eta_* = -\frac{2kd_2^2 f_* (1+\varepsilon) e^{-kH_2} \operatorname{th} kH_1}{\left(1+e^{-2kH_2}\right) D_1}.$$

Performing inverse Fourier transforms, we obtain

$$\eta(x,z) = \frac{1}{4\pi^2}\int_{-\infty}^{\infty} e^{i\mu x}d\mu \int_{-\infty}^{\infty} e^{i\nu z}\eta_* d\nu = \frac{1}{2\pi^2}\operatorname{Re}\int_0^{\pi} d\theta \int_0^{\infty} k e^{ikr\sin(\theta+\varphi)}\eta_* dk, \tag{4}$$

where the substitution x = r cos φ, z = r sin φ is made. A similar expression exists for the function ζ (x, z) as well.

The functions ζ_* and η_* have simple poles being roots of the equation D(k, θ) = 0 or D_1(k, θ) = 0. It can be confirmed that with

$$\Lambda[V^2H_2\sin^2(\theta+\alpha) + H_1\sin^2\theta] - V^4\sin^2\theta\sin^2(\theta+\alpha) < \frac{\varepsilon\Lambda H_1H_2}{1+\varepsilon}$$

the equation D(k, θ) = 0 has the two positive roots $\bar{k}_{1,2}$ ($\bar{k}_1 < \bar{k}_2$), otherwise there is only one root $\bar{k}_2$. The equation D_1(k, θ) = 0 has no more than one positive root $\bar{k}_1$ and only under the condition

$$V^2H_2\sin^2(\theta+\alpha) + (1+\varepsilon)H_1\sin^2\theta < \varepsilon\Lambda H_1H_2.$$

In selecting the integration contour in the k-plane in (4) we will use the Rayleigh method for introducing small dissipative forces [1] proportional to the velocities of fluid particles. In the initial problem (1)-(3) changes are experienced only by the dynamic conditions at the free surface in (2) and at the discontinuity in (3), which now will have the form

$$L_1\varphi_1 + \beta\varphi_1 = g\zeta,\ \rho_2L_2\varphi_2 - \rho_1L_1\varphi_1 + \beta(\rho_2\varphi_2 - \rho_1\varphi_1) = g(\rho_2-\rho_1)\eta,$$

where $\beta > 0$ is a dissipation coefficient which is small in value. The solution of problem (1) with these boundary conditions shows that the poles of the integrand in (4) with $\beta \to 0$ have the form k = $\bar{k}$ + i$\beta\gamma$, where, for example, under the "solid lid" condition

$$\gamma = \frac{2\bar{k}_1\left[V\sin(\theta+\alpha)\operatorname{cth}\bar{k}_1H_1 + (1+\varepsilon)\sin\theta\operatorname{cth}\bar{k}_1H_2\right]}{\varepsilon\Lambda - \bar{k}_1^2\left[(1+\varepsilon)H_2\sin^2\theta/\operatorname{sh}^2\bar{k}_1H_2 + V^2H_1\sin^2(\theta+\alpha)/\operatorname{sh}^2\bar{k}_1H_1\right]}.$$

Accordingly, in (4) the integration contour is selected in quadrant I or quadrant IV as a function of the sign on sin (θ + φ); all its real poles are "bypassed" by semicircles on which with $\gamma < 0$ Im k < 0, with $\gamma < 0$ Im k > 0. In [2] this circumstance was not taken into account and all the poles were "bypassed" from below.

As a result, the integral representations for the sought-for functions can be written in the form of the sum of single integrals governed by the presence of the poles and the double integrals arising as a result of integration along the imaginary axis, which henceforth will be discarded from consideration since they describe local effects in the neighborhood of the rise and rapidly decrease with an increase in r.

The final expression for the function η(r, φ) (and similarly for ζ (r, φ)) has the form

$$\eta(r,\varphi) = -\frac{1}{\pi}\sum_{j=1}^{2}\int_{a_j}^{b_j}\bar{k}_j\sin(\bar{k}_j\sin(\theta+\varphi))\operatorname{Res}\eta_*(\bar{k}_j,\theta)\,d\theta,$$

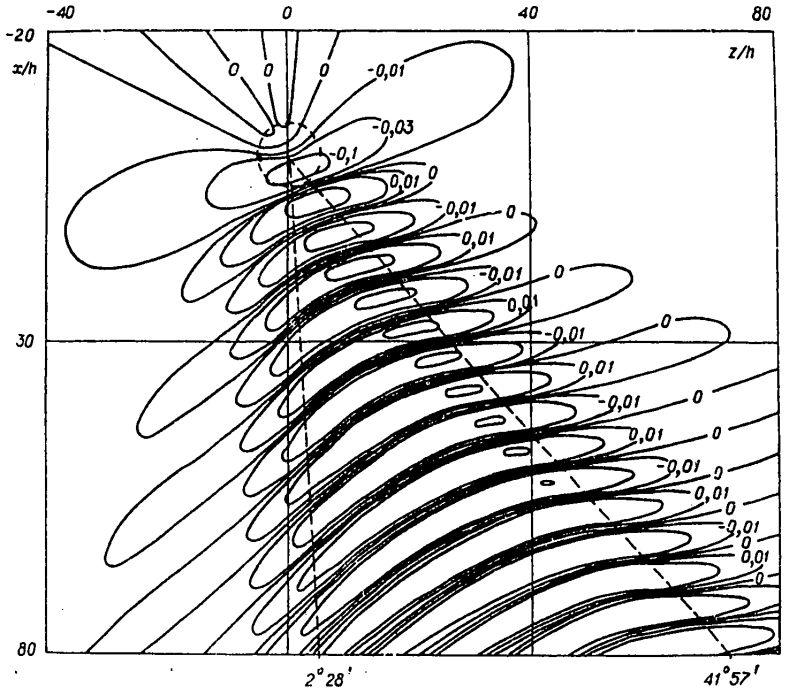

Fig. 2.

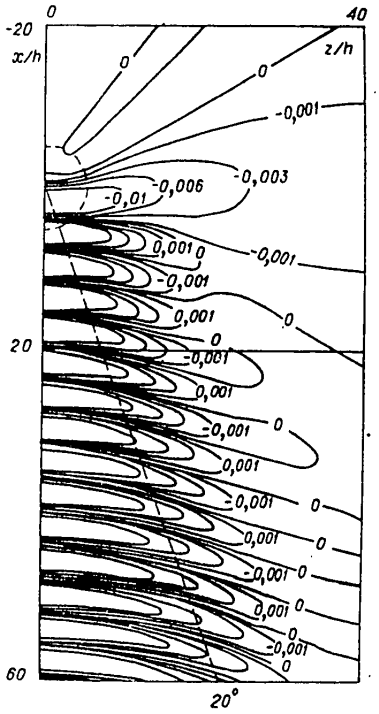

Fig. 3.

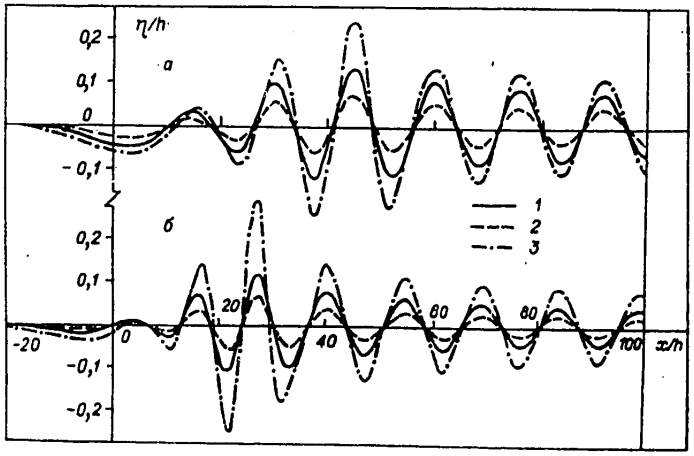

Fig. 5.

where $\bar{k}_i$ is the root of the equation $D(k, \theta) = 0$ or $D_1(k, \theta) = 0$ and integration is carried out using those intervals of the θ values in which sgn $(\sin(\theta+\varphi))$ = sgn (γ).

With satisfaction of the specific computations the form of the axisymmetric rise on the bottom was stipulated in two types:

$$f(r) = 1 - r^2/d^2 \quad \text{with} \quad 0 \leqslant r \leqslant d,\ f(r) = 0 \quad \text{with} \quad d < r < \infty, \qquad f_*(k) = 4\pi J_2(kd)/k^2, \tag{5}$$

where J_2 is a second-order Bessel function of the first kind.

$$f(r) = d^3/(d^2 + 2r^2)^{3/2} \qquad f_*(k) = \pi d^2 \exp(-dk/2)/2, \quad \text{with} \quad 0 \leqslant r < \infty, \tag{6}$$

with which the volumes of both rises coincide and are equal to $S = \pi d^2/2$. As a comparison we also investigated the case of flow around a dipole situated at the bottom at the point x = 0, z = 0 with the axis directed along the x-axis and a moment equal to S. In this case $f_* = S$. As is well known (see, for example, [4]), such an approximation is used when investigating internal waves generated by a moving body.

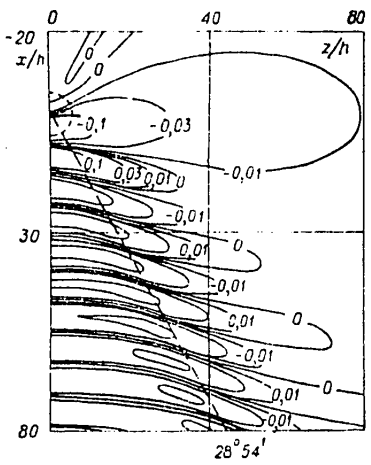

Fig. 1.

Numerical computations of the function $\eta(x, z)$ were made for two V and α values with $\Lambda = 100$, $\varepsilon = 10^{-2}$, $H_1/h = 2$, $H_2/h = 5$. Figures 1-4 represent isolines of the function $\eta(x, z)/h$ with V = 1, $\alpha = 0.45°$ (Figures 1, 2) and V = 0.5, $\alpha = 0.45°$ (Figures 3, 4) for an obstacle described by function (5) with d = 5; the dashed lines represent the boundaries of wave zones determined by the stationary phase method like in [2]. The circle with its center at the origin of coordinates corresponds to the boundary of the rise. With $\alpha = 0$ the pattern of the current is symmetric relative to the x-axis. In Figures 1, 2 the isolines are defined with the following levels: 0, $\pm 10^{-2}$, $\pm 3 \cdot 10^{-2}$, $\pm 10^{-1}$, $\pm 3 \cdot 10^{-1}$; in Figures 3, 4 -- 0, $\pm 10^{-3}$, $\pm 3 \cdot 10^{-3}$, $\pm 6 \cdot 10^{-3}$, $\pm 10^{-2}$, $\pm 3 \cdot 10^{-2}$.

It should be noted that with these values of the initial parameters the difference between the solutions obtained with use of the full conditions at the free boundary and the "solid lid" condition does not exceed 1%. The vertical displacements at the free surface are several orders of magnitude less than at the discontinuity.

An investigation of the influence of the form of an obstacle on the amplitude of internal waves indicated that a dipole approximation gives exaggerated values. Figure 5 represents the function $\eta(x, z)/h$ as a function of x with z/h = 20 and the mentioned Λ, ε, H_1, H_2 values for V - 1(a - α = 0, b - α = 45°). Curves 1-3 correspond to the rises stipulated by expressions (5), (6) and the dipole

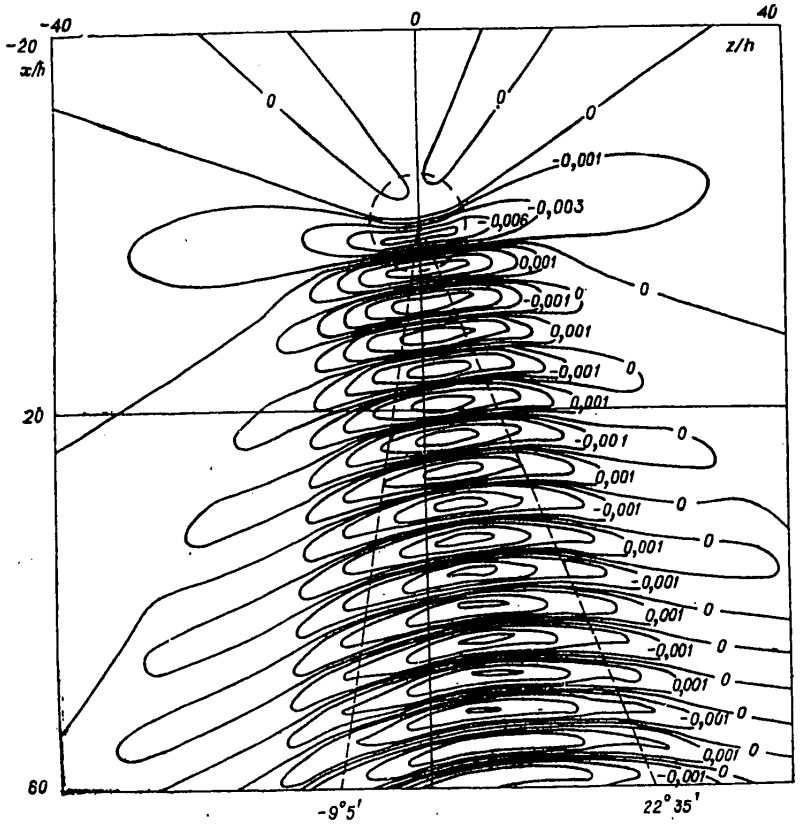

Fig. 5.

approximation. With V = 0.5 and different α the amplitudes of the waves for both types of rises become very close, but their discrepancy with the dipole approximation is still more substantial than with V = 1.

The author of [3] investigated the stability of waves developing at the discontinuity of two unbounded flows directed at an angle to one another. The results in that study are easily applied to the case of flows of finite depth when the "solid lid" conditions are satisfied at the free surface. Waves with a wave number k will be stable if

$$\frac{k}{(1+\varepsilon)\operatorname{th} kH_1 + \operatorname{th} kH_2} < \frac{\Lambda\varepsilon}{(1+\varepsilon)[V\sin(0+\alpha)-\sin 0]^2}.$$

For the stationary problem considered above the resulting wave movement is always stable.

BIBLIOGRAPHY

1. Sretenskiy, L. N., TEORIYA VOLNOVYKH DVIZHENIY ZHIDKOSTI (Theory of Wave Movements of a Fluid), Moscow, Nauka, 1977.

2. Kochina, I. N., "Waves at the Interface of Two Fluids Flowing at an Angle to One Another," PMM (Applied Mathematics and Mechanics), Vol 19, No 5, 1955.

3. Gandin, L. S., "Stability of Waves at Interface of Flows Directed at an Angle to One Another," IZV. AN SSSR, SER. GEOFIZICHESKAYA (News of the USSR Academy of Sciences, Geophysical Series), No 3, 1957.

4. Miles, J. W., "Internal Waves Generated by a Horizontally Moving Source," GEOPHYSICAL FLUID DYNAMICS, Vol 2, p 1, 1971.

5303
CSO: 1865/129

UDC 532.593

ASSOCIATED INTERNAL WAVES IN FLUID WITH EXPONENTIAL DENSITY DISTRIBUTION

Novosibirsk ZHURNAL PRIKLADNOY MEKHANIKI I TEKHNICHESKOY FIZIKI in Russian No 6, Nov-Dec 81 (manuscript received 13 Oct 80) pp 47-54

[Article by S. A. Makarov and Yu. D. Chashechkin, Moscow]

[Text]

Abstract: On the basis of the modified stationary phase method proposed in [1, 2], the authors of [3] in a plane and a three-dimensional case determined surfaces of a constant phase of internal waves excited by a body moving at an arbitrary angle to the horizon, satisfactorily coinciding with the experimentally observed waves. With allowance for the integral transforms in [4, 5], the author of [6] used numerical methods for examining, in a linear formulation, the plane and spatial problem of wave movements arising during flow around submerged "inflow" and "outflow" of identical intensity by a uniform flow of a density-stratified fluid. The asymptotic solution for the wave field excited by the "inflow"-"outflow" system, moving in an exponentially stratified fluid, was obtained in [7, 8]. These solutions describe the wave pattern arising during the movement of a body at high velocities. The objective of this study is a determination of the amplitude-phase characteristics of associated internal waves in a fluid with an exponential density distribution with a uniform horizontal motion of the body in a wide range of motion regimes (including movements at low velocities) with their subsequent comparison with the results of laboratory experiments. In the solution no allowance is made for dissipative and diffusional effects (that is, the change in the density of particles during their motion is not taken into account) or the influence of the free surface. It is assumed that the fluid is of infinite depth.

The system of hydrodynamic equations determining the field of velocities v has the form

$$(\partial/\partial t + \mathbf{v}\nabla)\rho\mathbf{v} = -\nabla p + \rho\mathbf{g},\ (\partial/\partial t + \mathbf{v}\nabla)\rho = 0,\ \nabla\mathbf{v} = m, \tag{1}$$

where t is time; ρ is density; p is pressure; g is the acceleration of gravity; m(x, y, z, t) is the distribution of inflows and outflows in the fluid; $\nabla = l\partial/\partial x + m\partial/\partial y + n\partial/\partial z$.

The examination is made in the laboratory coordinate system OXYZ (the X-axis is directed along the line of movement of the body, the Z-axis is directed vertically upward) and the coordinate system $OX^*YZ(x^* = x - Ut)$ is related to the body.

The problem is solved in the Boussinesq approximation. The dimensional parameters of the problem are: $\rho_0(z) = \rho_0(0) \exp[-z/\Lambda]$ is the density of the fluid; the stratification scale is $\Lambda = [d \ln \rho_0(z)/dz]^{-1}$; the period T and the frequency of free internal oscillations in the fluid is $N = \sqrt{g/\Lambda}$, $T = 2\pi/N$; d is the vertical dimension and L is the horizontal dimension of the body and U is the velocity of its motion; η_0 is the amplitude and A is the phase of the internal wave.

The dimensionless parameters: $Fr = U^2/N^2d^2$ is the internal Froude number; $C = \Lambda/d$ is the ratio of scales; $\Psi = L/d$ is the lengthening of the body; $x^0 = x^*N/AU$, $y^0 = yN/AU$, $z^0 = zN/AU$ are dimensionless coordinates.

Eddy-free flow around a body by a current of a uniform ideal fluid is equivalent to flow around a combination of inflows and outflows [9]. This result can also be applied to a stratified fluid in the case of small gradients when the density of the fluid changes insignificantly at distances of the order of the dimension of the body [6].

The motion of a dipole and a system consisting of an inflow of equal intensity situated at the distance 2a is considered.

The linearized system (1), with allowance for the correlation between the vertical deviation of a surface of constant density from an equilibrium position $\eta(x, y, z, t)$ and the vertical velocity component [7], is reduced to the following equation:

$$\left\{\frac{\partial^2}{\partial t^2}\left(\frac{\partial^2}{\partial x^2}+\frac{\partial^2}{\partial y^2}+\frac{\partial^2}{\partial z^2}\right)+N^2\left(\frac{\partial^2}{\partial x^2}+\frac{\partial^2}{\partial y^2}\right)\right\}[\rho_0(z)\eta(x,y,z,t)] = \frac{\partial}{\partial t}\frac{\partial}{\partial z}[\rho_0(z)m(x,y,z,t)]. \tag{2}$$

The values m(x, y, z, t) for the movement of plane and three-dimensional bodies are given in [6, 7].

We will seek a solution of equation (2) with zero boundary conditions at infinity. Steady wave motion is examined.

The internal waves forming during the uniform motion of a body in a stratified fluid are called "associated" because the wave pattern is stationary in the coordinate system related to the body.

The asymptotic solution of equation (2), taking into account that with uniform horizontal motion of the body $\omega = -\alpha U$, has the form [1]

$$\eta(x^*, y, z) = \frac{4\pi^2}{r^*} \sum \frac{BF(\alpha, \beta, \gamma) \exp[i(\alpha x^* + \beta y + \gamma z)]}{|\nabla_k G| \sqrt{|K|}} + O\left(\frac{1}{r^{*2}}\right) \tag{3}$$

with $r^* \to \infty$ along any radius-vector q; summation is carried out for all points $k = \{\alpha, \beta, \gamma\}$ on the wave number surface determined by the dispersion expression

$$G(\alpha, \beta, \gamma) = (\alpha U)^2(\alpha^2 + \beta^2 + \gamma^2) - N^2(\alpha^2 + \beta^2) = 0, \tag{4}$$

at which the normal to the surface is parallel to q and

$$\frac{\mathbf{r}^* \cdot \nabla_k G}{\frac{\partial G}{\partial \omega}} > 0 \left(\nabla_k = \mathbf{l}\frac{\partial}{\partial \alpha} + \mathbf{m}\frac{\partial}{\partial \beta} + \mathbf{n}\frac{\partial}{\partial \gamma}\right) \tag{5}$$

under the condition that the surface (4) has a nonzero Gaussian curvature K at each of these points [1]. The coefficient B is dependent on the sign of the curvature and the configuration of the wave number surface (4), $F(\alpha, \beta, \gamma)$ is a Fourier transform of the right-hand side of equation (2).

By analogy with [1], in a plane case (coordinates $\{x, z\}$) the asymptotic solution (2) is

$$\eta(x^*, z) = \sqrt{\frac{8\pi^3}{r^*}} \sum \frac{BF(\alpha, \gamma) \exp\left[i\left(\alpha x^* + \gamma z + \frac{\pi}{4} \operatorname{sgn} K\right)\right]}{|\nabla_k G| \sqrt{|K|}} + O\left(\frac{1}{r^*}\right) \tag{6}$$

where $r^* \to \infty$ along any radius-vector q; summation is carried out for all points $k = \{\alpha, \gamma\}$ by the curve

$$G(\alpha, \gamma) = (\alpha U)^2(\alpha^2 + \gamma^2) - N^2\alpha^2 = 0,$$

where the normal to the curve is parallel to q and (5) is satisfied.

As indicated by formulas (3), (6), the constant-phase surfaces have the form $k \cdot r^* = A$. Since the r^* vector is parallel to the normal of the surface G = 0 at the point k, then

$$\mathbf{r}^* = \frac{A}{\mathbf{k} \cdot \nabla_k G} \nabla_k G. \tag{7}$$

It follows from solution of system (7) with (4) taken into account that the constant-phase surfaces in a three-dimensional case are described by the equation

$$(x^0)^2 = [(y^0)^2 + (z^0)^2]\left[\frac{1}{(z^0)^2} - 1\right], \tag{8}$$

which coincides with [3, 10]. In a plane case

$$(x^0)^2 + (z^0)^2 = 1. \tag{9}$$

Formulas (8), (9) were derived for a point source when there is no interference of the waves excited by its different parts, which can change the resultant patterns of the constant-phase surface.

The inequality (5) is the radiation condition, according to which all the waves are generated by a source and do not arrive from infinity. It follows from this that wave formation occurs only behind the moving body, that is, with $x^* < 0$, whereas in spherical coordinates $\{r^*, \varphi, \theta\}$, related to the body, $x^* = r^* \cos\theta$, $y = r^* \cos\theta$, $y = r^* \sin\theta \cos\varphi$, $z = r^* \sin\theta \sin\varphi$ with $\theta > \pi/2$.

The points $k = \{\alpha, \beta, \gamma\}$ of the wave number surface (4), at which the normal to the surface coincides with the selected direction $r^* = (x^*, y, z)$, is found from the system

$$(\alpha U)^2(\alpha^2 + \beta^2 + \gamma^2) - N^2(\alpha^2 + \beta^2) = 0, \quad [\nabla_k G \cdot \mathbf{r}^*] = 0. \tag{10}$$

The vector equation of system (10) contains two linearly independent equations. Taking into account α, β and γ determined from (10):

$$\pm\frac{N}{U}\sin\varphi\cos\theta,\ \beta = \pm\frac{N}{U}\frac{\cos^2\theta}{\sin\theta}\sin\varphi\cos\varphi,\quad \gamma = \pm\frac{N}{U}\frac{1-\cos^2\theta\sin^2\varphi}{\sin\theta}$$

the wavelength is

$$\lambda = \frac{2\pi}{\sqrt{\alpha^2+\beta^2+\gamma^2}} = \frac{UT}{\sqrt{1+\frac{x^{*2}y^2}{(y^2+z^2)^2}}} = \frac{UT\sin\theta}{\sqrt{1-\sin^2\varphi\cos^2\theta}}. \tag{11}$$

In the plane y = 0 the wavelength is everywhere identical and equal to $\lambda_0 = UT$; outside this plane λ tends to zero with approach to the X-axis.

In the case of uniform horizontal motion of the dipole in a deep fluid with a weak stratification the vertical displacement η, determined from (3), coincides with the solution in [7]. With small U (accordingly large k) in the solution in [7] there is a singularity in the form 1/U.

In the case of movement of the inflow-outflow system it follows from (3) that

$$\eta_1(r^*, \theta, \varphi) = \frac{R^2}{r^*}\frac{\sqrt{a^2+R^2}}{a}\frac{\sqrt{1-\sin^2\varphi\cos^2\theta}}{\sin\theta},$$
$$\sin\left(\frac{Na}{U}\sin\varphi\cos\theta\right)\cos\left(\frac{Nr^*}{U}\sin\varphi\right) + O\left(\frac{1}{r^{*2}}\right), \tag{12}$$
$$r^* \to \infty,\ \pi/2 < \theta < \pi \qquad (\text{with } \theta = \pi,\ K = 0).$$

The vertical displacement (12) does not become equal to zero when U→0. With transformation to a laboratory coordinate system $\eta_1(x, y, z, t)$ at a fixed point x, y, z ($y \neq 0$) does not tend to zero when $t \to \infty$, the same as the solution in [7].

In a plane case with flow around a dipole it follows from (6) that

$$\eta_2(x^*, z) = \sqrt{\frac{2\pi}{r^*}}R^2\frac{z}{r^*}\sqrt{\frac{N}{U}}\cos\left(\frac{Nr^*}{U} - \frac{\pi}{4}\right) + O\left(\frac{1}{r^*}\right), \tag{13}$$
$$r^* \to \infty,\ x^* < 0,$$

with flow around the inflow-outflow system

$$\eta_3(x^*, z) = \sqrt{\frac{2\pi}{r^*}} \frac{R}{\operatorname{arctg}\left(\frac{a}{R}\right)} \frac{z}{x^*} \sqrt{\frac{U}{N}} \times \sin\left(\frac{Na}{U}\frac{x^*}{r^*}\right)\cos\left(\frac{Nr^*}{U} - \frac{\pi}{4}\right) + O\left(\frac{1}{r^*}\right), \quad r^* \to \infty,\ x^* < 0. \tag{14}$$

Both $\eta_2(x, z, t)$ and $\eta_3(x, z, t)$ tend to zero when $t \to \infty$, but only (14) becomes equal to zero when $U \to 0$.

The above-mentioned singularities of the solutions for point disturbances -- of a dipole [7], and of an inflow-outflow pair (12) -- are indicative of the non-equivalence of substitution of the motion of a three-dimensional body in a non-viscous fluid to motion of point disturbances not only with low velocities [7], but with high velocities, when $Fr \gg 1$, and can be eliminated by substitution of the delta functions in system (1) by a series of classical functions of the type

$$\frac{\exp[-r^2/l^2]}{(l\sqrt{\pi})^3} \to \delta(\mathbf{r}), \quad l \to 0. \tag{15}$$

The considered case of flow around distributed inflow and outflow at the distances $bl < r \ll \Lambda\ (b \gg 1)$ is equivalent to flow around point inflow and outflow of equal intensity $M_1 = M_0\ \mathrm{erf}^3(b)$, which corresponds to flow around an ovoid, where M_0 is the intensity of the point sources [9].

Then, from (3), with (15) taken into account, it follows that in the Boussinesq approximation ($\lambda_0 = UT \ll \Lambda$)

$$\eta^+(r^*, \theta, \varphi) = \exp\left[\frac{l^2}{4\Lambda^2}\right]\exp\left[-\left(\frac{\pi l}{\lambda}\right)^2\right]\frac{R^2}{r^*}\frac{\sqrt{a^2+R^2}}{a}\frac{\sqrt{1-\sin^2\varphi\cos^2\theta}}{\sin\theta} \times \sin\left(\frac{Na}{U}\sin\varphi\cos\theta\right)\cos\left(\frac{Nr^*}{U}\sin\varphi + \operatorname{sgn}(\sin\varphi)\frac{l^2N}{2\Lambda U}\frac{1-\sin^2\varphi\cos^2\theta}{\sin\theta}\right) + O\left(\frac{1}{r^{*2}}\right), \quad r^* \to \infty, \quad \frac{\pi}{2} < \theta < \pi. \tag{16}$$

The second exponential factor leads to a rapid attenuation of (16) with $U \to 0$ and exerts a small influence with large U. In the case of high velocities $\eta^+ \sim 1/U$ with a decrease in velocity the amplitude $|\eta_0^+|$ of the vertical displacement (16) has maxima at the points U_n, determined with $l \ll \lambda_0/\pi$ from the condition

$$\frac{Na}{U_n}|\sin\varphi\cos\theta| = \frac{\pi}{2} + \pi n, \quad n = 0, 1, 2, \ldots \tag{17}$$

With an increase in l the maxima of amplitude are displaced insignificantly in the direction of greater U.

The dependence of the amplitude of internal waves on the flow-around velocity in the case of small U, such that $Fr_a = U^2/(N^2a^2) < 1$, is attributable to the interference of waves from coherent sources (inflow and outflow), situated at the distance

2a. In the XZ-plane the maxima of the amplitude are observed with $U = U_n$, determined from

$$\frac{Na}{U_n}|\cos\theta| = \frac{\pi}{2}(2n+1), \quad n = 0, 1, 2, \ldots, \tag{18}$$

it therefore follows that

$$2a|\cos\theta| = n\lambda_n + \lambda_n/2, \ \lambda_n = U_n T,$$

which is the interference condition. The appearance of $\lambda_n/2$ is related to the opposite effect of inflow and outflow.

It follows from (18) that in the case of low velocities ($Fr_a<1$) there are several maxima of amplitude at different θ_n angles

$$|\cos\theta_n| = \frac{U}{Na}\frac{\pi}{2}(2n+1), \quad n = 0, 1, 2, \ldots \tag{19}$$

With an increase in velocity the maxima are displaced toward the wake axis.

With motion of an elongated body with the lengthening $\xi = a/R$ the amplitude of the internal wave is $|\eta_0^+| \sim 1 + \xi^2$ with $Fr_a \gg 1$, which coincides with [6]; with $Fr_a<1$ $|\eta_0^+| \sim \sqrt{1 + 1/\xi^2}$ and decreases with an increase in lengthening.

With motion of distributed inflow-outflow the form of the constant-phase surface differs somewhat from (8), since the phase "additive"

$$\operatorname{sgn}(\sin\varphi)\frac{l^2 N}{2\Lambda U}\frac{1-\sin^2\varphi\cos^2\theta}{\sin\theta},$$

enters into (16), whose value increases with approach to the X-axis.

From (16), with transformation to a laboratory coordinate system OXYZ, it follows that

$$\begin{aligned}\eta^+(O, y, z, t) = &-\exp\left[\frac{l^2}{4\Lambda^2}\right]\exp\left[-\frac{N^2 l^2}{4U^2}\left(1+\frac{(Ut)^2 y^2}{(y^2+z^2)^2}\right)\right]\times\\ &\times\frac{\sqrt{a^2+R^2}}{a}\frac{R^2}{\sqrt{y^2+z^2}}\sqrt{1-\frac{z^2}{y^2+z^2}\frac{(Ut)^2}{(Ut)^2+y^2+z^2}}\times\\ &\times\sin\left(\frac{Na}{U}\frac{z}{\sqrt{y^2+z^2}}\frac{Ut}{\sqrt{(Ut)^2+y^2+z^2}}\right)\cos\left\{\frac{N}{U}\sqrt{(Ut)^2+y^2+z^2}\times\right.\\ &\left.\times\left[\frac{z}{\sqrt{y^2+z^2}}+\frac{l^2}{2\Lambda}\frac{\operatorname{sgn}(z)}{\sqrt{y^2+z^2}}\left(1-\frac{z^2}{y^2+z^2}\frac{(Ut)^2}{(Ut)^2+y^2+z^2}\right)\right]\right\}+\\ &+O\left(\frac{1}{(Ut)^2+y^2+z^2}\right), \quad \sqrt{(Ut)^2+y^2+z^2}\to\infty, \quad t>0.\end{aligned} \tag{20}$$

Expression (20) becomes equal to zero for $t\to\infty$ when y = 0 due to a decrease in the term

$$\sqrt{1-\frac{z^2}{y^2+z^2}\frac{(Ut)^2}{(Ut)^2+y^2+z^2}},$$

with $y \neq 0$ due to a decrease in the second exponential factor. The frequency of oscillations with an increase in time tends to

$$\frac{N}{\sqrt{y^2+z^2}}\left[z+\frac{l^2}{2\Lambda}\frac{y^2}{y^2+z^2}\right]\simeq N\frac{z}{\sqrt{y^2+z^2}}.$$

The first oscillations have a period which is somewhat greater than $T(\sqrt{y^2+z^2})/z$.

The asymptotic solution is applicable at great (in comparison with the wavelength) distances from the source:

$$r^* \gg \lambda_0. \tag{21}$$

The linearity criterion is the inequality

$$|\eta_0| \ll \lambda.$$

If $\lambda \leqslant \pi l$, the linear solution (16) is correct when there is satisfaction of the condition

$$r^* \gg \frac{\lambda_0 R^2}{e(\pi l)^2}\frac{\sqrt{a^2+R^2}}{a}\left|\sin\left(\frac{Na}{U}\sin\varphi\cos\theta\right)\right|, \tag{22}$$

which with $Fr_a \lesssim 1$ is equivalent to $$r^* \gg \frac{R^2\lambda_0}{\lambda^2}\frac{\sqrt{a^2+R^2}}{a},$$

and with $Fr_a \gg 1$ $$r^* \gg \frac{2\pi R^2\sqrt{a^2+R^2}}{\lambda^2}|\sin\varphi\cos\theta|.$$

here e is the base of natural logarithms.

If $\lambda > \pi l$, the linear solution (16) is correct when there is satisfaction of the inequality

$$r^* \gg \frac{R^2\lambda_0}{\lambda^2}\frac{\sqrt{a^2+R^2}}{a}\left|\sin\left(\frac{Na}{U}\sin\varphi\cos\theta\right)\right|, \tag{23}$$

which with $Fr_a \lesssim 1$ is equivalent to

$$r^* \gg \frac{\lambda_0 R^2}{e(\pi l)^2}\frac{\sqrt{a^2+R^2}}{a},$$

and with $Fr_a \gg 1$

$$r^* \gg \frac{2R^2\sqrt{a^2+R^2}}{e\pi l^2}|\sin\varphi\cos\theta|,$$

It follows from (22), (23) that there is a region near the X-axis where a linear solution is incorrect.

An experimental investigation of associated internal waves was carried out in a laboratory basin measuring 1.5 x 0.4 x 0.4 m filled with an aqueous solution of common salt with a uniform concentration (density) gradient, Λ = 4.4 m, N = 1.5 sec^{-1}, T = 4.2 sec. The phase patterns were registered using an IAB-451 shadow instrument; amplitudes were registered with a "single-point" conductivity contact converter [11]. The boundaries of the dark and light bands on the shadow photograms are the wave crests and troughs, the blackening density is proportional to the wave amplitude. Our experiments indicated that as a result of the entrainment effect in the stratified fluid (blocking effect) the velocity and density profiles of the fluid change at distances of the order of the diameter ahead of and behind the body. It can therefore be assumed that internal waves are generated by the entire system consisting of the body and the fluid entrained by it. Due to the presence of viscosity the entrained fluid has the form of an ovoid.

Figure 1 shows the wave pattern in the plane XZ arising during the horizontal motion of an elongated body d = 1 cm, L = 8 cm with the velocity U = 1 cm/sec, T = 4.2 sec. The bend in the wave surfaces observed on the cited kinogram is attributable to a phase jump by π with a change in the sign on $\sin((Na/U)\cos\theta)$. The θ_p angles at which the bend occurs are determined from the condition

$$(Na/U)\,|\cos\theta_p| = \pi p,\ p = 1, 2, 3,\ldots \qquad (24)$$

In this case ($\theta_p = 56°$, p = 1) it follows from (24) that 2a = 7.6 cm; this approximately coincides with L.

As a result of the blocking effect a similar pattern can be observed during the motion of a sphere (Fig. 2, y = 0, d = 2 cm, U = 1.02 cm/sec, T = 4.2 sec, Fr = 0.11, $\theta_1 = 20°$). The a value determined from (24) is 2.25 cm.

Fig. 3 shows the wave pattern in the plane XZ arising during horizontal motion of a sphere d = 2 cm with a velocity U = 0.64 cm/sec, T = 4.2 sec, Fr = 0.044. With a decrease in velocity there is an increase in the effective horizontal dimension of the region of excitation of internal waves. On the shadow kinogram there is a bend of the phase surface at the angle $\theta_p = 39°$ (p = 2) and the interference maximum of the amplitude at an angle $\theta_n = 22°$ (n = 2) to the axis of motion. The substitution of the indicated θ_n and θ_p values into formulas (18), (24) gives close values for the half-distance between the centers of the sources a_1 = 3.6 cm, a_2 = 3.45 cm.

The resulting solutions (13), (14), (16) are antisymmetric relative to the plane (line) z = 0 in a three-dimensional (plane) case. Mathematically this is associated with a change in the sign on $\sin\varphi$ or (z) with transition from the upper half-space (half-plane) into the lower, and physically -- with opposite initial displacements in these half-spaces (half-planes). Figures 1-3 show that the wave crest in the upper half-plane corresponds to a trough in the lower. [Figures 1-3 are not reproduced here.]

Figure 4 is a trace showing measurement of the vertical displacement of fluid particles $\eta(0, y, z, t)$ in the case of horizontal motion of the sphere d = 2.5 cm with the velocity U = 1.65 cm/sec, T = 4.2 sec, Fr = 0.19 at the point y = 0, z =

5 cm. The points 1, 3, 5 represent troughs and the points 2, 4, 6 represent wave crests. The arrival times of the wave crests and depressions computed on the basis of (16) at the measurement points t_n = 2.9, 5.5, 7.8, 10, 12.1, 14.2 sec (n = 1, 2,...,6) coincide well with the experimentally observed values even for the first waves. For this case the solution (16) agrees with the experimental data with the choice a = 2.5 cm, $l \simeq 1$ cm; then the computed ratios of amplitudes of oscillations

$$\frac{|\eta_0|_{n+2}+|\eta_0|_{n+1}}{|\eta_0|_{n+1}+|\eta_0|_n}$$

(n = 1, 2, 3, 4) are equal to 1.4, 1.38, 1.25, 1.2. It follows from the trace that these ratios are 0.88, 1.56, 1.24 and 1.14. With an increase in distance to the source there is a decrease in the difference between the computed and observed values.

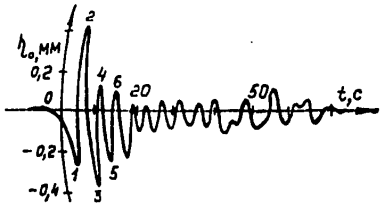

Fig. 4.

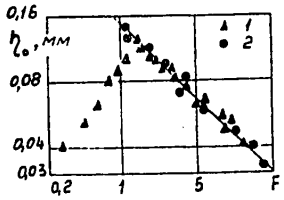

Fig. 5.

Figure 5 shows the dependence of the maximum displacement of particles in an internal wave in the case of horizontal motion of a sphere of the diameter d = 1 cm in a fluid with Λ = 4.2 m (points 1) and Λ = 17 m (points 2) at the point y = 0, z = 12 cm. The slope of the straight line on the graph corresponds to the dependence $Fr^{-1/2}$, which coincides with the law of decrease in amplitude $\eta_0 \sim 1/U$ with $Fr \gg 1$; with $Fr < 0.8$ $l \simeq 1.3$ cm.

In the case of motion of a sphere at great velocities ($Fr > 1$) $l < d/4$, $a < d$ and decreases with an increase in velocity.

The resulting solution (16) agrees satisfactorily with the data from laboratory experiments already at distances of the order of $2\lambda_0$.

Since with $Fr \ll 1$ the wavelength is less than or of the order of the dimensions of the body, in determining the amplitude characteristics of internal waves it is necessary to take the influence of viscosity into account.

BIBLIOGRAPHY

1. Lighthill, M. J., "Studies on Magneto-hydrodynamic Waves and Their Anisotropic Wave Motions," PHIL. TRANS. ROY. SOC. OF LONDON, Vol 252A, No 1014, 1960.

2. Lighthill, M. J., "On Wave Generated in Dispersive Systems by Travelling Forcing Effects With Applications to the Dynamics of Rotating Fluids," J. FLUID MECH., Vol 27, Pt 4, 1967.

3. Peat, K. S. and Stevenson, T. N., "Internal Waves Around a Body Moving in a Compressible Density-Stratified Fluid," J. FLUID MECH., Vol 70, Pt 4, 1975.

4. Wu, T. Y. T. and Mei, C. C., "Two=Dimensional Gravity Waves in a Stratified Ocean," PHYS. FLUIDS, Vol 10, No 3, 1967.

5. Mei, C. C., "Surface Wave Pattern Due to a Submerged Source Travelling in a Stratified Ocean," REPORT HYDRODYNAM. LAB. MASS. INST. TECHNOL., No 92, 1966.

6. Sturova, I. V., "Wave Movements Arising in a Stratified Fluid During Flow Around a Submerged Body," PMTF (Applied Mathematics and Technical Physics), No 6, 1974.

7. Miles, J. W., "Internal Waves Generated by a Horizontally Moving Source," GEOPHYSICAL FLUID DYNAMICS, Vol 2, 1971.

8. Dokuchayev, V. P. and Dolina, I. S., "Radiation of Internal Waves by Sources in an Exponentially Stratified Fluid," IZV. AN SSSR: FIZIKA ATMOSFERY I OKEANA (News of the USSR Academy of Sciences: Physics of the Atmosphere and Ocean), Vol 13, No 6, 1977.

9. Kochin, N. Ye., Kibel', I. A. and Roze, N. V., TEORETICHESKAYA GIDROMEKHANIKA (Theoretical Hydromechanics), Part I, Moscow, GIFML, 1963.

10. Nekrasov, V. N., Trokhan, A. M. and Chashechkin, Yu. D., "Generation of Internal Waves in a Plane-Stratified Medium by a Uniformly Moving Hydrodynamic Source (Three-Dimensional Problem)," KRATKIYE TEKSTY DOKLADOV VII VSESOYUZ. SIMPOZIUMA PO DIFRAKTSII I RASPROSTRANENIYU VOLN (Short Texts of Reports at the Seventh All-Union Symposium on Wave Diffraction and Propagation), Vol 3, Moscow, 1977.

11. Levtsov, V. I. and Chashechkin, Yu. D., "Highly Sensitive Converter for Conductivity of Fluids," TEZISY DOKLADOV IV VSESOYUZ. KONF. "METROLOGIYA V RADIOELEKTRONIKE" (Summaries of Reports at the Fourth All-Union Conference "Metrology in Radioelectronics"), Moscow, VNIIFTRI, 1978.

5303
CSO: 1865/129

UDC 532.5.51

PARAMETRIC RESONANCE IN STRATIFIED FLUID

Novosibirsk ZHURNAL PRIKLADNOY MEKHANIKI I TEKHNICHESKOY FIZIKI in Russian No 6, Nov-Dec 81 (manuscript received 6 Mar 81) pp 168-174

[Article by V. A. Vladimirov, Novosibirsk]

[Text]

Abstract: Parametric resonance is one of the widespread types of instability of mechanical systems. Parametrically excited oscillations constitute a somewhat broader class of phenomena. A mathematical determination of this class of oscillations is usually given [1] for systems whose equations of motion are reduced to ordinary differential equations in time. The parametric oscillations are related to the coefficients (parameters) of these equations by a periodic dependence on time. Such oscillations differ from forced oscillations, for which the explicit dependence on time is contained in the equations only additively, in the form of periodic forces. A standard example of the equations of parametric oscillations is the Mathieu equation and its generalizations. The first investigation of parametric oscillations was an experimental study by Faraday [2] in which a study was made of the oscillations of the free surface of a fluid in a vessel. However, later it was for the most part the applications to the mechanics of solid and elastic bodies which were developed [1, 3, 4]. An exception is the problem of oscillations of the free surface of a fluid in a vertically oscillating vessel. It was demonstrated in [5-7] that the displacement of the free surface in a linear approximation is reduced to the Mathieu equation and accordingly there are resonance frequencies at which the surface is unstable. Allowance for viscosity in this problem was introduced in [8]. It is only during the last decade that studies have begun on the parametric instability of more complex flows. The authors of [9, 10] made a study of parametric resonance in convection problems. The instability of Rossby waves was investigated in [11, 14]. Studies [15, 16] were devoted to the instability of internal waves in a stratified fluid. Source [15] gives

a number of considerations on the possibility of an increase in microscale disturbances against a background of an internal wave. A theoretical investigation of the parametric instability of a plane internal wave in the Boussinesq approximation is given in [16]. It is shown that a wave of a finite amplitude can be unstable. Within the range of small amplitudes parametric instability undergoes transition into known [17] resonance interactions of waves.

In this article a study is made of parametric resonance in a stratified fluid. In the cases of vertically oscillating vessels with a fluid and a horizontal plane-parallel flow it was possible to obtain the instability conditions and it is shown that instability of the same kind is observed in internal waves. Here the idea of the similarity of the physical conditions of the motion of a fluid in an oscillating vessel and in a wave is important. The differences are that the oscillations are not solid-body oscillations and their frequencies are not stipulated arbitrarily. However, if a long internal wave is examined, then locally (for short-wave disturbances) the conditions are close to those of a solid oscillating fluid. The studied type of instability of internal waves was omitted from consideration in [16]. An investigation of the mechanisms by which the destruction of internal waves can occur is of great interest in relation to the applications in oceanology [15-18]. Parametric resonance possibly can compete with the mechanism proposed in [18]. The latter essentially involves the appearance of zones in a wave in which the density increases upward. We also note the interesting hypothesis [11, 12, 15, 16] that the parametric instability of wave movements can be the mechanism of a "loss of predictability" of the current and the generation of turbulence.

1. We will examine a rectangular vessel filled with an ideal incompressible fluid. At the initial moment in time (t = 0) the fluid occupies the volume $0<x<a$, $0<y<b$, $0<z<c$. The density of the fluid is $\rho_0 = Ae^{-\beta y}$ ($A>0$, β are constants). The uniform gravity field has only a y-component (0, -g, 0). The buoyancy (Brunt-Väisälä) frequency is $N^2 = \beta g = \text{const}$. The vessel moves in the y-direction with the velocity $\dot{Y}(t) = dY/dt$; Y(t) is a periodic function (oscillations of a finite amplitude). "Non-flowthrough" conditions are satisfied at the boundaries of the vessel. The state of rest of the fluid relative to the vessel is a solution of the equations of motion. Its stability must be investigated.

We will transform to a coordinate system related to the vessel:

$$\bar{x} = x,\ \bar{y} = y - Y(t),\ \bar{z} = z,\ \bar{t} = t.$$

In these coordinates the equations of motion of the fluid have the same form as in the initial coordinates; only the gravity field g is replaced by $G \equiv g + \ddot{Y}$. The linearized system of equations for the disturbances has the form

$$\rho_0 u_t = -p_x,\ \rho_0 w_t = -p_z,$$
$$\rho_0 v_t = -p_y - \rho G,\ \rho_t + \rho_0' v = 0,\quad u_x + v_y + w_z = 0, \tag{1.1}$$

the line over x, y, z, t has been omitted. The notations u, v, w are used to designate the x, y, z components of velocity disturbances; ρ, p are density and pressure disturbances. The subscripts denote the partial derivatives, $\rho'_0 \equiv d\rho_0/dy$. The substitution $\sigma = p/\rho_0$, $r = \rho/\rho_0$ reduces (1.1) to a system of equations with coefficients not dependent on x, y, z

$$u_t = -\sigma_x,\ w_t = -\sigma_z,$$
$$v_t = -\sigma_y + \beta\sigma - Gr,\ r_t - \beta v = 0,\ u_x + v_y + w_z = 0, \tag{1.2}$$

allowing a separation of variables. For r, the equation

$$Dr_{tt} + \beta G(r_{xx} + r_{zz}) = 0, \tag{1.3}$$

follows from (1.2), where $D = \Delta - \beta\partial/\partial y$; Δ is a triangular Laplace operator. The substitution $r = \varphi e^{\beta y/2}$ transforms (1.3) into

$$(\Delta - \beta^2/4)\varphi_{tt} + \beta G(\varphi_{xx} + \varphi_{zz}) = 0. \tag{1.4}$$

The eigenfunction of the problem is

$$\varphi = R(t)k_1k_3 \cos k_1x \sin k_2y \cos k_3z, \tag{1.5}$$

where $k_1, k_2, k_3 \equiv (n_1/a, n_2/b, n_3/c)$; n_1, n_2, n_3 are arbitrary whole numbers. The components u, v, w, computed from (1.2), (1.5), satisfy the boundary conditions. It follows from (1.4), (1.5) that

$$\ddot{R} + B(N^2 + \beta\ddot{Y})R = 0, \tag{1.6}$$

where

$$B \equiv (k_1^2 + k_3^2)/(k^2 + \beta^2/4);\quad k^2 \equiv k_1^2 + k_2^2 + k_3^2.$$

Equation (1.6), as a result of the periodicity of Y(t), is the Hill equation [19]. With $Y = C\cos\omega t$ it is reduced to the Mathieu equation:

$$\ddot{R} + B(N^2 - \beta\omega^2 C \cos\omega t)R = 0,$$

whose canonical form is

$$R_{\tau\tau} + (a - 2q\cos 2\tau)R = 0, \tag{1.7}$$

where $\tau = \omega t/2$; $a = 4BN^2/\omega^2$; $q = 2BC$. The stability of the solutions (1.7) was studied in detail in [19, 20]. On the plane a, q (with $a > 0$) the unstable regions constitute "tongues" emanating from the points $a = m^2$, $m = 1, 2, 3, \ldots$ With small amplitudes C of vessel oscillations the solutions (1.7) are unstable in narrow zones around the points:

$$\omega = 2NB^{1/2}/m. \tag{1.8}$$

Such an instability is called parametric resonance [1, 3, 4], the number m is the order of resonance. Since B 1, for the existence of resonance of the order m it is necessary that $\omega < 2N/m$. For these dimensions of the vessel a, b, c and the buoyancy frequency N there is a four-parameter (with respect to n_1, n_2, n_3, m) set of frequencies ω of oscillations of the vessel (1.8) in which there is resonance. In all cases here and in the text which follows by the term "instability" is meant an exponential increase in the solutions with $t \to \infty$.

The preceding results were obtained for equilibrium density stratification $N^2 \equiv \beta g > 0$. At the same time it follows from (1.7) that with satisfaction of the conditions

$$\sqrt{2B|N^2|}/\omega < CB|\beta| < 1/2 + 2B|N^2|/\omega^2 \tag{1.9}$$

the oscillations of the vessel make stable a state with an increase in density upward ($N^2 < 0$). If the amplitude of the oscillations C is small, the right-hand side of (1.9) is always satisfied. The left-hand side gives the condition

$$\omega C > (2g/|\beta|B)^{1/2}. \tag{1.10}$$

The discussed property of stabilization of a nonequilibrium state is an analogue of the known result for a pendulum for which the upper position becomes stable with oscillations of the suspension point [21]. Still closer analogues are stabilization of Rayleigh-Taylor instability oscillations [22] and convection [23]. However, in contrast to these stablization cases it is impossible to achieve a nonequilibrium stratified fluid. In (1.10) this corresponds to an impairment of the inequality when $B \to 0$. Small B values are attained either with $k_1^2 + k_3^2$ or when $k_2 \to \infty$. Due to the limited dimensions of the vessel the first case is excluded. Accordingly, waves which are short in a vertical direction are dangerous. It is possible that here the stabilization can be achieved by the introduction of viscosity.

Another interesting corollary (1.7) is the instability of a flow in the absence of a gravity field g = 0. The instability condition (approximate [20]) is:

$$|C| > (2|\beta|)^{-1}.$$

Such an instability can be important for predicting the behavior of a stratified fluid under weightlessness conditions.

Allowance for the viscosity of a fluid leads to a replacement of the operator $\partial/\partial t$ before the velocity components in (1.1) by $\partial/\partial t - \nu\Delta$. Under the condition of a constancy of the coefficient of kinematic viscosity ν = const in place of (1.4) we obtain the equation

$$(\Delta - \beta^2/4)[\varphi_{tt} - \nu(\Delta + \beta^2/4 + \beta\partial/\partial y)\varphi_t] + \beta G(\varphi_{xx} + \varphi_{zz}) = 0.$$

The solution of the problem with satisfaction of the attachment conditions at the boundaries of the vessel is extremely complex and can be considered as a generalization of [8, 10]. We will examine an infinite vessel. After separation of the variables

$$\varphi = R(t)\, e^{i(k_1 x + k_2 y + k_3 z)}$$

we obtain the equation

$$\ddot{R} + \lambda \dot{R} + B(N^2 + \beta \ddot{Y})R = 0, \tag{2.1}$$

being a generalization of (1.6). This equation is the Hill equation (or Mathieu equation with Y = C cos ω t) with friction. The form of the friction coefficient is unusual:

$$\lambda = \nu(k^2 - \beta^2/4 - ik_2\beta).$$

For example, with $N^2 + \beta \ddot{Y} = 0$ from (2.1) for different k it is possible to obtain both attenuation and growth. Such a behavior of R(t) is related to the unlimited character of the selected solutions (1.1) with any fixed t. In the Boussinesq approximation (see below) the solutions are limited and $\lambda = \nu k^2$, which always corresponds to attenuation.

3. A direct generalization of the considered problem is the problem of the vertical oscillations of a horizontal plane-parallel flow of an ideal incompressible stratified fluid. The flow is directed along the x-axis; the velocity value is U = U(y). Retaining the notations in section 1, we obtain a system of equations for linear disturbances:

$$\rho_0(Lu + U'v) = -p_x,\ \rho_0 Lv = -p_y - \rho G,\ \rho_0 Lw = -p_z, \qquad L\rho + \rho_0' v = 0,\ u_x + v_y + w_z = 0, \tag{3.1}$$

where $L \equiv \partial/\partial t + U\partial/\partial x$. It follows from (3.1) that $(\Delta + \beta\partial/\partial y)L^2\rho + \beta G(\rho_{xx} + \rho_{zz}) - 2(U'L\rho_x)_y = 0$. The investigation of stability of solutions of this equation is extremely complex. However, for disturbances not dependent on the x-coordinate, we again obtain an equation of the type (1.3):

$$(\partial^2/\partial z^2 + \partial^2/\partial y^2 + \beta\partial/\partial y)\rho_{tt} + \beta G\rho_{zz} = 0,$$

which is solved by the substitution $\rho = \varphi e^{-\beta y/2}$ with subsequent separation of variables. The results obtained are the same as in sections 1 and 2 with the sole difference that $k_1 = 0$.

4. In the preceding examples it was demonstrated that fluctuations of the volume of a stratified fluid as a whole can lead to an instability in accordance with the parametric resonance mechanism. It is natural to expect that non-solid (differential) oscillations of the medium and especially internal waves (see introduction) also have similar properties. The principal difficulties in investigating the stability of internal movements in a stratified fluid involve a complexity of the initial equations even in the absence of their adequately simple partial solutions. The solution involves a changeover to approximations either in the solutions or directly in the equations. By "approximation" in the solutions it is understood that the main wave movement investigated for stability is stipulated approximately (for example, in the form of a finite number of amplitude terms in the series). Mathematically this operation has the sense of a replacement of the coefficients in the equations investigated for stability by their approximate (analytically

simpler) values. Examples of the direct simplification of the equations of motion are the Boussinesq approximation [17] or the β-plane approximation [11, 13, 24]. The problem of the mathematical correctness of this sort of examination is exceedingly complex. However, the scientific and practical importance of the problem is a justification of activity at the "physical level of rigor." Below we will give two examples of approximations in solutions and in the equations for the problem of stability of internal waves.

Assume that there is an ideal incompressible stratified fluid filling the entire space. The uniform gravity field g is directed along the y-axis. The undisturbed density of the fluid is $\rho_0 = Ae^{-\beta y}$; the buoyancy frequency is $N^2 = \beta g = \text{const}$ (the notations are the same as in section 1). We will examine the problem of the stability of an internal wave of a special form; in its stipulation we will limit ourselves to expressions which are linear with respect to amplitude. The form of such a wave is stipulated by the representation

$$u = 0,\ v = Y_t(x,\ t) = \partial Y/\partial t,$$

where u and v are the x- and y-velocity components.

The Y(x, t) function represents a traveling or standing wave in the form cos (kx - Nt) or cos kx cos Nt, etc. The frequency of this wave coincides with the buoyancy frequency N. By analogy with section 1 we will perform transformation of coordinates

$$\bar{x} = x,\ \bar{y} = y - Y(x,\ t),\ \bar{z} = z,\ \bar{t} = t,$$

which corresponds to transformation to coordinates "oscillating" together with the fluid. Thus, density in an internal wave is not dependent on time $\rho = \rho_0(\bar{y})$. For the vertical component v we introduce $\bar{v} = v - Y_t$, so that the main state is rest $u = 0$, $\bar{v} = 0$. The linearized system of equations, being an analogue of (1.1), has the form

$$\begin{gathered} \rho_0 u_t = -p_x + Y_x p_y,\ \rho_0 w_t = -p_z, \\ \rho_0(v_t + Y_{xt}u) = -p_y - \rho(g + Y_{tt}), \\ \rho_t + \rho_0'(v - Y_x u) = 0,\quad u_x - Y_x u_y + v_y + w_z = 0. \end{gathered} \tag{4.1}$$

The line over the notations has been omitted. We will examine a disturbance of the special form:

$$v = v(x,\ t),\ r = r(x,\ t),\ u = w = p = 0.$$

For $r = \rho/\rho_0$ we have

$$r_{tt} + (N^2 + Y_{tt})r = 0. \tag{4.2}$$

This equation is an analogue of (1.6). With $Y = \Phi(x)\cos Nt$ (4.2) is reduced to the Mathieu equation in which x plays the role of a parameter. Since the forcing frequency is equal to the main frequency there is a second resonance [3, 20] and the wave is unstable even for small amplitudes Φ. For a traveling wave $Y = C\cos(kx - Nt)$ and (4.2) is also reduced to the Mathieu equation, but only at the points

sin kx = 0. Hence it follows that there is also instability in this case. We note further that terms with Y enter differently into system (4.1). The derivatives are $Y_x \sim C/\lambda$, where C is amplitude, λ is wavelength. If this ratio is assumed to be small and it is neglected, then (4.1) is reduced to (1.1) with the single difference that the Y_{tt} value is dependent on the x-coordinate. For disturbances which are short-wave relative to x this system of equations in the first approximation coincides with (1.1).

Now we will examine the approach through approximations in the equations. The Boussinesq approximation [17] is a known simplification of the equations of motion for a stratified fluid:

$$d\mathbf{u}/dt = -\nabla p/\bar{\rho} - \theta \mathbf{g},\ d\theta/dt - \beta v = 0,\ \operatorname{div} \mathbf{u} = 0, \tag{4.3}$$

where u is the velocity vector; $\theta \equiv (\rho - \bar{\rho})/\bar{\rho}$; ρ is the total density, differing little from $\bar{\rho}$ = const; $\beta = \beta(y) \equiv -\rho'_0(y)/\bar{\rho}$. With $\beta > 0$ the system (4.3) has precise solutions -- plane waves:

$$(u,\ v,\ 0,\ p) = (-l/k,\ 1,\ i\beta/\omega,\ -\omega l/k^2)Ce^{i\psi}, \tag{4.4}$$

where $\omega = \pm kN/\sqrt{k^2 + l^2}$; C = const, $\psi = kx + ly - \omega t$.

It was demonstrated in [16] that these solutions may be unstable. At the same time it appears that some of the terms in the equations of motion discarded in the derivation of (4.3) can also give parametric instability. For a demonstration of this assertion it is adequate to note that in the problem of an oscillating vessel (see section 1) the use of equations (4.3) does not lead to instability. It is clear that such an approach is incorrect: the small discarded terms of the equations give an effect accumulating in a resonance fashion. In order to retain in the equations the instability discussed in section 1, in the first equation (4.3) it is necessary to return the earlier discarded term $\theta du/dt$. This operation is equivalent to a transformation to the Boussinesq approximation in a coordinate system related to the vessel. After this, a linearized system of equations of the stability problem follows from (4.3):

$$v_t = -p_y/\bar{\rho} - \theta(g + \ddot{Y}),\ u_t = -p_x/\bar{\rho},\ w_t = -p_z/\bar{\rho},\ \theta_t - \beta v = 0, \tag{4.4}$$
$$u_x + v_y + w_z = 0.$$

Comparison with system (1.1) shows that (4.4) is its simplified variant. It follows from (4.4) that

$$\Delta\alpha_{tt} + \beta G(\alpha_{xx} + \alpha_{zz}) = 0, \tag{4.5}$$

where $\alpha \equiv \theta/\beta$; $G \equiv g + \ddot{Y}$. Then the problem is solved by the separation of variables (see section 1). With β = const equation (4.5) is a simplification of (1.4). Allowance for viscosity leads, as already mentioned above, to the appearance in (4.5) of a dissipative term in the simplest form

$$\Delta(\alpha_{tt} - \nu\Delta\alpha_t) + \beta G(\alpha_{xx} + \alpha_{zz}) = 0.$$

In exactly the same way, allowance for the above-mentioned term of the equations leads to the appearance of an additional (in comparison with [16]) instability of the solutions (4.4). We will write the equations of motion in a coordinate system with the x-axis directed along the wave vector k and the y-axis directed along the velocity vector in the wave. The velocity and density fields assume the form

$$(U,\ V,\ \Theta) = (0,\ 1,\ i\beta/\omega)Ce^{i(\varkappa x-\omega t)},$$

where $\omega = N \cos \varphi$; φ is the angle between the x-axis and the horizontal plane; $\varkappa^2 \equiv k^2 + l^2$. The linearized system of equations of the problem for stability has the form

$$Lu = -p_x - g\theta \sin \varphi,\ Lv + V_x u = -p_y - \theta(g \cos \varphi + V_t),$$
$$Lw = -p_z,\ u_x + v_y + w_z = 0,\ L\theta + \Theta_x u - \beta v = 0, \qquad (4.6)$$

where $L \equiv \partial/\partial t + V\partial/\partial y$. We will examine disturbances of the special form:

$$v = v(x,\ t),\ \theta = \theta(x,\ t),\ p = p(x,\ t),\ u = w = 0.$$

It follows from (4.6) that

$$\theta_{tt} + (N^2 \cos^2 \varphi + \beta V_t \cos \varphi)\theta = 0.$$

Since the frequency of the change in V is equal to $\omega = N \cos \varphi$, for $V = C \cos(\varkappa x - \omega t)$ there is second resonance. We emphasize that the results in this section are of an illustrative character and constitute no proofs.

In conclusion we note the following. The problem of investigation of stability in the linear approximation of equilibrium of an ideal stratified fluid in a vertically oscillating vessel is reduced to solution of the Mathieu equation (1.7). For an equilibrium density stratification there can be an instability of the parametric resonance type. Stabilization by oscillations of nonequilibrium stratification is possible only for part of the spectrum.

In a horizontal plane-parallel flow of a stratified fluid subjected to vertical oscillations there are disturbances of a special form for which the same results as for an oscillating vessel are correct.

An approximate investigation for the stability of internal waves in an unbounded stratified fluid shows that for them there is an instability in accordance with the parametric resonance mechanism close in type to instability in an oscillating vessel.

As a development of our general concepts concerning the mechanisms of instability in a stratified fluid we will formulate the following. If the oscillations of the fluid are such that the mass velocity has a normal component toward surfaces of constant density, there can be an exponential increase in linear disturbances in accordance with the parametric resonance mechanism.

BIBLIOGRAPHY

1. Shmidt, G., PARAMETRICHESKIYE KOLEBANIYA (Parametric Oscillations), Moscow, Mir, 1978.

2. Faraday, M., "On a Peculiar Class of Acoustical Figures, and on Certain Forms Assumed by a Group of Particles Upon Vibrating Elastic Surfaces," PHIL. TRANS. ROY. SOC., Vol 121, p 299, 1831.

3. Landau, L. D. and Lifshits, Ye. M., MEKHANIKA (Mechanics), Moscow, Nauka, 1965.

4. Yakubovich, V. A. and Starzhinskiy, V. M., LINEYNYYE DIFFERENTSIAL'NYYE URAVNENIYA S PERIODICHESKIMI KOEFFITSIYENTAMI I IKH PRILOZHENIYA (Linear Differential Equations With Periodic Coefficients and Their Applications), Moscow, Nauka, 1972.

5. Moiseyev, N. N. and Rumyantsev, V. V., DINAMIKA TELA S POLOSTYAMI, SODERZHASHCHIMI ZHIDKOST' (Dynamics of a Body With Cavities Containing Fluid), Moscow, Nauka, 1955.

6. Sretenskiy, L. N., TEORIYA VOLNOVYKH DVIZHENIY ZHIDKOSTI (Theory of Wave Movements of a Fluid), Moscow, Nauka, 1977.

7. Benjamin, T. B. and Ursell, F., "The Stability of the Plane Free Surface of a Liquid in Vertical Motion," PROC. ROY. SOC., Vol 225, p 505, 1954.

8. Krushinskaya, S. I., "Oscillations of a Heavy Viscous Fluid in a Moving Vessel," ZhVMMF [expansion of this Navy Ministry journal unknown], Vol 5, No 3, 1965.

9. Gershuni, G. Z. and Zhukhovitskiy, Ye. M., KONVEKTIVNAYA USTOYCHIVOST' NESZHIMAYEMOY ZHIDKOSTI (Convective Stability of an Incompressible Fluid), Moscow, Nauka, 1972.

10. Markman, G. S. and Urintsev, A. L., "Parametric Excitation of Convective Motion in a Fluid Heated From Above," IZV. SEV.-KAVK. NAUCH. TSENTRA VYSSH. SHKOLY. YESTESTV. NAUKI (News of the Northern Caucasus Scientific Center of Advanced Educational Institutes. Natural Sciences), No 1, 1977.

11. Lorenz, E. N., "Barotropic Instability of Rossby Wave Motion," J. ATMOS. SCI., Vol 29, p 258, 1972.

12. Lilly, D. K., "A Note on Barotropic Instability and Predictability," J. ATMOS. Sci., Vol 30, No 1, 1973.

13. Mied, R. P., "The Instabilities of Finite-Amplitude Barotropic Rossby Waves," J. FLUID MECH., Vol 86, No 2, 1978.

14. Dolzhanskiy, F. V., Kurganskiy, M. V. and Chernous'ko, Yu. L., "Laboratory and Theoretical Investigation of Barotropic Rossby Waves in a Rotating Annular Channel," IZV. AN SSSR: FAO (News of the USSR Academy of Sciences: Physics of the Atmosphere and Ocean), Vol 15, No 6, 1979.

15. McEwan, A. D. and Robinson, R. M., "Parametric Instability of Internal Gravity Waves," J. FLUID MECH., Vol 67, No 4, 1975.

16. Mied, R. P., "The Occurrence of Parametric Instability of Internal Gravity Waves," J. FLUID MECH., Vol 78, No 4, 1976.

17. Phillips, O. M., DINAMIKA VERKHNEGO SLOYA OKEANA (Dynamics of the Upper Layer of the Ocean), Leningrad, Gidrometeoizdat, 1980.

18. Orlanski, I., "On the Breaking of Standing Internal Gravity Waves," J. FLUID MECH., Vol 54, No 3, 1972.

19. Whittaker, E. T. and Watson, D. N., KURS SOVREMENNOGO ANALIZA (Course in Modern Analysis), Vol 1, Moscow, FML, 1963.

20. Abramovits, M. and Stigan, I., SPRAVOCHNIK PO SPETSIAL'NYM FUNKTSIYAM (Handbook on Special Functions), Moscow, Nauka, 1979.

21. Kapitsa, P. L., "Dynamic Stability of a Pendulum With an Oscillating Suspension Point," ZhETF (Journal of Experimental and Theoretical Physics), Vol 21, No 5, 1951.

22. Briksman, V. A., "Parametric Stabilization of Interface of Fluids," DAN SSSR (Reports of the USSR Academy of Sciences), Vol 226, No 5, 1976.

23. Zen'kovskaya, S. M. and Simonenko, I. B., "Influence of High-Frequency Vibration on Development of Convection," IZV. AN SSSR: MZhG (News of the USSR Academy of Sciences: Mechanics of Fluids and Gases), No 5, 1966.

24. Batchelor, G., VVEDENIYE V DINAMIKU ZHIDKOSTI (Introduction to Fluid Dynamics), Moscow, Mir, 1973.

5303
CSO: 1865/129

UDC 551.465

SPECTRA OF CURRENT FIELDS IN OCEAN DETERMINED ALONG TRAJECTORIES OF FREELY DRIFTING SOFAR SYSTEM BUOYS

Moscow DOKLADY AKADEMII NAUK SSSR in Russian Vol 263, No 4, Apr 82 (manuscript received 10 Jul 81) pp 993-996

[Article by K. V. Konyayev and G. I. Merinova, Acoustics Institute imeni N. N. Andreyev, Moscow]

[Text] Within the framework of the Soviet-American POLYMODE experiment for studying the synoptic variability of currents in the ocean the Local Dynamic Experiment was carried out by the American side. About 40 neutral-buoyancy buoys of the SOFAR (Sound Fixing and Ranging) system were released in May 1978 in a square measuring 150 x 150 km with its center at about 31°N and 69°W and were set at equilibrium at the horizons 700 and 1300 m; their position was registered by on-shore and self-contained acoustic stations each 8 hours for a period of 6 months. An analysis of the trajectories of these and earlier released buoys made it possible to determine a number of characteristics of synoptic movements [1, 2]. Among the spectral characteristics of the field of currents computations were made only of the so-called time spectrum Lagrangians -- the spectrum of a number of velocity readings without allowance for the spatial location of these readings.

In December 1980 the data on buoy trajectories were transmitted to the Soviet side and it became possible to carry out their complete spatial-temporal spectral analysis. The potential possibility of such an analysis is quite obvious: in physical space and time the trajectories of the buoys relatively densely fill some volume, creating a quite full idea concerning the three-dimensional realization of the field.

Representing the three-dimensional realization in the form of a set of time functions, determined on the buoy trajectories, the three-dimensional amplitude spectrum of the realization can be written in the form of time integrals (written for the u-component of the velocity vector):

$$S_u(k, l, f) = \sum_j \int u_j(t) \exp\{-i2\pi[kx_j(t) + ly_j(t) + ft]\}\, dt,$$

where x, y, t are the horizontal space coordinates and time, the x-axis is directed to the east, the y-axis -- to the north; k, l, f are the space and time frequencies; j is the number of the buoy; $u_j(t)$ is the u-component of the velocity vector; $x_j(t)$, $y_j(t)$ are the coordinates of the j-th buoy; integration is

carried out during the entire observation time only for negative time frequencies. The three-dimensional spectrum of kinetic energy of horizontal movements is equal to (4 degrees of freedom)

$$g(k, l, f) = (S_u S_u^* + S_v S_v^*)\Delta/2IT,$$

where Δ is the mean area covered by one float (determined as the first part of the ratio of the maximum of the space spectral window to the volume under this window); I is the number of buoys; T is the equivalent observation time. With change to the time spectrum the integration is carried out by areas (10 x 16)$\cdot 10^{-3}$ cycle/km separately for the western and eastern half-planes of space frequencies (about 25 degrees of freedom for the background part of the spectrum).

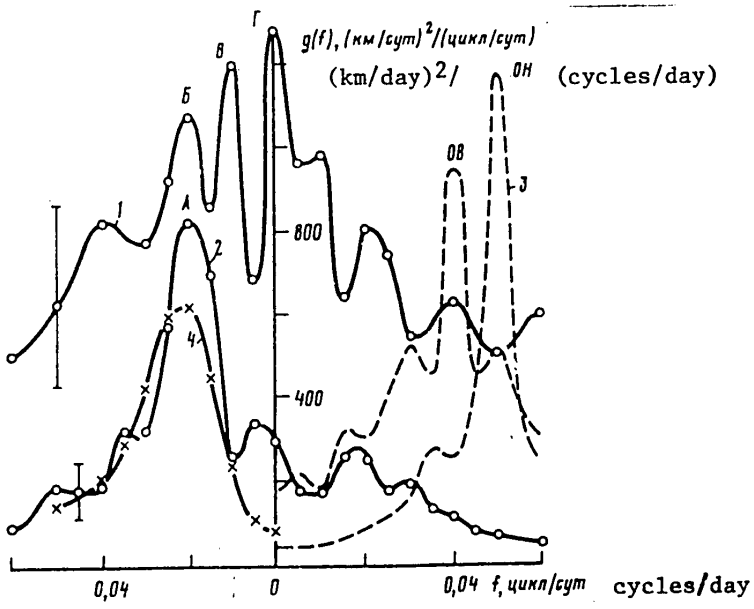

Fig. 1. Western (at left) and eastern (at right) time spectra of kinetic energy of horizontal movements at horizons 700 (1, peaks B, C, D) and 1300 m (2, peak A) and spectral windows OB and OH for these same horizons (3), 4 -- western spectrum at horizon 1300 m during first 60 days; vertical lines -- 80% confidence intervals for background part of spectrum.

Rossby waves can make a contribution only to the western time spectrum. The spectral window is computed as the response to identical readings of the velocity components, equal to 3 km/day and arranged on the existing trajectories (in order not to overburden the diagrams the windows on them have been displaced from the zero frequency). Due to movement of the buoys together with

the mean flow the observed time frequencies coincide with the true frequencies and the boundaries of the corridors of the possible parameters of Rossby waves can be determined directly from the dispersion expressions [3].

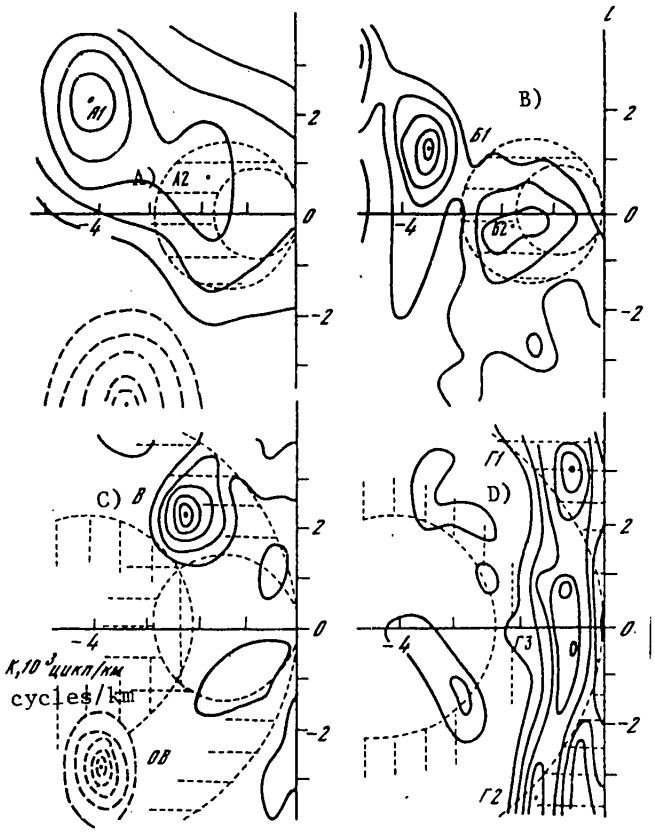

Fig. 2. Space spectra corresponding to the principal peaks of the time spectra (isolines 95, 80, 60, 40, 20% of maximum). The dashed lines correspond to the space spectral windows OB and OH; the horizontal and vertical dashed curves represent the corridors of possible parameters of Rossby waves of the zero and first modes respectively.

In the analysis we used series of coordinates following with an interval of 1 day from 12 May through 13 November 1978. For the horizons 700 and 1300 m the normalizing values are: Δ = 10.5 and $4.6 \cdot 10^3$ km^2, T = 111 and 130 days, I = 20 and 22; the mean velocities and velocity dispersions for these horizons are (separately for the u- and v-components) -0.6 and 0.4 km/day, 101 and 86 (km/day)^2, -1.6 and 0 km/day, 25 and 30 (km/day)^2.

The nature of the dropoff of the time spectra is determined to a great extent by the shape of the side lobes of the spectral window so that the true spectrum drops off appreciably more rapidly than the measured spectrum (Fig. 1). The

western spectra contain narrow peaks which correspond to the most compact space spectra peaks (Fig. 2). Peak A was formed for the most part by the oscillations observed during the first 60 days: the area under the peak during the entire time was 12 $(km/day)^2$, and during the first 60 days -- 28 $(km/day)^2$. Peaks A2 and B2 fall in the corridor of the parameters of barotropic Rossby waves (frequencies for the boundaries of the corridors f$\pm$0.005 cycle/day) and the peaks A1 and B1 do not fall far from this corridor and from the dispersion surface of the baroclinic waves approaching close to this section of the spectrum near the point $K = -4 \cdot 10^{-3}$ cycle/km. It is more probable that these oscillations are barotropic waves since their intensities differ little at the two horizons. The B peak lies in the corridor of the barotropic waves and not far from the circular corridor of the baroclinic waves. It is more probable that these are baroclinic oscillations since they are not traced at the horizon 1300 m. The peaks $\Gamma 1$, $\Gamma 2$, $\Gamma 3$ correspond to oscillations with periods greater than 200 days. The group velocity of the waves (peaks A, B, C) is directed to the southeast [4]. The space spectrum of the oscillations with frequencies 0-0.06 cycle/day at the 700-m horizon occupies a relatively broad angular spectrum with a maximum in the northwest quadrant, and at the horizon 1300 m almost does not differ from the space spectrum at a frequency of 0.02 cycle/day (peaks A1, A2). The space spectrum of oscillations with frequencies 0.10-0.14 cycle/day in the western sector at the 700-m horizon is virtually uniform, but at the horizon 1300 m is close to zero around the zero space frequency (the 20% spectral isoline is $(6\text{-}11)\times10^{-3}$ cycle/km distant from the zero frequency). The elimination of low space frequencies from the spectrum is evidence of a predominance of nearly immobile turbulence transported by orbital motion in the waves.

Table 1

Parameter	A1	A2	B1	B2	B	G1	G2	G3
Number of mode	0?	0	0?	0	1	0	0	0
Period, days	50	50	50	50	100	200	200	200
Length, km	210	500	270	550	310	320	270	1000
Direction, °N	300	285	290	260	315	350	200	270
Kinetic energy (approximate), $(km/day)^2$	6	4	6	4	10	4	4	4

The parameters of the principal waves are given in Table 1.

According to data from anchored measurement instruments operating from 6 September 1977 through 30 August 1978 in the region 29°N and 70°W at the horizons 700 and 1400 m (Soviet part of POLYMODE), the pattern of the space-time spectrum is close to that considered on the basis of total intensity, period and length of the predominant waves; the clearest spectral peaks correspond to oscillations with the observed periods 50 and 85 days (true periods 60 and 130 days); the 50-day waves are also propagated to the northwest sector; however, in general, in contrast to this case, there is a predominance of waves moving to the southwest.

It follows from this analysis that about one-third of the kinetic energy of horizontal movements in this region of the ocean was carried by narrow-band Rossby waves of the lower modes, moving for the most part to the west and

northwest. At the 700-m horizon the oscillations were created for the most part by 5-6 different waves, and at the 1300-m horizon -- by two waves; most of the kinetic energy of these two waves was concentrated in the first third of the observation time.

BIBLIOGRAPHY

1. Rossby, T, Voorhis, A. D. and Webb, D., J. MARINE RES., Vol 33, No 3, p 355, 1975.

2. Freeland, H. J., Rhines, R. B. and Rossby, T., IBID., Vol 33, No 3, p 383, 1975.

3. Konyayev, K. V. and Sabinin, K. L., DAN (Reports of the USSR Academy of Sciences), Vol 253, No 4, p 970, 1980.

4. Longuet-Higgins, M. S., PROC. ROY. SOC., Vol A-279, No 1379, p 446, 1964.

5303
CSO: 1865/142

TERRESTRIAL GEOPHYSICS

UDC 534.222.2

RADIATION OF ELASTIC WAVES IN UNVENTED EXPLOSION

Moscow IZVESTIYA AKADEMII NAUK SSSR: FIZIKA ZEMLI in Russian No 2, Feb 82 (manuscript received 8 Jan 81) pp 23-29

[Article by S. Z. Dunin, O. V. Nagornov and Ye. A. Popov, Moscow Engineering Physics Institute]

[Text]

Abstract: A study was made of the radiation of elastic waves during an explosion in a porous medium with the dilatancy effect taken into account. The character of radiation of elastic energy at different moments in time was investigated. The spectral composition of the radiated seismic signal, the influence of the strength parameters of the medium, porosity and dilatancy coefficient on the elastic energy radiated during an explosion were analyzed.

In connection with the use of explosions there has been a great increase in interest in the problem of radiation of elastic waves in ground and rocks. This is attributable primarily to the problems involved in the seismic safety of shots and seismic prospecting [1, 2].

A number of models have been proposed for computing seismic waves forming during an explosion; a review of these was given in [3]. In these studies it is assumed that elastic waves are radiated by some spherical source whose radius is known as the elastic radius. The elastic radius is assumed equal to the radius of the destruction zone. As indicated by experimental data (such as [4]), the radiation of elastic waves already begins during the movement of the destruction wave front. The author of [5] gave an approximate estimate of the elastic energy radiated prior to the time of stopping of the plasticity wave front. The author of [6] examined the influence of an elastic precursor on motion in the near zone of an explosion for solid rock on the assumption that behind the shock wave front the medium becomes fluid, the shear destruction condition is satisfied at the wave front and the velocity of the wave front is linearly related to mass velocity behind it.

Source [1] gave a schematic representation of the powerful explosion phenomenon. According to [1], as a result of the evaporation of rock a spherical cavity is formed (as indicated by the experimental data in [7] and a theoretical estimate [8], 60-100

tons is evaporated per kiloton of charge). The vapor pressure in the cavity considerably exceeds the strength parameters of the medium. Further development of the explosion can be broken down into three principal stages. In the first, hydrodynamic stage it is assumed that the medium behaves like a fluid, that is, the difference in radial and azimuthal stresses is neglected. This stage ends when the mean pressure in the medium is comparable with the theoretical strength of the crystalline matter. The strength properties of the medium become extremely important in the second stage. When the velocity of the wave front is comparable to the velocity of propagation of longitudinal waves the radiation of an elastic wave begins. In this third stage the elastic properties of the medium play an important role. In [9] an estimate was made of the radiated seismic wave within the framework of the above-mentioned scheme on the assumption that the radius R_0 from which the radiation of an elastic wave begins and the maximum radius of the plastic zone R_p are close. Experimental data show that in the case of both field [4] and in the case of laboratory [10] explosions $R_p/R_0 \sim 3$-5.

Next we will be interested only in characteristics related to the radiation of an elastic wave and we will drop the hydrodynamic phase of the explosion. In this article we will examine the problem of radiation of elastic waves in a porous medium with the dilatancy effect taken into account. The nature of the radiation of elastic energy at different moments in time is investigated. The influence of the strength parameters of the medium, porosity and the dilatancy coefficient on the quantity of elastic energy radiated during an explosion is analyzed. The spectral composition of the radiated seismic signal is analyzed.

In the case of an underground shot in a homogeneous medium compressed by lithostatic pressure a destruction wave is propagated from a cavity of the radius a_0 with the initial pressure p_0. The Mises-Schleicher plasticity condition

$$\sigma_r-\sigma_\theta=-k+m(\sigma_r+2\sigma_\theta),$$

is satisfied behind the wave front. Here σ_r and σ_θ are the radial and azimuthal directions; k, m are constants. The flow behind the front is described by the equations of conservation of mass and momentum and the dilatancy equation, which are written in a spherically symmetric coordinate system in Lagrange variables (r_0, t). The equation of motion is

$$\rho_0 r_0^2 r^{\alpha-2}\frac{\partial u}{\partial t}=-\frac{\partial}{\partial r_0}\left[r^\alpha\left(p+\frac{k}{3m}\right)\right], \tag{1}$$

where $\alpha = 6m/(2m+1)$, $p(r_0,t)$, u is mass velocity, $r(r_0,t)$ is the Eulerian coordinate of the point r_0.

The continuity equation is

$$\frac{\partial r}{\partial r_0}=\frac{r_0^2}{r^2}\frac{\rho_0}{\rho}, \tag{2}$$

where $\rho(r_0,t)$ is particle density, ρ_0 is initial density. The dilatancy equation, with allowance for the continuity equation, is

$$\Lambda\frac{\partial}{\partial t}\ln(\rho r^3)+\frac{\partial}{\partial t}\ln\rho=0, \tag{3}$$

where Λ is the dilatancy rate [11].

Experimental data and theoretical computations [4, 12] show that in porous media the principal mechanism of energy dissipation is related to shock compression in the wave front, that is, to an irreversible packing of pores. We will make the following simplifying assumption. At the front the destructible medium attains its limiting compression $\varepsilon_{fr} = 1 - \rho_0/\rho_{fr}$. The subscript "fr" denotes values of the parameters at the front; the subscript "0" denotes values of the parameters in the undisturbed medium. Henceforth we will assume that $\varepsilon_{fr} = \text{const} = \varepsilon$.

At the front of the destruction wave there is satisfaction of the conditions of conservation of mass and momentum

[Φ = front]

$$u_\Phi = \varepsilon \dot{R}(t), \tag{4}$$

$$p_\Phi = \rho_0 \varepsilon \dot{R}^2(t) + p_h, \tag{5}$$

where R(t) and $\dot{R}(t)$ are front radius and velocity, p_h is lithostatic pressure at the depth h.

The dilatancy rate Λ for porosities 5-15% can be considered constant [1]. Then equation (3) is integrated

$$\rho(r_0, t) = \rho_\Phi \left(\frac{r_0}{r(r_0, t)}\right)^{2-n}, \tag{6}$$

where $n = (2-\Lambda)/(1+\Lambda)$.

The integration of the continuity equation (2), with (6) taken into account, gives the relationship

$$r^{n+1}(r_0, t) = (1-\varepsilon) r_0^{n+1} + \varepsilon R^{n+1}(t), \tag{7}$$

where r falls between the radius of the cavity and the radius of the wave front:

$$((1-\varepsilon) a_0^{n+1} + \varepsilon R^{n+1}(t))^{1/n+1} \leqslant r \leqslant R(t).$$

We introduce the dimensionless parameters $\tau = c_0 t/a_0$, $x_0 = r_0/a_0$, $Y(\tau) = R(t)/a_0$, where c_0 is the velocity of propagation of longitudinal waves in the undestroyed medium.

The equation of motion (1) after integration in the range from r_0 to R(t), with allowance for (4), (5), (7), with $x_0 = 1$, assumes the form:

$$A(Y) Y\dot{Y} + B(Y)\dot{Y}^2 + C(Y) = 0, \tag{8}$$

where

$$A(Y) = \int_{1/Y}^{1} d\xi\, \xi^2 z^{\alpha-n-2}(\xi),$$

$$z(\xi)=(\varepsilon+(1-\varepsilon)\xi^{n+1})^{1/n+1},$$

$$B(Y)=1+nA(Y)-n\varepsilon\int_{1/Y}^{1}d\xi\,\xi^{2}z^{\alpha-2n-3}(\xi),$$

$$C(Y)=\frac{p_h}{\varepsilon\rho_0c_0^2}-\frac{k}{3\varepsilon m\rho_1c_0^2}-z^{\alpha}\left(\frac{1}{Y}\right)\frac{p(\tau)-\frac{k}{3m}}{\varepsilon\rho_0c_0^2},$$

where $p(\tau)$ is the pressure on the wall of the explosion cavity, which conforms to the adiabatic law:

$$p(\tau)=[1-\varepsilon+\varepsilon Y^{n+1}(\tau)]^{-\frac{2\gamma}{n+1}}.$$

Equation (8) with the initial conditions

$$Y(0)=1,\quad \dot{Y}(0)=\sqrt{\frac{p_0-p_h}{\varepsilon\rho_0c_0^2}} \tag{9}$$

was solved numerically prior to the moment in time τ_1, when the velocity of the wave front was greater than the velocity of the longitudinal waves c_0. After the velocity of the destruction wave front becomes comparable to c_0, the "detachment" of the elastic precursor (forerunner) begins. In this stage the medium in front of the wave front is disturbed by the elastic precursor and the conditions at the destruction wave front assume the form

$$u-\dot{R}=\frac{\rho_1}{\rho_\Phi}(v-\dot{R}),\qquad p_\Phi-p_h=-\sigma_r+\rho_1\left(1-\frac{\rho_1}{\rho_\Phi}\right)(v-\dot{R})^2, \tag{10}$$

where ρ_1, v, σ_r are density, mass velocity, and radial stress (negative during compression) in the elastic wave.

The parameters of the elastic wave are expressed through one unknown function $f(\xi)$ -- the potential of elastic displacements -- in the following way (the medium is considered ideally elastic):

$$v=c_0\left[\frac{f(\xi)}{x}+\frac{f(\xi)}{x^2}\right],$$

$$\sigma_r=-\rho_1c_0^2\left[\frac{f(\xi)}{x}+2\frac{1-2\nu}{1-\nu}\left(\frac{f(\xi)}{x^2}+\frac{f(\xi)}{x^3}\right)\right]-p_h, \tag{11}$$

$$\sigma_\theta=-\rho_1c_0^2\left[\frac{\nu}{1-\nu}\frac{f(\xi)}{x}-\frac{1-2\nu}{1-\nu}\left(\frac{f(\xi)}{x^2}+\frac{f(\xi)}{x^3}\right)\right]-p_h,$$

$$\rho_1=\frac{\rho_0}{1-f(\xi)/x}.$$

Here $\xi=\tau-x$, $x=r/a_0$, ν is the Poisson coefficient.

At the destruction wave front we assume that one of the following conditions is satisfied:

$$\sigma_\theta-\sigma_r=\tau_s \tag{12}$$

or

$$\sigma_r = -\sigma_*. \tag{13}$$

We will assume that the lithostatic pressure is great and radial detachment fissures do not develop.

Omitting intermediate computations, we write a system of equations for determining the unknown functions $Y(\tau)$ and $f(\xi)$ with $\tau > \tau_1$:

$$\dot{Y}A(Y)Y + B(Y)\dot{Y}^2 + C + D = 0, \tag{14}$$

$$\frac{\dot{f}}{Y} = \frac{\sigma_*}{\rho_0 c_0^2} - \frac{2(1-2\nu)}{1-\nu}\left[\frac{f}{Y^2} + \frac{f}{Y^3}\right] - \frac{p_h}{\rho_0 c_0^2},$$

where the latter equation is taken with $x = Y(t)$ and

$$D = \frac{\sigma_*}{\varepsilon\rho_0 c_0^2} + v_1^2 - 2\dot{Y}v_1, \tag{15}$$

$$v_1 = \frac{\sigma_*}{\rho_0 c_0^2} + \frac{3\nu-1}{1-\nu}\frac{f}{Y^2} - \frac{2(1-2\nu)}{1-\nu}\frac{f}{Y^3}.$$

This system of equations (written with allowance for the destruction criterion (13)) is integrated numerically with the following initial conditions:

$$Y = Y(\tau_1),\ \dot{Y} = \dot{Y}(\tau_1),\ w(\tau_1) = 0,\ \ v(\tau_1) = 0, \tag{16}$$

where $w(\tau_1)$ is dispacement in the elastic wave at the initial moment in time, $Y(\tau_1)$, $\dot{Y}(\tau_1)$ are the values of the radius and wave front velocity at the time τ_1, obtained from solution in the preceding stage.

It is assumed that when the velocity of the destruction wave front is compared with the mass velocity of the particles in front of it (when $\tau = \tau_2$) there will be no further destruction of the medium but the radiation of elastic waves will continue. From this moment ($t = t_2$) an analytical solution is obtained for the well-known Sharpe problem [13]:

$$\sigma_r = -\sigma_* \quad \text{when} \quad x = Y(\tau_2), \tag{17}$$

and as the initial conditions for the potential of elastic displacements we will take its values f and $\dot{f}$, obtained in the preceding stage.

The elastic energy radiated during the explosion was computed using the formula

$$e(t) = 4\pi\rho_0 a_0^3 c_0^2 \int_0^{c_0 t/a_0} [f(\tau)]^2\, d\tau. \tag{18}$$

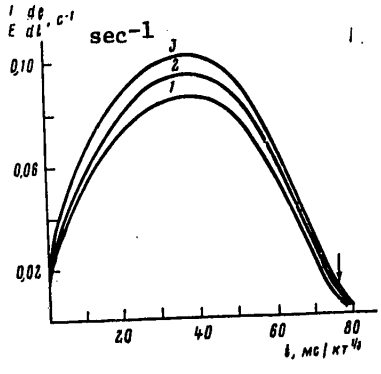

Fig. 1. Dependence of velocity of radiation of elastic energy on time. 1) $\Lambda = 0$, 2) $\Lambda = 0.05$, 3) $\Lambda = 0.11$, E is the explosion energy; the arrow indicates the time t_2.

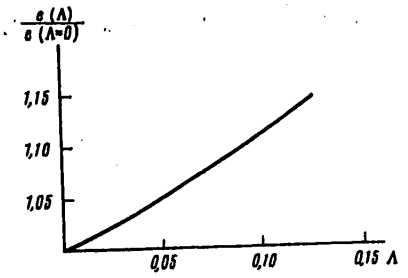

Fig. 2. Dependence of irradiated elastic energy on dilatancy coefficient.

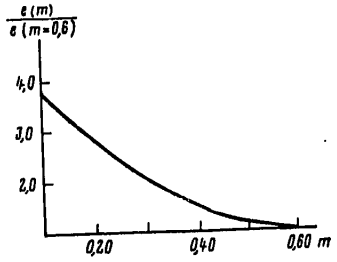

Fig. 3. Dependence of radiated elastic energy on dry friction coefficient.

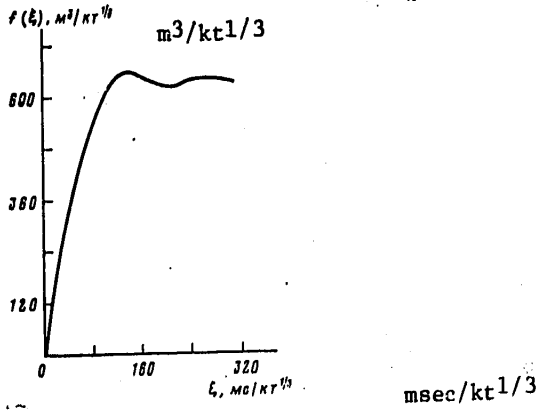

Fig. 4. Dependence of potential of elastic displacements on time.

Figure 1 is a graph of the dependence of the velocity of radiation of elastic energy de(t)/dt on time with different dilatancy coefficients. It can be seen from this dependence that most of the elastic energy is radiated up to the moment $t_2 = \tau_2 a_0 / c_0$, that is, with motion of the destruction wave. It exceeds by a factor of approximately 4-10 the elastic energy radiated after the destruction wave stops. With an increase in the dilatancy coefficient the quantity of radiated elastic energy increases. For example (Fig. 2), the elastic energy radiated with $\Lambda = 0$ is 12% greater than the elastic energy radiated with $\Lambda = 0.1$. The radius of the destruction zone in a dilatating medium ($\Lambda = 0.1$) is 10% greater than in a nondilatating medium. The ratio $R_p/R_0 = 3.8\text{-}4.2$, depending on Λ. Figure 3 shows the dependence of the radiated elastic energy on the dry friction coefficient with a porosity of

9%. With a decrease in the dry friction coefficient from 0.60 to 0.15 the quantity of radiated elastic energy increases by a factor of 3.5. The radius of the plasticity zone increases by 40%. In this case the increase in the fraction of radiated elastic energy is related to a decrease in energy dissipation due to plastic flow.

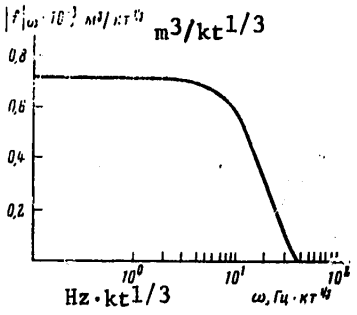

Fig. 5. Dependence of derivative of potential of elastic displacements on frequency.

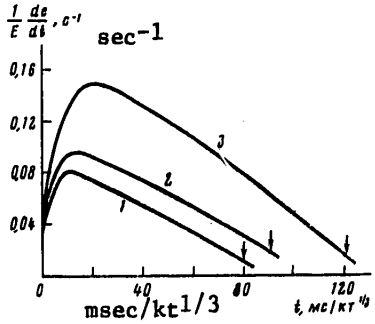

Fig. 6. Dependence of velocity of radiation of elastic energy on time with different porosity. 1) 13%, 2) 9%, 3) 5%, E -- energy of explosion; the arrow indicates the time t_2.

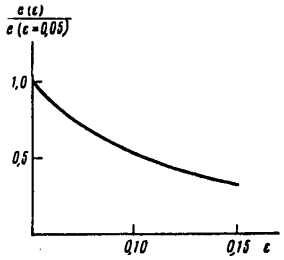

Fig. 7. Dependence of radiated elastic energy on porosity.

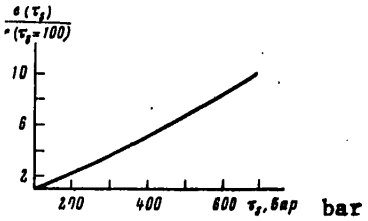

Fig. 8. Dependence of quantity of radiated elastic energy on cohesion coefficient.

If the medium conforms to the Tresk plasticity condition

$$\sigma_\theta - \sigma_r = \tau_s, \tag{19}$$

then equation (1) assumes the form

$$\rho_0 r_0^{\alpha-1} r^{\alpha-1} \frac{\partial u}{\partial t} = -\frac{\partial}{\partial r_0}\left[p + 2\tau_s \ln \frac{r}{r_0}\right]. \tag{20}$$

For $\tau < \tau_1$ the coefficient C in equation (8) must be assumed equal to:

$$C_1 = \frac{1}{\varepsilon \rho_0 c_0^2}\left[p_h + 2\tau_s \ln Y(\tau) - p_0\left[1 - \varepsilon + \varepsilon Y^{n+1}\right]^{-\frac{5\gamma}{n+1}}\right],$$

and when $\tau_1<\tau<\tau_2$ the system of equations (14) assumes the form:

$$A(Y)Y\dot{Y}+B(Y)\dot{Y}^2+C_1+D_1=0, \tag{21}$$

$$\frac{f}{Y}+3\left[\frac{f}{Y^2}+\frac{f}{Y^3}\right]-\frac{1-\nu}{1-2\nu}\frac{\tau_s}{\rho_0 c_0^2}=0, \tag{22}$$

$$D_1=\frac{1}{\varepsilon}\frac{1+\nu}{1-\nu}\left[\frac{f}{Y^2}+\frac{f}{Y^3}\right]+v_2^2-2\dot{Y}v_2,$$

$$v_2=\frac{1-\nu}{1-2\nu}\frac{\tau_s}{\rho_0 c_0^2}-\frac{2f}{Y^2}-\frac{3f}{Y^3}.$$

The system of equations (21), (22) with the initial conditions (16) was integrated numerically with parameters characteristic for rock salt [14]. As a result of the computations it was possible to ascertain the dependence of reduced potential on time (Fig. 4) and the frequency dependence of the derivative of the potential of elastic displacements (Fig. 5).

A contribution to the high-frequency spectral component is made by the leading part of the elastic precursor radiated during the motion of the destruction wave front.

We also computed the dependence of the velocity of radiation of an elastic wave on time for different porosities (Fig. 6). We note also, as in the case of the condition of destruction at the front by means of crushing (13), that the part of elastic energy radiated after stopping of the destruction front is an order of magnitude less than the fraction radiated before stopping: the effective source of elastic waves is seemingly situated between the cavity and the elastic boundary. Such a character of elastic wave radiation was experimentally observed in [2]. With an increase in porosity from 5 to 15% the fraction of radiated energy decreases by half (Fig. 7). The radius of the plasticity zone R_p decreases since the fraction of energy going to shock compression increases with an increase in porosity.

A study was made of the dependence of the radiated energy on the cohesion coefficient τ_s with a fixed 10% porosity (Fig. 8). It can be seen that the fraction of radiated elastic energy increased by a factor of 5 with an increase in τ_s with τ_s = 0.8 kbar in comparison with τ_s = 0.2 kbar (the radius of the plasticity zone increased by a factor of 1.5).

Summary

1. A study was made of the dynamics of radiation of elastic waves from a spherical unvented (underground) source. It was shown that most of the elastic energy is radiated prior to the stopping of the destruction front, which must be taken into account in formulating a model of an effective spherical source.

2. A dependence of the fraction of radiated energy on the parameters of the medium (porosity, strength, dilatancy coefficient) was established.

3. The dependence of reduced potential on frequency and time was determined. The leading part of the radiated elastic precursor makes a contribution to the high-frequency spectral component.

The authors express appreciation to Ye. Ye. Lovetskiy, V. K. Sirotkin and V. S. Fetisov for useful discussions.

BIBLIOGRAPHY

1. Rodionov, V. N., et al., MEKHANICHESKIY EFFEKT PODZEMNOGO VZRYVA (Mechanical Effect of an Underground Explosion), Moscow, Nedra, 1971, 220 pages.

2. Vasil'yev, Yu. N., et al., "Study of Structure of an Explosion Center in Soft Ground," IZV. AN SSSR: FIZIKA ZEMLI (News of the USSR Academy of Sciences: Physics of the Earth), No 12, pp 40-50, 1972.

3. Kogan, S. Ya. and Polikarpov, A. M., "Comparison of Different Models of a Seismic Source of an Underground Explosion," IZV. AN SSSR: FIZIKA ZEMLI, No 1, pp 32-43, 1976.

4. Rodin, G., SEISMOLOGIYA YADERNYKH VZRYVOV (Seismology of Nuclear Explosions), Moscow, Mir, 1974, 190 pages.

5. Lovetskiy, Ye. Ye., "Some Problems of the Theory of an Explosion in Porous Ground," IZV. AN SSSR. OTN. MEKHANIKA I MASHINOSTROYENIYE (News of the USSR Academy of Sciences. Department of Technical Sciences. Mechanics and Machine Building), No 6, pp 36-43, 1959.

6. Koryavov, V. P., "Influence of a Precursor on Motion in the Near Zone of an Explosion," IZV. AN SSSR. FIZIKA ZEMLI, No 10, pp 74-79, 1974.

7. Butkovich. T. R., "Calculation of the Shock Wave From an Underground Nuclear Explosion in Granite," J. GEOPHYS. RES., Vol 70, No 4, pp 825-892, 1965.

8. Dunin, S. Z. and Sirotkin, V. K., "Expansion of the Gas Cavity in Brittle Rock With Allowance for the Dilatance Properties of the Ground," ZH. PRIKL. MEKH. I TEKHN. FIZ. (Journal of Applied Mechanics and Technical Physics), No 4, pp 106-109, 1977.

9. Kostyuchenko, V. N. and Rodionov, V. N., "Radiation of Seismic Waves During Powerful Underground Explosions in Solid Rocks," IZV. AN SSSR: FIZIKA ZEMLI, No 10, pp 65-73, 1974.

10. Tsvetkov, V. M., et al., "Mechanism of Fracturing of a Solid Medium by an Explosion," DOKL. AN SSSR (Reports of the USSR Academy of Sciences), Vol 231, No 5, pp 1067-1069, 1976.

11. Nikolayevskiy, V. N., "Correlation Between Body and Shear Plastic Deformations and Shock Waves in Soft Ground," DOKLADY AN SSSR, Vol 177, No 3, pp 542-545, 1967.

12. Lovetskiy, Ye. Ye., Maslennikov, A. M. and Fetisov, V. S., "Energy Dissipation During an Explosion in a Porous Elastico-Plastic Medium," ZH. PRIKL. MEKH. I TEKHN. FIZ., No 6, pp 134-140, 1979.

13. Sharpe, J. A., "The Production of Elastic Waves by Explosion Pressure," GEOPHYSICS, Vol 7, No 2, pp 144-154, 1942.

14. Khristoforov, B. D., et al., "Influence of Porosity on the Parameters of Dynamic Compression of NaCl," IZV. AN SSSR: FIZIKA ZEMLI, No 8, pp 31-40, 1971.

5303
CSO: 1865/136

UDC 528.532.291

NEW DEVELOPMENTS IN GRAVIMETRIC METHODS AND INSTRUMENTATION

Moscow IZMERENIYE SILY TYAZHESTI in Russian 1981 (signed to press 16 Oct 81) pp 2, 93-96

[Annotation, table of contents and abstracts from collection of articles "Gravity Measurement," responsible editor Yu. D. Bulanzhe, corresponding member, USSR Academy of Sciences, Izdatel'stvo "Nauka", 950 copies, 96 pages]

[Text] Annotation. This collection of articles is devoted to the development and also an evaluation of the accuracy of gravimetric instrumentation and methods for work with it. The authors discuss the overall accuracy of sea gravimeters of the AMG type for 10 years. Also examined is the possibility of an effective protection of the geophysical instruments against microseisms. The collection is intended for specialists in the field of geodesy and gravimetry.

Contents

UDC 528.532.291

DETERMINATION OF GRADUATION OF GR/K2 'DELTA-2' GRAVIMETERS BY TILT METHOD

[Abstract of article by Rukavishnikov, R. B.]

[Text] A study was made of calibration by the tilt method of two quartz astaticized narrow-range gravimeters using a UEGP-1 apparatus at different temperatures (+25 and +35°C), whose constancy was maintained using a TEG thermostat. It was found that the value of a graduation of the investigated gravimeters is dependent on temperature and that the nonlinearity of the reading scale is considerably less than indicated in the certification data for the instruments. The relative error in determining the value of a graduation on the average is equal to $\pm 2 \cdot 10^{-4}$ and the error in determining scale corrections is ±0.02 mgal. The use of the proposed method and apparatus for calibrating instruments of the mentioned type makes it possible to increase the reliability in determining their constants and the accuracy in gravimetric measurements as a whole. Figures 2, tables 1, references 5.

UDC 528.271:519.281.2

ACCURACY IN OBSERVATIONS WITH AMG GRAVIMETERS ON EXPEDITIONS OF THE INSTITUTE OF PHYSICS OF THE EARTH USSR ACADEMY OF SCIENCES DURING 1968-1977

[Abstract of article by Boyarskiy, E. A. and Pushchina, L. V.]

[Text] The article describes the method and cites estimates of the accuracy of observations with AMG sea gravimeters on the basis of the results of 10 expeditions of the Institute of Physics of the Earth, USSR Academy of Sciences. The evaluation was made using three methods: 1) on the basis of internal convergence, that is, on the basis of a comparison of simultaneous observations by two or three methods; 2) on the basis of repeated observations at the points of intersection of runs; 3) on the basis of a comparison with the results of other expeditions. Figures 3, tables 8, references 5.

UDC 528.271:519.281.2

ERRORS IN MEASUREMENTS WITH GRAVIMETERS IN STANDARD POLYGONS IN AUSTRALIA IN 1973 AND IN EASTERN EUROPE IN 1974

[Abstract of article by Boyarskiy, E. A.]

[Text] The random and systematic errors in measurements with gravimeters in standard polygons are analyzed. It is shown that there is a constant error which characterizes the gravimeter in all measurements in this link. This error changes from link to link and from instrument to instrument randomly: its mean square value for the GAG-2 is $\pm 47 \mu$gal; for the Zhs-12 it is $\pm 30 \mu$gal; for the Lacoste-Romberg -- $\pm 17 \mu$gal. Tables 5, references 7.

UDC 528.532.291

SOME PROBLEMS IN THE ADJUSTMENT OF AN AMG SEA GRAVIMETER IN CALIBRATION BY THE TILT METHOD AND DETERMINATION OF SKEW ANGLES BETWEEN GRAVIMETER SENSING SYSTEMS

[Article by Svetlosanova, Z. P.]

[Text] The author examines the possibility of increasing the quality of adjustment of the AMG gravimeter during calibration by the tilt method. The article describes a method for gravimeter adjustment with use of a special device for the separate registry of sensing systems. Also given are the results of determination of the skew angle between the sensing systems of a group of AMG gravimeters. Recommendations are given on the practical use of the UEG-11 apparatus for eliminating skews. Figures 1, tables 3, references 3.

UDC 550.310

ANTISEISMIC PROTECTION OF GEOPHYSICAL INSTRUMENTS

[Article by Dubovskoy, V. B., Grushinskiy, A. N., Zayonchkovskiy, M. A. and Leont'yev, V. I.]

[Text] The article sets forth a theory for a passive antiseismic platform and gives an analysis of the possibility of creating an effective antiseismic platform with a feedback. Evaluating the accuracy characteristics of presently existing standard-produced sensors of horizontal and vertical accelerations, the authors come to the conclusion that it is more effective to have protection against microseisms by means of a low-frequency passive platform. The article gives the amplitude and phase-frequency characteristics and recommends the optimum parameters. Figures 2, references 2.

UDC 529.786.2

ECONOMICAL THERMOSTATING OF GAG-3 GEODETIC GRAVIMETER

[Article by Dubovskoy, V. B., Leont'yev, V. I. and Zayonchkovskiy, M. A.]

[Text] A study was made of the advantage of a proportional thermostating system. The authors give the comparative characteristics of schemes with independent and dependent temperature sensors. There is a detailed analysis of the problem of creating a nongradient temperature field. The authors provide an optimum design for a thermostat using a Dewar vessel. The model of a thermostat constructed with an analysis of the principal sources of errors has high accuracy parameters: the thermostating coefficient is not less than 10^{-4}, the homogeneity of the temperature field is not worse than $(2-3)\cdot10^{-5}$ °C, the influence of thermal impacts is weak. The considered thermostating system can be used extensively in precise measurement apparatus. Figures 2, tables 1, references 4.

UDC 528.532.291

GEOMETRY OF HIGHLY SENSITIVE LEVELS

[Abstract of article by Dobrokhotov, Yu. S.]

[Text] A method is proposed for constructing the section profile of an entire working surface of a highly sensitive level. Control computations for models formed by circles of different radii indicated that the errors introduced by simplifications of rigorous theory are negligible in comparison with the measurement errors in the investigation of levels. The practical use of the proposed method is shown in the example of three second levels. Figures 12, references 4.

UDC 528.532.291

LEVEL-TYPE TILTMETER

[Abstract of article by Dobrokhotov, Yu. S.]

[Text] The article describes a tiltmeter with a sensitivity of 0.1-0."2 to be used in measurements of tilts of the earth's surface in active seismic and volcanic regions. Highly sensitive astronomical levels are used as the tiltmeter measurement elements. Methods for adjusting the instrument and determining its constants are set forth. Figures 3, references 2.

UDC 528.532.291

CALIBRATION BY THE METHOD OF TILT OF 'WORDEN MASTER' GRAVIMETERS

[Abstract of article by Rukavishnikov, R. B.]

[Text] The calibration of two quartz astaticized gravimeters of the "Worden Master" type produced by the American "Texas Instruments" Company is described. Investigations of instruments carried out with the unthermostated UEGP-1 apparatus and with the TEG thermostat at a temperature close to the thermostating temperature of the instruments are compared. It has been established that the relative error in determining the graduation value in both cases is approximately identical and equal to $(6-7)\cdot10^{-5}$; the error in determining the scale corrections in the first case is equal to ±0.025 mgal, and in the second -- ±0.008 mgal. The conclusion is drawn that the quality in determining the gravimeter constants is influenced clearly by the constancy of temperature in the course of the investigations, the number of repetitions and experience of the operator. Figures 1, tables 2, references 3.

UDC 550.34.012

POSSIBILITIES FOR THE REGISTRY OF MICROACCELERATIONS ABOARD SPACE VEHICLES

[Abstract of article by Dubovskoy, V. B., Zholobov, V. M., Zayonchkovskiy, M. A., Leont'yev, V. I., Leskov, L. V., Obydennikov, S. S. and Savicheva, V. V.]

[Text] The article gives an analysis of the factors causing accelerations of satellites and orbital stations and evaluates their possible causes. Making a comparative analysis of existing methods for measuring accelerations, the authors conclude that on the basis of highly sensitive geophysical instrumentation it is possible to create acceleration sensors greatly exceeding in their sensitivity those in standard production by industry. The authors describe a model of an accelerometer, which, having good noise immunity, is superior to known instruments and can be used successfully in solving a number of problems in space research. Figures 4, references 2.

5303
CSO: 1865/131

UDC 551.1

MULTISIDED INVESTIGATIONS OF THE EARTH'S CRUST AND UPPER MANTLE: RESULTS AND PROSPECTS

Moscow VESTNIK AKADEMII NAUK SSSR in Russian No 3, Mar 82 pp 110-114

[Article by V. V. Belousov, corresponding member, USSR Academy of Sciences]

[Text] The Scientific Council of the USSR Academy of Sciences on Multisided Investigations of the Earth's Crust and Upper Mantle during the last five years has coordinated work on study of structure and development of the earth's crust and upper mantle. This work was carried out by about 150 organizations of the USSR Academy of Sciences, USSR Geology Ministry and USSR Ministry of Higher and Secondary Specialized Education. The program for these studies belonged (and in the current five-year program belongs) to the group of programs entering into the plans of the USSR State Committee on Science and Technology.

The investigations have been carried out by geological, geophysical and geochemical methods in different structural zones of the Soviet Union for the purpose of clarifying the peculiarities of the tectonic, magmatic and metamorphic processes, for developing theoretical concepts concerning their mechanism and causes. Special efforts have been applied in order to integrate different methods and obtain a multisided geological-geophysical interpretation of the observed characteristics of structure of the earth's deep layers.

The studies were carried out in different directions, the scope of individual research areas was different, and in addition to major problems solutions were found for many special ones. We will attempt to summarize the principal results obtained in this work plan and also to draw some conclusions concerning the most important directions in further research of this type.

The most general result relates to the problem of inhomogeneities in the structure of the earth's crust and upper mantle and essentially involves a refinement of data on the distribution of these inhomogeneities, their nature, and the relationship of surface geological structures to them.

The fact that the earth's crust and upper mantle are inhomogeneous both vertically and horizontally and that these changes in its structure correspond to changes in structures at the surface was also known earlier. But in the course of recent years

there has been a refinement of our knowledge concerning such inhomogeneities. As a result it has been possible to separate the observed deep structures into a series of "models" corresponding to definite types of geological zones. Seismic models of the crust and mantle are the best developed.

For example, the plates of ancient platforms are characterized by a stable thickness of the earth's crust (approximately equal to 40 km), an increased mean seismic velocity in the crust (6.5 km/sec) with its separation into three layers of approximately identical thickness and a high seismic velocity at the top of the mantle (8.2-8.3 km/sec). The ancient crystalline shields are underlain by a still thicker crust (up to 50 km). The plates of the young platforms have a crust with a thickness of 35-40 km, the mean seismic velocities in them are lower than in the ancient platforms (about 6.4 km/sec), and at the top of the mantle the velocities vary between 7.9 and 8.1 km/sec.

All these figures pertain to the internal regions of the continent. They change appreciably toward its peripheries: there the thickness of the crust in these same structural conditions decreases to 28-35 km.

The deep depressions on the platform have a special structure. Aulacogens or grabens, such as the Dneprovsko-Donetskiy graben, are characterized by a decrease in crustal thickness under a downwarp in the basement (to 35 km), as a result of which the Mohorovicic discontinuity beneath the axis of the downwarp rises by 5-10 km relative to the surrounding regions.

Such depressions as the Caspian depression, where the consolidated crust is at a depth of more than 20 km and is covered by an equally thick sedimentary layer, stand out still more clearly in structure. Under the center of this type of depression the thickness of the entire crust decreases to 30 km and the thickness of its consolidated layer decreases to 10 km. A decrease in thickness occurs due to the consolidated crust, in which, in this connection, only the lower, most high-velocity part persists, that is, the densest layer. It therefore follows that in such depressions the granite (granite-gneiss) part disappears and the entire solid part of the crust consists of a "basalt" (granulite-basite) layer. In some cases beneath such depressions there are lenses of high-velocity matter of lesser density (7.8-7.9 km/sec) at the top of the mantle.

Zones of modern and recent rock formation are separated, as is well known, into epigeosynclinal and epiplatform zones. The first includes the Carpathians, Crimea and the Caucasus. In these zones there is a thickening of the crust to 50-60 km. The thickening takes in primarily the upper or middle layers, that is, the low- and intermediate-velocity layers. At the top of the mantle the velocities are close to 8 km/sec. The boundaries between the layers are traced less clearly than on the platforms. A circumstance of particular interest is that in the crust of such orogenic downwarps as the Kura or Transcarpathian downwarps there are high-velocity, dense and large inclusions.

Zones of epiplatform mountain formation, such as the Tien Shan or Pamir, in their deep structure are similar to the preceding, but here there is a general decrease in the velocities of seismic waves both in the crust and in the upper mantle.

Under the Alayskiy Range there are low-velocity layers in the crust forming local velocity inversions. The velocities at the top of the mantle are reduced to 7.5-7.9 km/sec.

The model for rift zones, an example of which is Lake Baykal and the adjacent regions, is characterized by a crust of reduced thickness (up to 35 km), convex relief of the Moho beneath the graben at the surface, both at the base of the crust (6.7 km/sec) and at the top of the mantle (7.7 km/sec).

In the volcanic regions of Kamchatka, in addition to a general decrease in crustal thickness (to 30 km), typical for the margins of the continent, there are pipelike bodies in the upper mantle with anomalously low seismic velocities. These bodies serve for conducting lava in channels.

Extremely important results were obtained by the deep seismic sounding method in the zone of transition from the continent to the Pacific Ocean. Together with the results of earlier studies, carried out in the oceans surrounding the Soviet Union, they indicated that with increasing distance from the land, with increasing depth of the sea, the continental crust is gradually wedged out, being replaced by an oceanic crust. On the island arcs the crustal thickness again increases; the crust either remains oceanic or there are indicators of a continental structure, in this case being anomalously thin. The transition of the crust to the mantle is considerably less clear than in the other zones. In the abyssal trenches the crust has an oceanic structure and is especially thin. The marginal sea - island arc system is characterized by reduced seismic velocities at the top of the mantle.

Until now we do not have adequate information on the structure of the deep layers of the upper mantle, and in particular, on the degree of expression of the asthenosphere -- a partially molten layer lying at a depth of 100-200 km. However, it can be considered established that in the mantle, to a depth of not less than 200 km, there are well-expressed horizontal inhomogeneities. Seismic and magnetotelluric investigations have shown that the distribution of the asthenospheric layers is extremely nonuniform. One cannot speak of a continuous asthenosphere. It is most probable that it is entirely absent beneath the crystalline shields, the geologically quietest. It is poorly expressed beneath the plates of the ancient platforms, but is best expressed and has a considerable thickness under regions of modern rift and mountain formation. In the rift zones and in regions of modern volcanism the partially molten matter of the asthenosphere penetrates into the uppermost layers of the mantle and forms lenses of anomalously low-density matter directly under the crust. It is known that observations of elastic waves reflected from the surface of the earth's core have indicated that in a more general plan the inhomogeneities associated with separation of the earth's surface into continents and oceans penetrate to a depth of at least 400 km.

There will be a considerable broadening of our information concerning deep inhomogeneities and concerning their nature if the seismic data are supplemented by gravimetric and geothermal data.

For example, there are exceedingly interesting results from the use of isostatic anomalies with their separation into different orders differing with respect to wavelength from thousands to hundreds and tens of kilometers. In this way it is

possible to discriminate a pattern of distribution of densities at different depths in the crust and upper mantle. Regional isostatic anomalies with a wavelength of a thousand kilometers are evidence of very deep inhomogeneities penetrating into the subasthenospheric layers of the mantle. Comparison of these anomalies with the latest endogenous geological activity indicates the presence of a direct correspondence between density distribution in the mantle and the degree of excitation of endogenous processes at the surface, that is, the degree of intensity of tectonic and magmatic processes. The minimum densities correspond to the greatest degree of excitation. In actuality, the least dense mantle is situated under the Pamir and Tien Shan, from whence it is propagated to the region of most recent tectonic activation in the southern part of Siberia and into the Baykal rift zone. This region of the less dense mantle differs sharply from the ancient East European Platform or the Anabarskiy shield with their quiet gravitational field, close to equilibrium.

Great complications are observed in the zone of transition from the continent to the Pacific Ocean. Here regional isostatic anomalies attain a high maximum. It is evidently caused by some heavy masses concentrated under the asthenosphere at a depth of several hundreds of kilometers. But if this regional background is removed and we turn to local isostatic anomalies, it is found that there is a far more complex pattern. Then positive anomalies persist on the island arcs, but in the abyssal trenches they become negative, the marginal seas being in an equilibrium state. If the influence of the crust is subtracted from the anomalies, local anomalies revealing the distribution of densities in the upper layers of the mantle are revealed. In this case beneath the marginal seas the anomalies become negative, but under the abyssal trenches -- positive.

These complexities indicate a different distribution of densities at different levels in the section of the transition zone. Such a great inhomogeneity of the medium is evidence of extremely energetic deep processes, which also corresponds to the geological data.

Geothermal observations are of decisive importance in understanding the nature of deep processes. Like density inhomogeneities, heat flows are associated with the latest endogenous activity; they are greater where the activity is greater and less in the quiet regions. High heat flows are associated with the latest epiplatform mountain formation (Pamir, Tien Shan) and the epigeosynclinal uplift of the Central Caucasus. High flows also chara terize the rift zone of Baykal and the transition zone from the continent to the Pacific Ocean. On the platforms there is usually a normal flow decreasing to subnormal on the crystalline shields.

It is easy to see that the seismological, gravimetric, geothermal and also magnetotelluric data agree well with one another. The conditions for such an agreement are evidently determined by the thermal regime of the deep layers. In actuality, in those regions where the heat flow and accordingly the temperatures are higher there is a well-expressed asthenosphere, reduced velocities at the top of the mantle and reduced densities of these same layers. Everywhere in the regions of increased heat flows at the surface there are modern or traces of relatively recent intensive tectonic, magmatic and metamorphic processes. In places where the heat flow is normal the asthenosphere is expressed weakly or is not expressed at all; the

velocities at the top of the mantle are normal, the crust is thick and recent and very recent endogenous activity at the surface is weak.

This correlation makes it possible to surmise that endogenous regimes, that is, combinations of tectonic, magmatic and metamorphic processes, for the most part are determined by the thermal conditions in the earth's deep layers. Excited regimes are orogenic, rift, active transitional zones; they are caused by corresponding thermal excitation of the upper mantle and crust, expressed, in particular, in intensified melting of the upper mantle. Quiet regimes -- platform, passive transition zones -- are associated with quiet thermal conditions. The circumstance that regimes of different degree of expression appear simultaneously at the earth's surface is a result of nonuniformity of the earth's heat field. Hence, to be sure, it is natural to assume that also a change in regimes in time, including so-called endogenous cycles, are caused by temporal evolution of thermal nonuniformities in the mantle and crust.

Thus, the results of a multisided geological-geophysical study of the earth's crust and upper mantle over the territory of the USSR create a basis for a generalized overview of the development of the earth's tectonosphere. This basis is the history of the earth's thermal field with all its spatial and temporal nonuniformities. Such a generalization is of both theoretical and practical importance since a clarification of the relationships between the upper mantle and the crust and an understanding of the character of the processes determining these relationships make it possible to interpret the mechanism and conditions of formation of different geological structures.

The observed inhomogeneities in the structure of the earth's crust and upper mantle, in combination with inhomogeneities in the thermal field, are evidence that the processes transpiring in the tectonosphere are not limited to mechanical movements, but are also accompanied by physicochemical transformations of matter.

In deep inhomogeneities it is natural to see a reflection of the processes which at the present time are in different stages of their development. We could reconstruct these processes if we were able to arrange the observed states in the sequence of their development in nature. If, for example, the mean section of the crust of an ancient platform is adopted as the initial section, and the observed anomalous section of the crust of the Caspian depression is adopted as the next section, forming in connection with downwarping of the earth's crust, we will interpret the absence of a granite-gneiss layer not as a primary phenomenon, but as a result of secondary transformations. As a result of the latter this layer in its elastic properties became indistinguishable from the basalt layer. Such a transformation could be a result of metamorphic processes with an increase in the initial density of the granite-gneiss layer. To be sure, this is only a hypothesis.

Still less of a definite nature can be said now concerning the nature of processes in this same region at the boundary of the crust and mantle, where, if conclusions are drawn on the basis of geophysical data, this boundary has been displaced upward relative to its initial position and crustal thickness was thus reduced. If crustal dilatation is excluded (and in the case of the isometric Caspian depression it is scarcely possible), one must think of rather radical transformations of

matter (for example, phase transitions) at this boundary.

Similar comparisons for other cases will enable us to speak of a decrease in the density of the upper layers of the mantle under the influence of intensified heating causing (or intensifying) partial melting. This occurs in regions of mountain and rift formation. A decrease in density of the upper mantle also occurs in the transition zone from the continent to the ocean. But at the same time in local downwarps (and in regions of mountain formation and in abyssal trenches) dense inclusions appear which are registered by both seismic and gravimetric methods. It can be postulated that dense inclusions represent injections of heavy magma.

However, such hypotheses are inadequate both for the solution of theoretical problems and especially for meeting practical requirements. In order to clarify the true nature of the correlation between depths and the surface there is need for models based on a comparison of the geophysical indices and embodying physicochemical materials. This requires an intensified development of the geophysical aspects of the considered problem.

It should be noted that the geochemical direction until now has been inadequately reflected in the program for multisided investigations of the earth's crust and upper mantle. Now the situation is improving. But even beyond the limits of this program, in world geochemical science, a great volume of data has been accumulated which can be used in a comparison with geophysical and geological data. Much information has been accumulated concerning conditions of magma formation and metamorphism. An analysis of the distribution of isotopes, radioactive and rare earth elements gives much for an understanding of physicochemical processes in the earth's deep layers. Data are available indicating the stratification of the upper mantle: beneath its upper layer, poor in alkalis and rare elements, there is evidently a layer containing these elements. All this is opening up broad paths to an understanding of evolution not only of the structure but also the matter of the crust and upper mantle, a revelation of the patterns of distribution of matter of different composition in the earth's deep layers in different geological zones.

Such a broader, more multisided approach to the study of the earth's deep layers will make it possible to hope that in the course of the five-year plan which is now beginning we will considerably advance in our understanding of the earth's deep layers and those processes which determine the development of the earth's crust and the distribution of matter in it, including those aspects which are of practical interest.

5303
CSO: 1865/139

PHYSICS OF ATMOSPHERE

ARTICLES ON STRUCTURE OF AURORAL SUBSTORM

Apatity STRUKTURA AVRORAL'NOY SUBBURI (REZUL'TATY MIM) in Russian 1980 (signed to press 23 Dec 80) pp 2, 154-159

[Annotation and abstracts from collection of articles "Structure of the Auroral Substorm (Results of Program for International Investigation of the Magnetosphere)", edited by M. V. Uspenskiy, candidate of technical sciences (responsible editor), A. G. Yakhnin and Ye. Ye. Timofeyev, Polyarnyy geofizicheskiy institut, Kol'skiy filial AN SSSR, 400 copies, 159 pages]

[Text] Annotation. The collection of articles gives the results of observations and investigations carried out at the Polar Geophysical Institute in implementing the program for International Investigation of the Magnetosphere. The authors examine problems relating to the physics of the radioaurora and the relationship between the radioaurora and other geophysical phenomena. A study was made of the characteristics of auroras in different substorm phases and also the dynamics of the equivalent current system at the time of breakup. Some characteristics of the polar ionosphere and geomagnetic pulsations are investigated. The collection is intended for scientific specialists, graduate students and students specializing in the field of solar-terrestrial physics and physics of the magnetosphere and ionosphere.

Abstracts

UDC 550.388

NEW EVIDENCE OF UNIFIED WAVE NATURE OF SYNCHRONOUS PULSATIONS IN RADIOAURORA AND GEOMAGNETIC FIELD

[Article by Kustov, A. V., Pudovkin, A. I., Kangas, I., Leynonen, I. and Uspenskiy, M. V.]

[Text] An analysis was made of the results of observations in the general zone of pulsations in the radioaurora and short-period pulsations of the geomagnetic field of class PIC, registered on 28 February 1978. Earlier it was proposed that both phenomena be interpreted as the result of the incidence of an Alfven wave from the magnetosphere. New information is given confirming this hypothesis. Figures 4, references 6.

UDC 550.388

CORRELATION BETWEEN RADIOAURORA AND PROTON AURORAS IN EVENTS OF 3 FEBRUARY AND 16 MARCH 1978

[Article by Fedorova, N. I., Totunova, G. F. and Sukhovanenko, P. Ya.]

[Text] A study was made of the joint behavior of regions of the radioaurora and proton auroras on the basis of simultaneous observations of radar reflections and surface optical spectral observations in the evening sector of local geomagnetic time. A good correlation was discovered between the region of the maximum intensity of H_β and the diffuse radioaurora in the evening sector. Ionization by protons gives a contribution to the electron concentration in the ionospheric E region comparable with the concentration of leaking electrons. Figures 2, references 16.

UDC 550.338

POLAR GEOPHYSICAL INSTITUTE PULSED DOPPLER APPARATUS FOR DRIFT MEASUREMENTS OF RADIOAURORA

[Article by Stepanov, G. S., Kustov, A. V., Miroshnikov, Yu. G. and Yakovlev, P. I.]

[Text] The article describes the new Polar Geophysical Institute pulsed Doppler radar intended for the geophysical diagnosis of the ionosphere within the framework of the international program for investigation of the magnetosphere. The radar was developed for three-position measurements of the cosine dependence of the Doppler scattering shift, together with the STARE system, and for investigation of the spatial and Doppler structure of short-period pulsations accompanying substorms and participation in diagnosis of artificial modification of the ionospheric E region by powerful SW radiation. The authors give the zones of radar visibility, aspect angles and positioning of geophysical instruments. The article gives examples of the spectra of reflected signals and a table (calendar) of available data for the experiment "Auroral Breakup-79." Figures 7, tables 2, references 15 items.

UDC 550.388

NATURE OF EAST-WEST ASYMMETRY OF ALTITUDES OF AURORAL SCATTERING

[Article by Timofeyev, Ye. Ye.]

[Text] This study is a review of data on the east-west asymmetry of radioaurora altitudes. This author analyzes the results of measurements at frequencies from 46 to 1210 MHz. It is shown that the asymmetry of altitudes is not a result of change in the current angle with the azimuth of observation; in order to eliminate the contradiction between experiment and the existing theory it is necessary to propose the presence, in general, of a slight slope to the east (about 1°) of the ionospheric current layers. Figures 1, references 17.

UDC 550.388

DETAILED ANALYSIS OF ALTITUDE CHARACTERISTICS OF RADIOAURORA IN EVENT OF 11 FEBRUARY 1979

[Article by Timofeyev, Ye. Ye., Miroshnikova, T. V. and Kukushkina, R. S.]

[Text] The author gives a comparison of the behavior of the altitudes of auroral scattering at a frequency of 90 MHz with other parameters of the ionospheric E region during the course of the event of 11 February 1979. It is shown that there is a systematic eastward slope of the radioaurora layers in the region of the westerly electrojet and there is no correlation between the altitude at which the radio ray is orthogonal to the geomagnetic field and the altitude of scattering. There is a correlation between the altitudes of the radioaurora and the lower edge of auroral E_s layers observed in one and the same ionospheric region. Figures 4, references 14.

UDC 550.388.8

LONGITUDINAL ELECTRIC FIELDS AS MAIN SOURCE OF ACCELERATION OF AURORAL PARTICLE FLUXES DURING DEVELOPMENT OF SUBSTORM

[Article by Yevlashin, L. S. and Yevlashin, L. M.]

[Text] On the basis of a joint analysis of the optical spectra of auroras and ionospheric data at the time of development of midnight isolated negative bays in the H component at Murmansk station the authors give a scheme for change in the parameters of the energy spectra of auroral protons and electrons, from which it can be seen that in the different phases of an elementary substorm there is an anticorrelation of variations of hardness of the energy spectra. This is evidence that the main source of acceleration of auroral particles operative during development of a substorm can be the electric field directed along the earth's magnetic lines of force. Figures 4, references 15.

UDC 550.388.8

DIFFUSE RADIOAURORA AND LONGITUDINAL CURRENTS IN EVENING SECTOR

[Article by Gustafson, G., Sverdlov, Yu. L. and Sergeyeva, N. G.]

[Text] A study was made of the correlation between the radioaurora and longitudinal currents. The meridional chain of radars operates at a frequency of 88 MHz. The longitudinal currents were measured by the "Triad" satellite. It was found that a diffuse radioaurora is associated with inflowing longitudinal currents. Figures 4, references 11.

UDC 550.385.37

LOCALIZATION OF Pc5 AND AURORAL OVAL

[Article by Raspopov, O. M. and Afanas'yeva, L. T.]

[Text] On the basis of materials from the network of surface observatories situated in the subauroral latitudes and auroral zone the authors describe the correlation between Pc5 and the auroral oval. The region of generation of Pc5 is related to the equatorial boundary of the oval with different levels of magnetic activity. It is known on the basis of satellite data that the excitation of Pc5 is associated with the drift of plasma inhomogeneities from the nighttime sector of the magnetosphere to its daytime part during the time of a substorm. The azimuthal drift of the source of oscillations is also detected on the basis of surface data. The drift velocity is $\sim$ 0.5-1.1 degree/min. The detected patterns are compared with the known theories of excitation of Pc5 pulsations. The most probable mechanism of generation of oscillations is drift instability developing on the inner boundary of the plasma layer in the morning sector of the magnetosphere during the time of the restoration phase of a substorm. Figures 3, tables 2, references 25.

UDC 550.388

RELAXATION CHARACTERISTICS OF AURORAL IONOSPHERE

[Article by Tagirov, V. R., Vlaskov, V. A., Chernous, S. A. and Kayla, K.]

[Text] This review gives a detailed examination of the experimental and fundamental theoretical data on measurement and computation of the reaction time of the auroral ionosphere to the injection of particles. Figures 7, tables 2, references 25.

UDC 550.388

FREQUENCY DEPENDENCE OF ALTITUDINAL VARIATION OF CONDUCTIVITY TENSOR OF MULTICOMPONENT IONOSPHERE

[Article by Pudovkin, A. M. and Pudovkina, Ye. V.]

[Text] The method for direct solution of a system of equations of motion is used in computing the components of the conductivity tensor of cold plasma. The article gives the altitudinal variations of the tensor components for frequencies 10^{-3}-10^{5} sec^{-1} for the daytime mean latitudinal six-component ionosphere under quiet conditions. Figures 6, tables 6, references 6.

UDC 550.338

ASYMMETRY OF AURORAL SCATTERING INDICATRIX

[Article by Zarnitskiy, Yu. F.]

[Text] A linear theory is used in analysis of the relative contribution of different factors capable of causing an asymmetry of the indicatrix of auroral USW

scattering in the polar ionosphere. It is shown that Kadomtsev-Nedospasov instability in the longitudinal current is capable of causing swinging of long-wave drift waves deflected from the orthogonal magnetic field by a considerable angle. The authors also briefly examine the influence of ohmic heating of ionospheric plasma on the development of Buneman-Fahl instability in the E layer. Figures 8, references 9.

UDC 550.338

LONG-PERIOD PULSATIONS OF SPECTRUM OF ENERGIES OF ENERGETIC AURORAL ELECTRONS IN MORNING HOURS

[Article by Pirs, G. P., Shumilov, O. I., Lazutin, L. L., Radkevich, V. A. and Zhulin, I. A.]

[Text] On the basis of measurements of X-radiation in the stratosphere during the SAMBO-79 experiment a study was made of long-period pulsations of the intensity and spectrum of energies of auroral X-radiation in morning. The article describes the case of synchronicity of long-period pulsations of intensity with similar pulsations of the spectral parameters of auroral X-radiation, which accompanied considerable activity of Pc5 geomagnetic pulsations. Figures 2, references 18.

UDC 550.385

DEVELOPMENT OF EQUIVALENT CURRENT SYSTEM DURING BREAKUP TIME

[Article by Yakhin, A. G., Sergeyev, V. A., Baumyokhann, V. and Raspopov, O. M.]

[Text] Data from the Scandinavian network of magnetometers are used in analyzing the development of an equivalent current system of a weak localized substorm. The results make it possible to propose the existence of a Birkeland system of currents with a current flowing in at the eastern edge and flowing out at the western edge of the auroral convexity. The growth of the current system occurs discretely; intensifications occur near the moments of flares of new arcs on the front of the auroral convexity. Figures 2, references 7.

UDC 550.338.8

IONOSPHERIC CONDUCTIVITY IN THE REGION OF THE EASTERN ELECTROJET AND RADIOAURORA AMPLITUDE

[Article by Starkov, G. V., Uspenskiy, M. V., Kayla, K., Pellinen, R. I., Grinval'd, R. A., Nil'sen, E. and Sofko, G.]

[Text] Data on the radioaurora are used in investigating ionospheric conditions around the equatorial arc of the auroral oval in the preliminary phase of a storm in the evening. The basis of the work is a detailed instrumental analysis of the local storm of 16 March 1978, selected by the Polar Geophysical Institute (NL 78-8) for a complex investigation within the framework of the experiment "Auroral Breakup-78." The authors demonstrate the existence of a stable conductivity

jump related to the most equatorial arc of the auroral oval. Equatorward from the oval the Hall conductivity is 3-5 times greater than the conductivity within the oval between the arcs, although the Pedersen conductivity there also differs insignificantly. This phenomenon has also been confirmed by other geophysical observations carried out simultaneously and by data of the Chatanikovskaya incoherent scattering station for other cases. It is demonstrated that the earlier experimentally determined linear relationship between the amplitude of the radioaurora and density of the ionospheric current is a special case of the more general case, which is the linear relationship of the radioaurora amplitude and the mean electron density in the scattering volume. The latter in some limits allows an anticorrelation between the electric field and amplitude of the experimentally determined radioaurora. Figures 7, references 35.

5303 - END -
CSO: 1865/74